

MUONIUM IN SOME INSULATING OXIDES AND DIAMOND

by

DAVID PHILIP SPENCER

B.Sc., The University of British Columbia, 1977

A THESIS SUBMITTED IN PARTIAL FULFILMENT OF
THE REQUIREMENTS FOR THE DEGREE OF
DOCTOR OF PHILOSOPHY

in

THE FACULTY OF GRADUATE STUDIES

Department of Chemistry

We accept this thesis as conforming
to the required standard

UNIVERSITY OF BRITISH COLUMBIA

February, 1985

© David Philip Spencer, 1985

22

In presenting this thesis in partial fulfilment of the requirements for an advanced degree at the UNIVERSITY OF BRITISH COLUMBIA, I agree that the Library shall make it freely available for reference and study. I further agree that permission for extensive copying of this thesis for scholarly purposes may be granted by the Head of my Department or by his or her representatives. It is understood that copying or publication of this thesis for financial gain shall not be allowed without my written permission.

Department of Chemistry

UNIVERSITY OF BRITISH COLUMBIA
2075 Wesbrook Place
Vancouver, Canada
V6T 1W5

Date: February, 1985

Abstract

Muonium can be regarded as an isotopic analogue of the hydrogen atom, with a positive muon replacing the proton. This thesis is concerned with searches for muonium in weak transverse and zero magnetic fields in a variety of non-magnetic oxide insulators with few nuclear moments, and in diamond, a semiconductor. The technique of Muon Spin Rotation (μ SR) was used, which can be thought of in analogy with NMR and EPR. It relies on measuring the direction of the muon spin with time via the unique signature of the parity violating decay of the muon, in which its decay positron is emitted preferentially along the muon spin direction. This can provide a sensitive measure of the interaction of the muon spin with its environment.

Muonium has been searched for successfully in α -quartz, fused quartz, hexagonal and fused germanium dioxide, magnesium oxide, and diamond; and unsuccessfully in tetragonal germanium dioxide, rutile, strontium titanate, zircon, and beryl. All the samples save the quartzes showed a large "missing fraction"; that is, not all the initial muon polarization could be accounted for. This indicates that muonium was formed but rapidly depolarized. The missing fractions were found to be very strongly temperature dependent in strontium titanate but only weakly in rutile. At room temperature, the observed muonium fractions were: α -quartz and fused quartz ($65 \pm 5\%$), hexagonal germanium dioxide $< 2\%$, fused germanium dioxide ($10 \pm 4\%$), magnesium oxide ($30 \pm 10\%$), and diamond ($33 \pm 4\%$). It is noteworthy that the fractions are very different in quartz and germanium dioxide, despite their structural analogy. The observation of muonium in diamond represents the first time that muonium has been seen in a room temperature semiconductor.

A spin-Hamiltonian new to μ SR was found in low-temperature α -quartz and hexagonal germanium dioxide, in which the hyperfine interaction is completely anisotropic. In low-temperature α -quartz in zero magnetic field this interaction gives rise to three signals whose frequencies are orientation independent, but whose amplitudes are strongly orientation dependent. By studying the orientation dependence it was determined that muonium occupies a site which is identical with that seen for hydrogen in EPR studies. This was the first time that muonium was

shown to behave just like an isotope of hydrogen in a solid. In hexagonal GeO_2 , eight frequencies were observed at 6K, in marked contrast to the observation of only three frequencies in structurally analogous α -quartz. The interpretation of this is that there are three or four different sites, the exact nature of which has not been determined.

Table of Contents

A.	Chapter I: Introduction	1
1.	The Muon and its Polarization	1
2.	The Muonium Atom	5
3.	Muon and Muonium Fractions	8
4.	MSR In Solids	9
B.	Chapter II: Experimental Apparatus	15
1.	Cyclotron, Beamlines and D.C. Separator	15
2.	Surface Muon Beams and Conventional Beams	17
3.	Data – Collection and Analysis	18
4.	Eagle: a Standard Surface Muon Apparatus	26
5.	Some Considerations in Apparatus Design	28
C.	Chapter III: Muonium Hyperfine Interactions	38
1.	Spin–Hamiltonian I: Isotropic Hyperfine Interaction	38
2.	Spin–Hamiltonian II: Axially Symmetric Hyperfine Interaction	41
3.	Spin–Hamiltonian III: Completely Anisotropic Hyperfine Interaction	43
4.	Superhyperfine Spin–Hamiltonian	46
D.	Chapter IV: A Brief Survey of Muonium Formation and Relaxation	48
1.	Gases	49
2.	Liquids	50
3.	Solids	51
E.	Chapter V: Results and Discussion	56
1.	Quartz	56
2.	Germanium Dioxide	85
3.	Magnesium Oxide	92
4.	Strontium Titanate	96
5.	Rutile	103

6.	Beryl and Zircon	106
7.	Diamond	106
F.	Chapter VI: Summary and Conclusions	112
G.	Appendix 1: A Muon Magic Beamline for TRIUMF	116
1.	Introduction	116
2.	State of the Art	116
3.	Alternatives	116
4.	Justification	118
5.	Design Considerations	119
6.	Conclusions	122
H.	Appendix 2: Solving the Anisotropic Hyperfine Hamiltonian	123
1.	Solve H_A , the Hyperfine Part	124
2.	Solve the Zeeman Part H_B	126
3.	Solve the Total H_T	127
I.	Appendix 3: The Superhyperfine Interaction Hamiltonian	146
	BIBLIOGRAPHY	147

List of Figures

1. A typical μ SR time histogram	3
2. A typical μ SR asymmetry plot	4
3. Muonium in fused quartz at 10 G	7
4. The muon signal in fused quartz at 85 G	10
5. M20 beam line	19
6. A typical μ SR apparatus	20
7. Comparison of WSFT and FFT	25
8. Interior of Eagle	27
9. Sketch of the variable collimator	29
10. Dependence of number and asymmetry of positron decays on energy	33
11. A^2N as a function of cutoff energy	34
12. Breit-Rabi diagram for the isotropic case	39
13. Breit-Rabi diagram for the cylindrically symmetric case	42
14. Breit-Rabi diagram for the completely anisotropic case	45
15. Low-field beating of muonium in α -quartz	62
16. Anisotropy of splitting in quartz	63
17. Muonium oscillation at zero applied magnetic field in α -quartz	64
18. Fourier transforms of low temperature α -quartz data	66
19. Diagram of the hydrogen site in α -quartz	70
20. High statistics muonium signal	72
21. Fourier transforms of quartz data, unapodized and weakly apodized	74
22. Fourier transforms of quartz data, medium and strong apodizations	75
23. WSFT of high statistics quartz data	76
24. Relaxation rate versus temperature for α -quartz	79
25. Relaxation rate of the muonium signal in fused silica versus temperature	82
26. Muonium signal in the perpendicular telescope in zero applied magnetic field	84

27. Relaxation rate of the muonium signal in fused germania versus temperature	87
28. FFT of fused germanium dioxide in a 60 Gauss magnetic field	88
29. FFT and WSFT of hexagonal GeO ₂	89
30. Muonium signal in room temperature MgO	93
31. Relaxation rate of the muonium signal in MgO versus temperature	94
32. Amplitude of the muon signal in SrTiO ₃ versus temperature	97
33. Muon relaxation rate in SrTiO ₃ versus temperature	99
34. Asymmetry plot of early time data in SrTiO ₃ at zero and seven Gauss	101
35. Plot of early time data in SrTiO ₃ at 25 Gauss and in the perpendicular direction	102
36. Temperature dependence of the muon signal in TiO ₂	104
37. Plot of the observed signal in TiO ₂ at 20 K and 295 K	105
38. Asymmetry in diamond at room temperature and 6 K	108
39. Relaxation rate of muonium in diamond versus temperature	109

List of Tables

i. Some properties of the positive muon and of muonium	6
ii. Summary of results obtained	57
iii. Purities of materials used	58
iv. Comparison of muonium and hydrogen results in quartz	67
v. Frequencies observed in GeO_2	90

Acknowledgements

I wish to thank my supervisors, Don Fleming and Jess Brewer for their efforts, both mental and physical, over the years it has taken me to complete first my research, and then my thesis, and I hope that they feel it was all as worthwhile as I do. I must also single out John Coope for his assistance in showing me how to do the calculations of Appendix 2, naturally any errors or omissions are my own. Peter van den Bosch and Jon Nightingale were generous with their time and patience in making the document itself look as attractive as I believe it to be.

There are far more people I feel I should acknowledge than I could ever give individual attention to, so... I wish to thank Jim McIlroy and his "Beamline Boys" for their eternal cheerfulness and willingness to jump to my aid at moments of crisis; Don Arseneau, Masa Senba, Dave Garner, Dale Harshman, Carl Clawson, Eric Turner, Paul Percival, Tomo Uemura, Rob Kiefl, Rolf Keitel, Glenn McRae, Randy Mikula, Bob Butters, T.J. Ahrens, Joe Nagel, J. Weil, Y. Koga, and N. Drikitis.

I will single out my parents, for whose assistance I can never possibly be grateful enough and my parents-in-law, who have been of great help in seeing me through this. Most of all, to my wife Sylvia, who has put up with so much over the years, who has helped me in so many ways, and to whom I dedicate this, my thesis.

A. CHAPTER I: INTRODUCTION

1. THE MUON AND ITS POLARIZATION

The muon is a sub-atomic particle with about 200 times the rest mass of the electron, or about 1/9th the rest mass of the proton. It has a charge of either +1 or -1, decaying into a positron and two neutrinos, or an electron and two neutrinos respectively. This work will be concerned exclusively with positive muons.



The muon has a mean life of about 2.2 microseconds. This may seem short, but its parent, the pion, has a mean life of only 26 nanoseconds:



The muon lifetime is long enough though so that detecting it and measuring the elapsed time until the observation of its decay positron is relatively easy. Moreover, many interesting subjects can be studied in the microsecond range available.

The muon can be used in studying a wide variety of subjects, including charge exchange in gases [Fleming 84]¹, relaxation dynamics in both gases [Senba 84] and liquids [Stadlbauer 84], magnetic fields and relaxation phenomena in solids [Heffner 84], diffusion on surfaces [Harshman 84], the Lamb shift of the muonium atom in vacuum [Oram 84], and is used in particle physics experiments [Carr 84]. The acronym invented to describe the field is μ SR or MSR for Muon Spin Rotation (Resonance, Research...). The technique and its applications have been reviewed by Brewer et al. [75], Schenck [76, 81], and Heffner et al. [84] and has been the subject of three conferences, the proceedings of which have been published in *Hyperfine Interactions* [Gygax 79, Brewer 81b, Yamazaki 84].

¹The format which will be used for references is [first author's last name year of publication *modulo* 1900], unless the author's name has immediately preceded the reference in the text, in which case only the year *modulo* 1900 will appear.

What is it that makes the muon such a powerful tool? A very simple property – it is possible to determine the direction of the spin of a muon as a function of time. This is due to the non-conservation of parity in the weak interaction [Lee 56] which has two effects: the muon is produced 100% polarized in the direction of its momentum, and when it decays the positron produced tends to come off along the muon spin direction.

In practice, due to quantum mechanics for one thing, it is not the spin of an individual muon which is followed, but rather the spin of an ensemble of muons. Generally, however, this ensemble is generated by studying one muon at a time. That is, in a typical experiment, a muon stops in a target and begins precessing² in a magnetic field applied transverse to the spin direction. After some time it decays. The direction in which the decay positron is emitted and the elapsed time since decay are determined. Another muon stops in the target, and so on. After perhaps 100 million muons have been studied, the result is as shown in Figure 1, where the number of positrons detected in a particular direction is plotted against elapsed time until decay. The obvious exponential reflects the muon lifetime, while the oscillation is due to the precession of muons in the applied field³. The amplitude of this oscillation as a fraction of the number of counts is termed the asymmetry and is plotted in Figure 2⁴. In magnetic materials such as iron, the muon may also precess in a local magnetic field.

This phenomenon was first observed by R.L. Garwin et al. [57], in testing parity conservation, an experiment suggested by Lee and Yang⁵ [56]. Garwin et al. stopped muons in two different targets: graphite and nuclear emulsion. The amplitude of the oscillations observed in the nuclear emulsion was markedly less than that in graphite. Further experiments a year later by

²Strictly speaking, the modern interpretation of the meaning of quantum mechanics prohibits speaking of such things as the precession of a single spin. However, its usage here reflects convenience as well as continued use within the field.

³ Whenever the phrase "applied field" is used, it should be taken to mean "applied magnetic field".

⁴ This spectrum is a combination of spectra from two different directions, the left and the right, hence it is called a Left-Right spectrum. Backward-Forward and Up-Down spectra may also be formed. The directions used are usually from the muon's point of view.

⁵It was the second experiment to show parity violation, immediately following the classic ⁶⁰Co β decay experiment of Wu [57] et al.; indeed Garwin's paper immediately followed Wu's in Physical Review's Letters to the Editor.

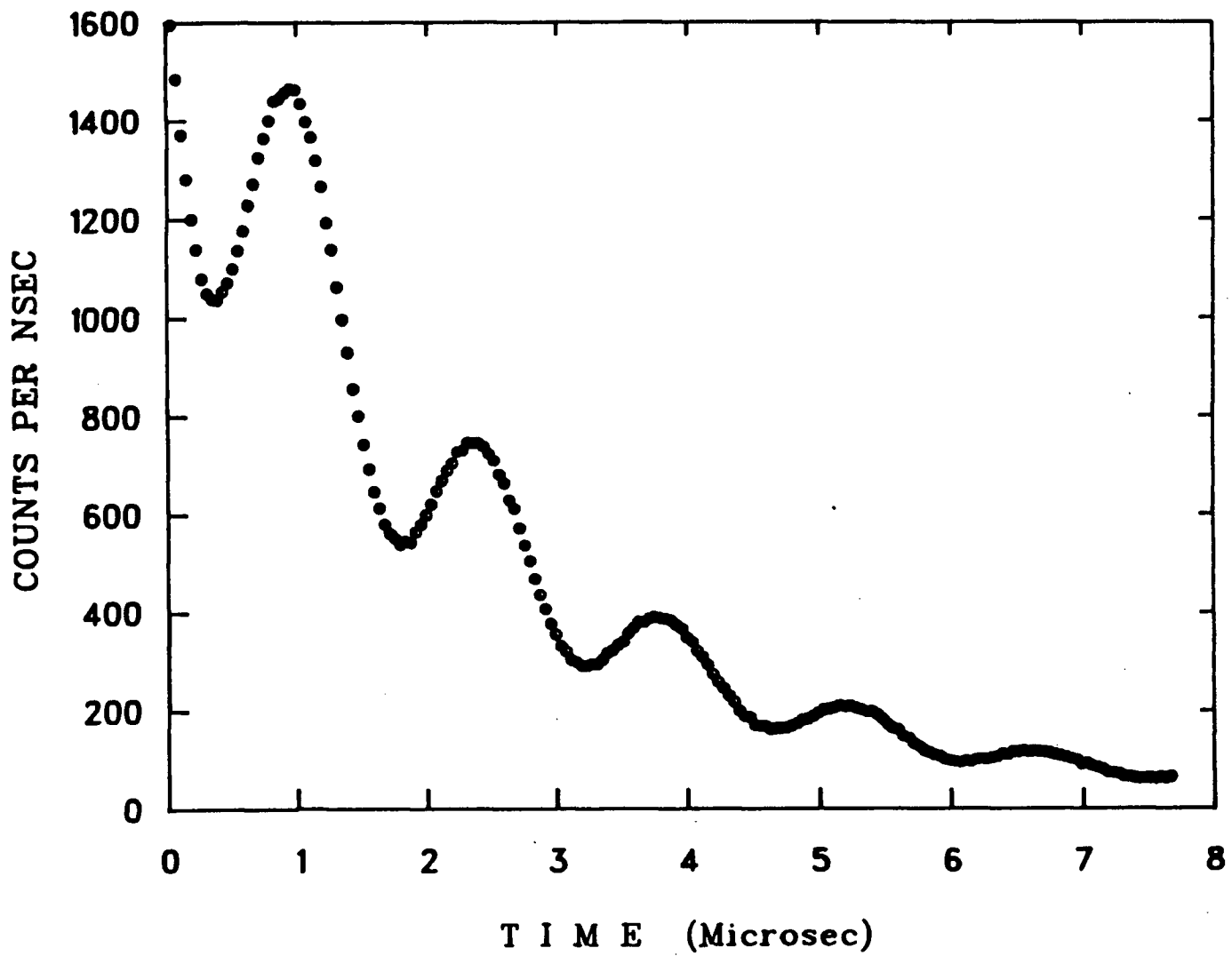


Figure 1
A typical μ SR time histogram. Aluminum at 60 Gauss.

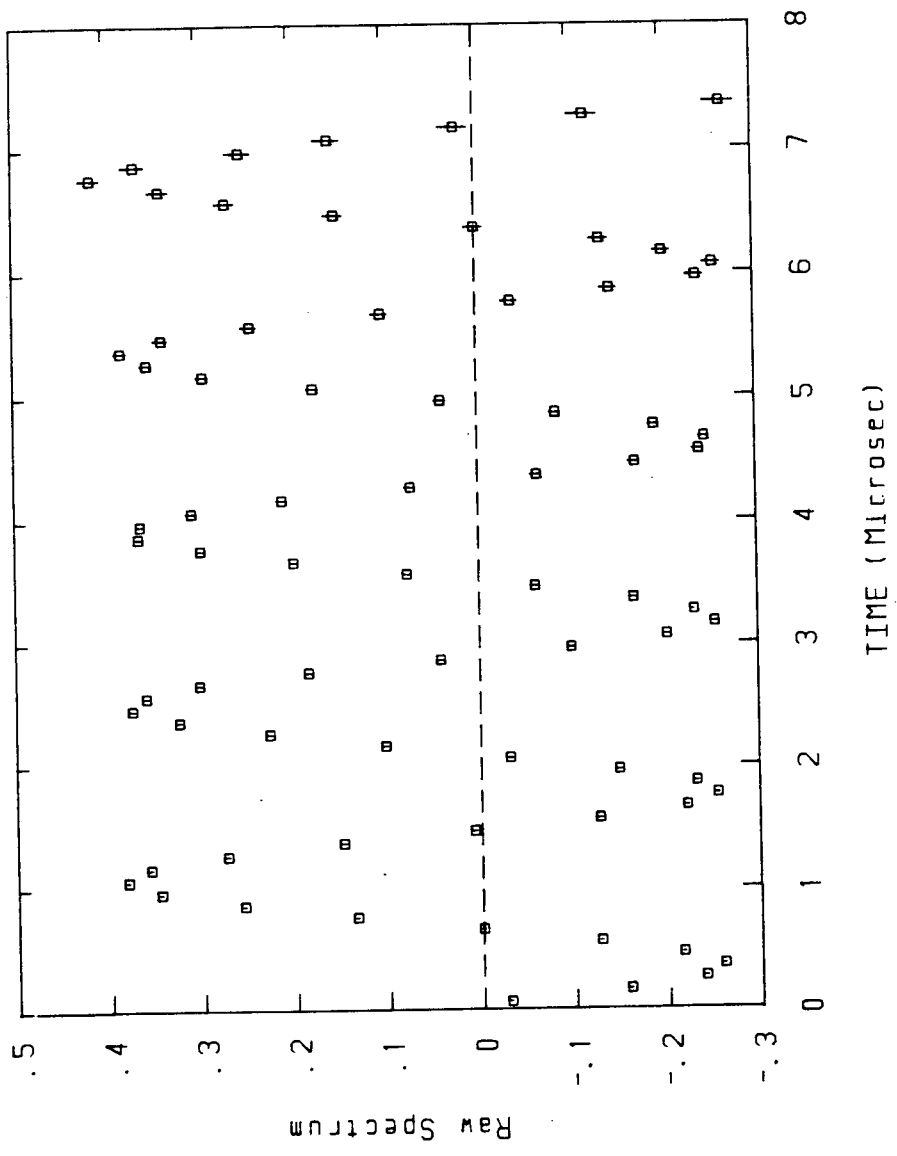


Figure 2
A typical μ SR asymmetry plot. Aluminum at 60 Gauss.

Swanson [58] in a variety of materials revealed the same wide variations in the "residual" muon polarization, from about 10% in benzene to 100% in typical metals. In non-magnetic materials, such differences are now known to be due to the thermalization process of the positive muon in matter.

2. THE MUONIUM ATOM

When a positive muon passes through, or stops in, matter, it may pick up an electron to form a $\mu^+ e^-$ bound state called muonium (Mu) ⁶ ⁷. Since the reduced masses of muonium and hydrogen are only very slightly different, properties such as ionization potential and radius are virtually identical, as shown in Table I. Consequently it behaves chemically like an isotope of hydrogen but one with a far greater mass difference than is available from deuterium or tritium. When the muon captures an electron, their spins may be either parallel or anti-parallel. If they are anti-parallel, the muon's spin will oscillate at the hyperfine frequency of 4463 MHz (for muonium in a vacuum) and be unobservable by conventional μ SR techniques. This results in only one-half the muonium ensemble being directly observable.

Any muonium formed may be readily distinguished from unreacted muons and/or muons in diamagnetic environments, as the characteristic Larmor precession frequency of muonium in a weak transverse field is about 103 times larger than that of the muon. This can be seen by comparing Figure 2, a plot of the muon asymmetry in aluminum at 60 Gauss, to Figure 3, a plot of muonium asymmetry in fused quartz in 10 G. Several phenomena can be observed:

1. the probability of muonium formation;
2. the rate at which the muonium signal vanishes;
3. the mechanism for its disappearance; and
4. the strength and directionality, if any, of the hyperfine coupling between the muon and its

⁶The spin of the electron may be either parallel to the muon spin, thus forming "triplet" muonium, or it may be anti-parallel, forming the so-called mixed muonium.
⁷The first written reference to this is in a paper by Friedman and Telegdi [57], which was published in the same volume of the same journal as Wu's and Garwin's papers. The dates indicate that the three papers were received at virtually the same time.

Table I Some properties of the positive muon and of muonium

Muon	Charge	= +1	
	Spin	= 1/2	
	Rest Mass	= 105.6596 MeV = 206.7685 m_e = 0.1126 m_p	
	Magnetic Moment	= 4.4905x10 ⁻²³ erg G ⁻¹ = 3.1833 μ_p = 0.004836 μ_e	
	g-Factor	= 2.0023318 = 1.000006 g_e	
	Mean Lifetime	= 2.197037 μ s	
	Gyromagnetic Ratio	= 13.5544 kHz G ⁻¹ = 3.18334 γ_p	
	Muonium	Rest Mass	= 0.1131 m_H = 207.8 m_e
		Reduced Mass	= 0.9952 m_e = 0.9956 μ_H
		Bohr Radius	= 0.5315 Å = 1.0044 a_{0H}
Ionization Energy		= 13.54 eV = 0.9956 I.E. _H	
Hyperfine Frequency		= 2.8044 x 10 ¹⁰ rad s ⁻¹ = 3.1423 ω_{0H} = 4463 MHz	

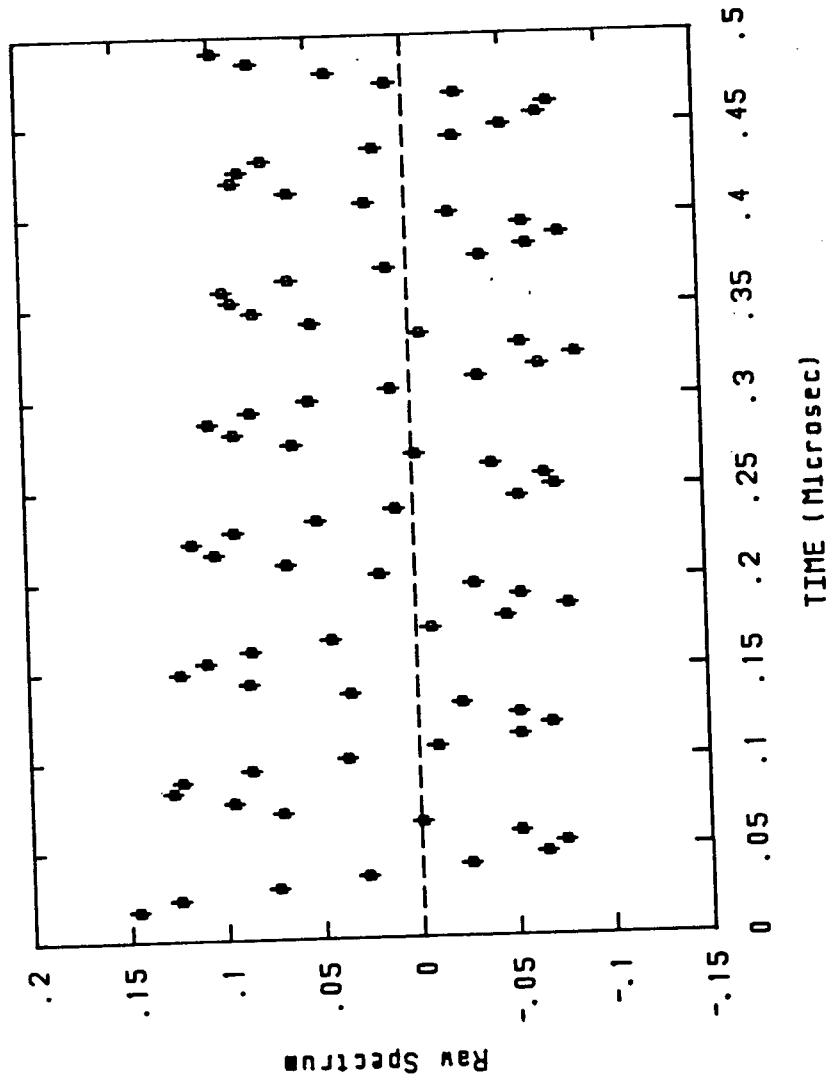


Figure 3
Muonium in fused quartz at room temperature in a field of 10 G.

electron.

These subjects, in solids, form the basis of this thesis and will be dealt with in more depth later.

Even in the first μ SR experiments, Garwin et al. [57], Friedmann and Telegdi [57], and Swanson [58] observed a decrease in the initial amplitude of the muon signal which was attributable to the formation of muonium. However, muonium was not observed directly until Hughes et al. [60] observed it in gaseous argon. The first observation of muonium in a solid was reported by Myasishcheva [68] in crystalline and fused quartz, in solid carbon dioxide and in ice. Muonium was not observed in a liquid until Percival et al. [76] observed it in water; the surprisingly late date was due to earlier workers having failed to remove all the dissolved oxygen.

3. MUON AND MUONIUM FRACTIONS

After stopping in a given medium, the muons can be found in either a diamagnetic environment or a paramagnetic environment. For present purposes, all the muons in diamagnetic environments, such as bare μ^+ or MuOH , will be treated as precessing at the same frequency, and the corresponding fraction of the stopped muons denoted as P_D . Those muons in paramagnetic environments will be separated into two groups: muonium atoms in which the hyperfine interaction is comparable to that in vacuum, and is nearly isotropic; and muonium-like species, such as muonic radicals⁸ [Roduner 84] and anomalous muonium [Brewer 73, Patterson 84] in which the hyperfine interaction is far reduced from that in vacuum and possibly highly anisotropic. The corresponding fractions are denoted P_{Mu} and P_{Mu^*} . These three fractions are calculated from the measured initial asymmetries relative to a standard sample, typically aluminum, as in Figure 2, in which 100% of the muons are in a diamagnetic environment. Since none of the work of this thesis observed any Mu^* states, it will now be dropped from this discussion. From inspection, the asymmetry in Figure 2 is about 0.30, the actual value coming from a fitting procedure which will be described later. The fractions P_D and P_{Mu} can be calculated from:

⁸Muonium itself is, of course, a radical.

$$P_D = \frac{A_D}{A_{\max}}, \quad P_{\text{Mu}} = \frac{2A_{\text{Mu}}}{A_{\max}} \quad (1.3)$$

where A_D , for example Figure 4, and A_{Mu} , for example Figure 3, are the measured initial amplitudes of the corresponding μSR signals and A_{\max} , for example Figure 2, is the measured initial amplitude in the standard sample. The factor of two present in the definition of P_{Mu} takes into account the loss of one-half the signal due to the formation of anti-parallel muonium.

The phrase "missing fraction" will occur repeatedly in this thesis, as it does in μSR literature. The missing fraction P_L , L for "lost", is that part of the initial asymmetry unaccounted for in the muon and muonium signals observed in a particular sample,

$$P_L = 1 - P_D - P_{\text{Mu}} \quad (1.4)$$

4. MSR IN SOLIDS

The hydrogen atom, and therefore the muonium atom, represents the simplest atomic defect in a solid, as it has no electronic core. This means that theoretical calculations of its behaviour may be done more rigorously, possibly leading to the interpretation of more complicated defects. Hydrogen is also a very common, and commercially important impurity in solids. The study of the muon can lead to a better understanding of the role of hydrogen as it can provide information otherwise unobtainable.

Of particular importance is the role of hydrogen in the semiconductors silicon and germanium, where it is not known what effects, if any, the large amounts of hydrogen present has on the properties of these two materials. While no hydrogen EPR signal has ever been substantiated in them, muonium and muonium-like states are observed and have been studied extensively, as shown by many of the papers in the Proceedings of the Yamada Conference VII, also known as $\mu\text{SR}83$ [Yamazaki 84].

The study of muons in solids is pursued for two reasons: what they can reveal about the materials themselves, and what they can reveal about the role of hydrogen in these materials. One example of the former is the measurement of Knight shifts [Schenck 81], and of the latter, muonium in silicon [Patterson 84]. The measurement of the frequency and relaxation can be used

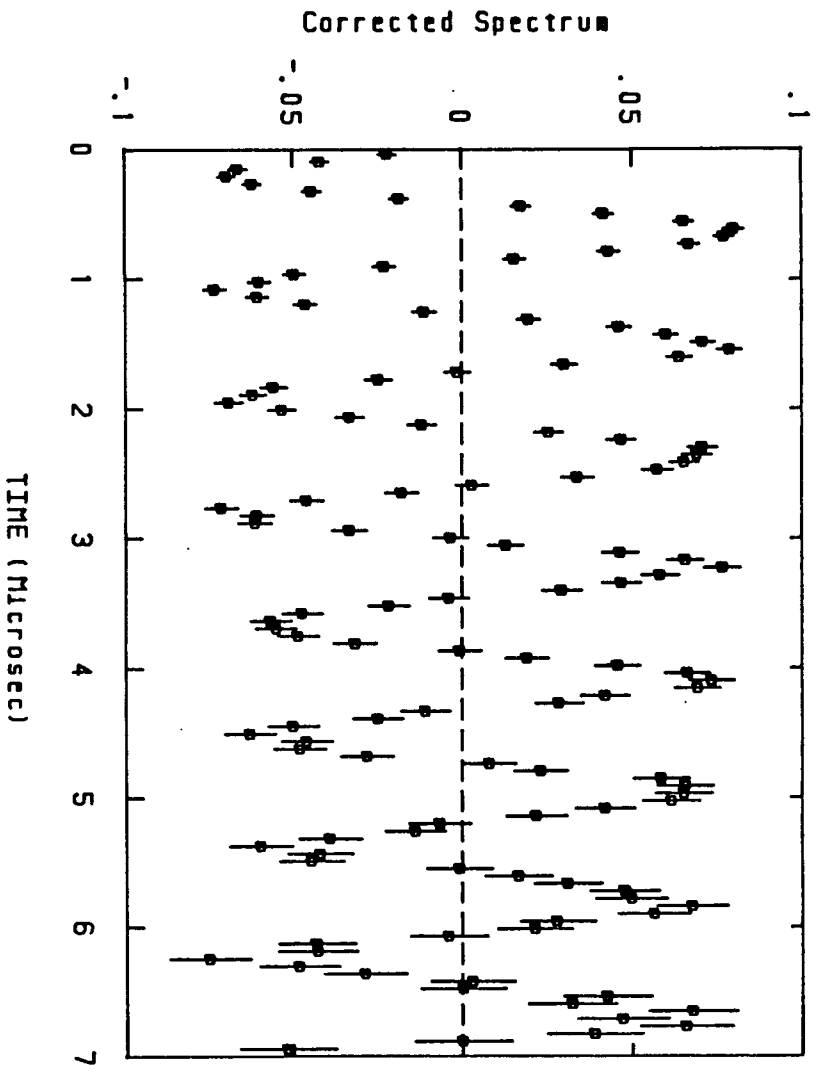


Figure 4
Muon signal in fused quartz at 85 G.

to identify the static and dynamic environments of the muon in the lattice. In the study of diffusion, the muon is important as it has a mass between the ultimate light interstitial, the positron, and the proton. For example, there is now evidence that quantum diffusion of the muon takes place in low-temperature copper [Kadano 84]. Muonium can be considered in much the same light as the muon, where the frequencies and relaxation rate provide information about the static and dynamic interaction of muonium with the lattice.

Using μ SR to study solids instead of the more conventional techniques of EPR and NMR has both advantages and disadvantages. Some of the advantages are:

1. Short lived species, with lifetimes down to 10 ns, can be observed;
2. In principle, the fate of all muons can be determined;
3. The large mass ratio between the proton and the muon allows isotopic effects to be measured more sensitively than with any other probe;
4. The muon diffuses much more readily than the proton;
5. Species are observed in μ SR which are unseen by standard EPR;
6. Relaxation can be observed in the absence of applied magnetic fields;
7. Muons can be injected into and studied in any material, with no concerns about solubility;
8. The muon is an infinitely dilute probe, as there is only one muon at a time, hence there are no probe-probe interactions.

Some of the disadvantages are:

1. The short lifetime leads to lower resolution;
2. The muon may not have reached its equilibrium state in the time available before decay;
3. For chemical reactions, there is no opportunity to study the reaction products with techniques such as infrared spectroscopy or via classical chemistry;
4. It requires a source of muons.

This last disadvantage is becoming less of a barrier with time as the field of μ SR has grown much more quickly in the 1970's since the introduction of machines such as those at the "meson

factories" at TRIUMF⁹, SIN¹⁰, and LAMPF¹¹ each of which increased the number of muons available by a factor of about 100 over that obtainable from the earlier machines. There are also other machines and more are becoming available all the time, some with even higher intensities. The technology of producing and transporting muons has also been improving, resulting in still further increases in availability.

When this present work was begun in 1978, muons had been studied in a variety of solid targets, but most of the results were for muons in diamagnetic environments; there were still relatively few solid systems in which muonium had been directly observed and could be studied, consisting of fused and crystalline quartz, solid CO₂, ice, silicon and germanium [Brewer 75]. It was not clear why muonium formed in some targets but not in others, and many of the results were in samples of unknown purity. There was a clear need for more systems in which to study the behaviour of muonium, more understanding of why muonium forms, and more detailed studies of muonium in some selected systems. Hence part of the motivation of the work of this thesis was to do a survey of what were felt to be likely candidates for muonium formation. Zero or low transverse fields were used as the spectra are much simpler to interpret than those from the longitudinal fields used by Ivanter et al. [72], for example. Higher transverse fields resulted in the signals being lost due to the time resolution of the available apparatus. As μ SR generally uses much lower applied fields than EPR and NMR, the Hamiltonians describing these properties had to be solved for their low field limits rather than their high field limits.

The materials used in this present work were chosen largely because:

1. they were not ferromagnetic nor were they expected to have significant paramagnetism;
2. hydrogen atoms had been observed in similar materials [Pake 73];
3. they were largely free of nuclear moments;
4. they were available in reasonable purity;
5. they were available as single crystals;

⁹*Tri-University Meson Facility* originally, although by the time it was actually built there were four universities involved.

¹⁰*Schweizerisches Institut für Nuklearforschung*

¹¹*Los Alamos Meson Physics Facility*

6. the samples had to be large enough in area and volume to stop a significant number of muons and
7. the materials were non-metals.

The absence of magnetism and nuclear moments was necessary as it was known from previous work [Brewer 75] that muonium would be unobservable in zero or low transverse fields in such systems. That is not to say that muonium might not be present, but it would be depolarized and hence unobservable, resulting in a missing fraction. Impurities may trap and depolarize muonium, possibly too quickly for the muonium signal to be observed. It was expected that muonium might be trapped at crystal boundaries and depolarized, and if anisotropies were present as first observed by Brewer et al. [73] in silicon, a polycrystalline material would broaden the signal considerably. The area and volume requirements have declined significantly over the time this work was in progress; the earliest experiments used a cube about four cm on a side, whereas later a 0.5 mm slice, 7 mm by 7 mm, was sufficient. Metals are not suitable as muonium cannot form due to the "sea" of conduction electrons present screening the muon.

One system, quartz, was studied in some detail, as it proved to exhibit properties previously unseen in μ SR. Another major motivation for the study of quartz was that it was well characterized by the EPR of hydrogen in quartz [Isoya 83, Perlson 74]. This allowed a comparison of the behaviour of muonium and hydrogen atoms, which had not previously been possible in any solid system. Although muonium is clearly just like a very light isotope of hydrogen (Table I), and is known to behave this way in gases [Garner 78] and liquids [Stadlbauer 84], at the time this thesis was begun, there was *no* direct evidence for this in solids. Since hexagonal germanium dioxide is structurally analogous to α -quartz, it was studied as well, in the expectation that a site for muonium could also be established, thus predicting the site for the hydrogen atom. As there is little hydrogen in hexagonal germanium dioxide [Goodrum 72], the hydrogen EPR experiment might be too difficult, so μ SR could contribute data otherwise unobtainable.

In addition to the insulators, muonium was also studied in diamond, a semiconductor. μ SR studies had been carried out in its structural analogues silicon and germanium, but only one

experiment [Swanson 58] had been carried out in diamond.

Since the start of this present work, the situation with respect to the state of knowledge of muonium in solids has changed dramatically due to a recent clever technical innovation at SIN [Kiefl 84]. By applying transverse fields as high as 12 kilogauss in an apparatus with high time resolution, it is now possible to observe muonium in materials with appreciable nuclear magnetic moments, such as potassium chloride. Some of their results will be discussed in Chapter V. It should be noted, however, that this new technique is not a substitute for, but rather it is complementary to, the zero and low transverse field work of this thesis.

B. CHAPTER II: EXPERIMENTAL APPARATUS

1. CYCLOTRON, BEAMLINES AND D.C. SEPARATOR

The experiments described in this thesis were carried out at TRIUMF, a cyclotron on the UBC campus. TRIUMF is a sector focussed machine, accelerating negative hydrogen ions to an energy of 500 MeV. Two electrons are then stripped off, leaving a positive hydrogen ion, or proton, which travels down a (primary) beam line at about 75% of the speed of light. These protons strike a "production target" of some material, generally beryllium or graphite, and undergo a variety of interactions, some of which produce positive pions. Several nuclear reactions are possible, for example:



These pions then decay to muons. The muons are transported down a (secondary) beam line to an "experimental" target where they are stopped.

For present intents and purposes a beam line is made of magnetic elements, dipole and quadrupole magnets, with the analogous optical elements being prisms and focussing lenses, respectively. As a prism changes the direction of impinging light, depending on wavelength, so does a dipole change the direction of a charged particle beam, depending on the ratio of momentum to charge. A quadrupole magnet behaves like a focussing lens except that a single quadrupole only focusses in one direction, e.g. vertical, while it defocusses in the other, e.g. horizontal. Hence quadrupole doublets or triplets are used, one focussing in each direction, resulting in a net focussing effect. Momentum and charge selection is performed by choosing only those particles which come through a dipole in a particular direction.

One of the difficulties with charged particles is that only the *ratio* of momentum to charge is selected. This means that a particle with a charge of +2 and a momentum of 2p will be bent in the same direction as a particle with a charge of +1 and a momentum of p. A much more serious problem is that particles of different masses can have the same momentum/charge ratio. Since

some of the other interactions which the proton may undergo in the production target generate copious quantities of positrons over a wide range of energies, this leads to the positive muon beam being contaminated with positrons. In fact, a ratio of positrons to muons of 40:1 has been observed — rather more like a positron beam contaminated with muons. Since the experimenter is generally interested in detecting positrons from muons decaying at rest this contamination can be quite a problem.

One way of solving this problem is to use a Wien filter [Jackson 62], a device which uses crossed electric and magnetic fields. The forces on a given particle are $q\mathbf{v} \times \mathbf{B}$ for the magnetic field, and $q\mathbf{E}$ for the electric field, where:

q is the charge on the particle;

\mathbf{v} is the velocity of the particle;

\mathbf{B} is the magnetic field; and

\mathbf{E} is the electric field.

The fields are perpendicular, and the values of the fields are chosen such that only a particle of a particular velocity is transmitted. Since momentum has already been selected, only a particular type of particle will be transmitted through this system. This device is frequently referred to as a "D.C. Separator" ¹² and in principle is capable of providing a muon beam 100% free of contamination. When operated at a sufficiently high voltage and magnetic field it will also rotate the spin of the muon relative to its momentum.

¹² This separation can be done using crossed, static fields in a D.C. Separator, or with just a single oscillating field in an "R.F. Separator". This latter device relies on the fact that the cyclotron output has a time structure, putting out protons in a burst every 44 nanoseconds. As a result, the pions, muons and positrons also have this feature. Since, for a given momentum, these three have different velocities, their time of flight to a particular point will be different. If the R.F. Separator oscillates at the same frequency as the cyclotron and a suitable phase is chosen, the unwanted particles can be steered away. Since its location is fixed, it usually works for only a particular momentum or perhaps several particular momenta, whereas the D.C. Separator has a continuous range.

2. SURFACE MUON BEAMS AND CONVENTIONAL BEAMS

There are two different types of muon beams used in μ SR, "conventional" and "surface". Conventional muons have historical precedence¹³, but surface muons are somewhat easier to describe, and were used for the bulk of the work described in this thesis.

In the center-of-mass frame the pion decays to produce a 4.1 MeV muon and a muon neutrino as in eq. I.2. Since the neutrino always has its spin anti-parallel to its momentum direction and since the spin of the pion is zero, the muon spin is also anti-parallel to its momentum direction, yielding 100% longitudinally polarized muons¹⁴. If this pion is at rest in the lab frame, the result is a 4.1 MeV muon in the lab frame as well – a rather simple case of relativistic kinematics. In the center-of-mass frame, this decay is isotropic. Surface muons arise when a low energy pion produced from proton bombardment in a reaction like (eq. II.1) stops at or near the surface of the production target. These muons come off with an energy of 4.1 MeV, yielding a momentum of 29.8 MeV/c¹⁵. Some then travel down a beamline through the various magnetic and electric fields present, and through a thin window to stop in the experimental target. Due to their low energy, they stop very easily, their total range being of the order of 140 mg/cm²¹⁶. This corresponds to roughly one metre of air at a pressure of one atmosphere or to 0.5 mm of quartz. The spin of these muons is pointing anti-parallel to their momentum direction in the center-of-mass pion frame, which here corresponds to the lab frame.

Conventional muons arise from pions which were of higher energy and escaped the production target completely to travel down a beamline where, due to their short lifetime, many of

¹³In fact, as an historical footnote, it could be said that Friedman and Telegdi's experiment in 1956 [57] used surface muons, and since Garwin used cloud muons, a case could be made for surface muons having historical precedence.

¹⁴The neutrino is said to have negative helicity, where helicity is defined as:

$$h = \frac{2\vec{p} \cdot \vec{\sigma}}{|\vec{p}|}$$

where $\vec{\sigma}$ is the spin and \vec{p} is the momentum direction, and is a good quantum number for neutrinos. Frequently other longitudinally polarized particles, such as muons, are spoken of as having helicity, but this is not strictly true.

¹⁵ A typical nuclear science unit: 1 MeV/c = 5.3x10⁻²² kg-m/sec.

¹⁶ Another typical nuclear science unit: the range in centimetres of a particle is naturally dependent on the density of the material, and in fact, the range in different materials scales fairly well with just the density, so that R(nuclear science) = R(length units)/ ρ (density) is quite useful.

them decay in flight. In the lab frame, due to relativistic kinematics, those pions which decay "forward" (in the centre-of-mass frame), that is, down the beamline, produce muons with very different energies from those resulting from pions decaying "backward" (in the centre-of-mass frame), or up the beamline. However, if the initial pion momentum was high enough, those from forward decays and backward decays will travel down the beamline *in the lab frame*, but two different types of conventional muon result, forward and backward muons, with very different momenta.

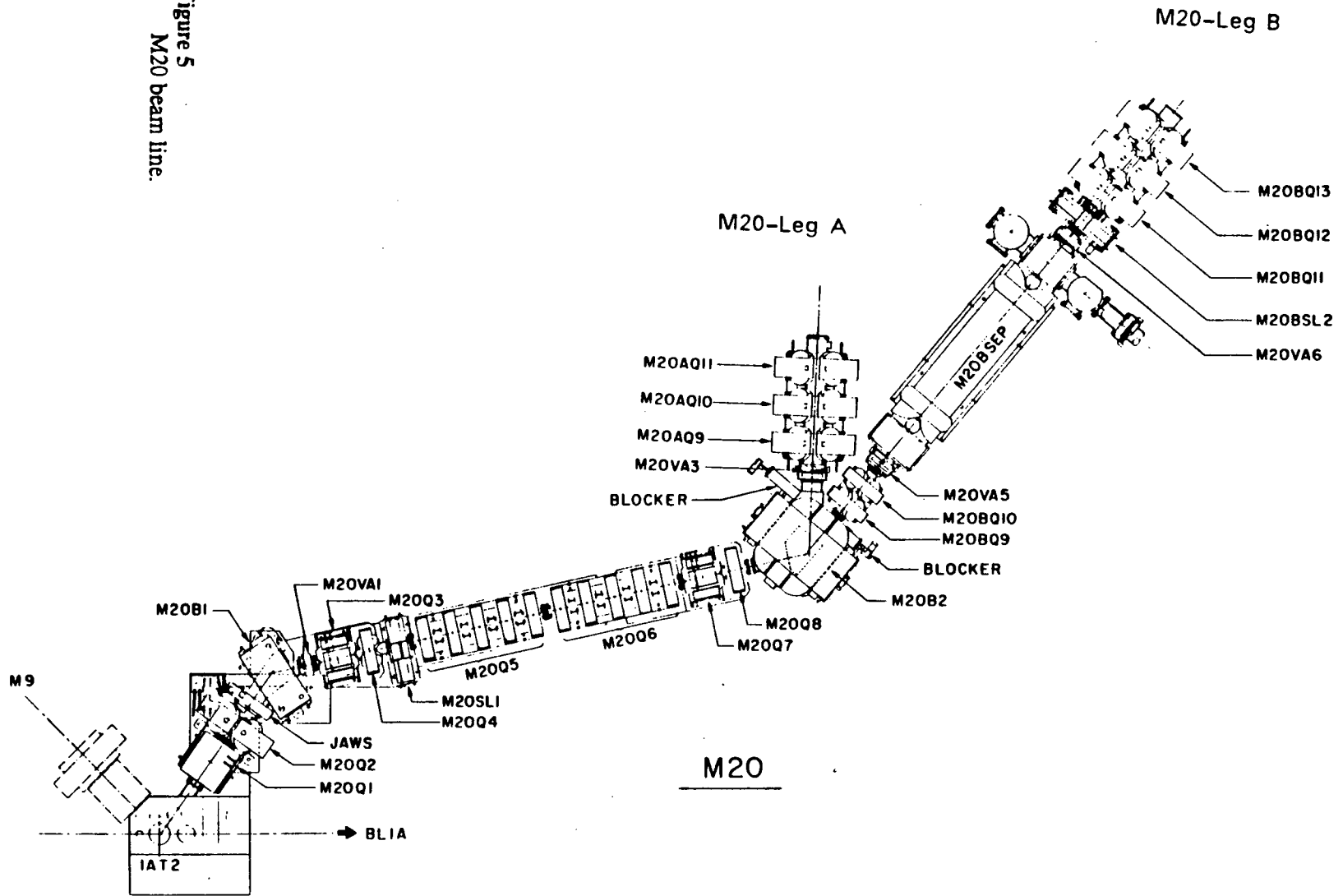
The spins of forward and backward muons point in opposite directions; the spin of a forward muon, like the surface muon, is anti-parallel to its momentum direction, and the spin of a backward muon is parallel to its momentum direction. There are, of course, muons with momenta between these extremes, but since their polarization is also intermediate, they are of lower utility. A typical momentum for a forward muon might be 170 MeV/c (kinetic energy = 94 MeV), for a backward muon 80 MeV/c (27 MeV). The corresponding ranges would be about 34 g/cm² and 5 g/cm². Clearly these ranges are far higher than those for surface muons, and so they are quite inappropriate for targets such as low pressure gases or thin solids.

In order to transmit surface muons, the beamline must have all its magnets set for the same momentum. Conventional muons, however, require that the momentum selected be different in different parts of the beamline in order to admit pions of one momentum and release muons of a different momentum. With reference to Figure 5, the muons from pions which decay in the center or decay section are "captured" by the quadrupoles and the second dipole, B2, is set so that the forward muons go down leg B while the backward muons go down leg A.

3. DATA - COLLECTION AND ANALYSIS

Figure 6 shows a schematic diagram of a typical μ SR apparatus. The collimator is typically about 2.5 cm thick lead or brass and is used to define the "spot size" of the beam. In practice most of the muons coming out of the beampipe stop in the collimator. The remaining muons pass through and "fire" the M₁ and M₂ counters, typically plastic scintillator, and most of

Figure 5
M20 beam line.



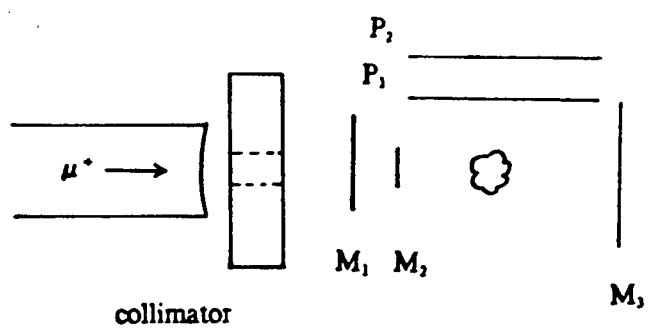


Figure 6
Schematic diagram of a typical μ SR apparatus.

these muons stop in the target. Some may miss the target or pass through it and strike the M_3 counter. A "good" muon is thus a signal from M_1 and M_2 and no signal from M_3 . It is then said that M_1 and M_2 are in coincidence and M_3 is in anti-coincidence, which may be written in Boolean notation $M_1 \cdot M_2 \cdot \bar{M}_3$. The muons which stop in the target precess in the magnetic field¹⁷ and eventually decay. Some of the resulting positrons pass through positron counters P_1 and P_2 . In the jargon of the trade, P_1 and P_2 form a positron telescope. A good event is thus $M_1 \cdot M_2 \cdot \bar{M}_3 \cdot P_1 \cdot P_2$, with a delay allowed between $M_1 \cdot M_2 \cdot \bar{M}_3$ and $P_1 \cdot P_2$, but not otherwise.

The measurement of this delay is the key to doing the experiment, and the observed delay is recorded for each event¹⁸. The maximum delay allowed is controlled by a "data gate" which opens when a muon is detected and closes at some pre-determined time later, typically eight microseconds or some 3.6 muon lifetimes. If a positron has not been detected by then, it is assumed it will never be detected. All of the work of this thesis used the time-differential μ SR technique [Brewer 75, Garner 79], which is the most commonly used, although time-integral techniques are extremely useful in some applications [Schenck 81, Heffner 84]. This discussion applies principally to the time-differential technique.

One of the things which may happen is that a second muon may enter during the time the data gate is open. This is known as "pile-up". If a positron is detected, it may not be possible to distinguish which muon it came from, so no events are accepted until the current data gate, which is re-started for every muon detected, has expired. Only after that will a new muon-positron pair be considered a good event. Consequently, if the incident muon rate is too high there will be no good events at all.

There is an optimum rate which is given by [Garner 79]:

$$N = \frac{1}{2T} \quad (\text{II.2})$$

¹⁷ As drawn, the magnetic field is perpendicular to the page, so the muons precess in the plane of the page.

¹⁸ Some time elapses between when the muon passes through the counter and when it stops in the target. This is not usually important in condensed matter as it is very nearly the same for each muon.

where N is the number of incident muons per second and T is the length of the data gate in seconds. A typical T is eight microseconds, which yields an optimum incident muon rate of 62,500 per second. Further discussion of this can be found in Appendix 1.

The data gate is selected according to the type of experiment being done. For example, if the signal is long-lived, a longer gate might be used. The incident muon rate can be adjusted by changing the size of the collimator (see Figure 6). The times of decay are recorded with a certain coarseness, known as time per bin, which is also varied according to the type of experiment being done. The data consists of a number of bins, perhaps 2000 per telescope, containing the number of events for each time interval. The data from each telescope then constitutes a time histogram such as in Figure 1.

After the data has been collected, it is fitted to an equation like:

$$N(t) = N_0 e^{-t/\tau} (1 + \sum_i [A_i e^{-\lambda_i t} \cos(\omega_i t + \phi_i)]) + B_g \quad (\text{II.3})$$

where $N(t)$ is the number of events recorded at time t from the muon stop, and the parameters are defined as:

N_0 is the normalization;

τ the muon lifetime;

A_i the initial amplitude of the i th signal;

λ_i the relaxation rate of the i th signal;

ω_i the frequency of the i th signal;

ϕ_i the phase of the i th signal; and

B_g the time-independent background.

In general, there may be more than one signal present. The fitting is via a chi-squared minimization, where:

$$\chi^2 = \sum_i \frac{(N_{io} - N_{ie})^2}{\sigma_i^2} \quad (\text{II.4})$$

where: χ^2 is the chi-squared;

N_{iO} is the Number of events observed in bin i ;

N_{ie} is the Number of events expected in bin i ;

σ_i is the uncertainty in the number of events in bin i .

Bin i corresponds to time $t = i \Delta t$, where Δt is the time per bin.

Since Poisson statistics are applicable, $\sigma_i = \sqrt{N_{iO}}$, so

$$\chi^2 = \sum_i \frac{(N_{iO} - N_{ie})^2}{N_{iO}} \quad (\text{II.5})$$

The ideal value for χ^2 when the equation describes the data perfectly and Poisson statistics apply, is

$$\chi_{\text{ideal}}^2 = n - f \quad (\text{II.6})$$

where n is the number of bins fit and f is the number of parameters used. There is, however, a distribution around this value due to statistical fluctuation. More importantly, if the model from which the fitting equation is derived does not describe the data correctly, the calculated minimum value of the χ^2 may be much higher than the ideal value. In this case, the calculated value will depend on the number of events collected, growing larger with higher statistics, while the ideal value does not change with the number of events collected.

The minimizations done in this work used the general non-linear least squares fit program MINUIT [James 71] running mainly on a VAX 11/780 located at TRIUMF. This program provides best-fit values for the parameters of interest and their associated errors. When fitting μ SR data, all the parameters are floating, but with limits. That is, they are allowed to vary freely and independently between some upper and lower bounds. It is also possible to "fix" one or more parameters, if their values are known *a priori*.

Some analysis was also done using Fast Fourier Transforms (FFT) [Brewer 82], which are particularly useful for data where several frequencies are expected. One of the problems with using an FFT is that in μ SR data, the errors in the data are larger for longer times. Thus, the

signal to noise ratio in the FFT deteriorates if longer times are transformed. If an apodization¹⁹ function is used which handles this correctly²⁰, the signal is unavoidably broadened. Another problem with an FFT is that of "ringing". Since only a finite length of time is being transformed, every signal will have a number of side-lobes [de Haseth 82]. This makes it difficult to find a small peak close to a large one. Apodization can also be used to suppress this ringing, and there are apodization functions which minimize the broadening for a given amount of suppression [Norton 76]. Unfortunately, none of these functions corresponds to the form given above for "correct" statistical weighting.

Since a search for weak or closely adjacent signals formed a large part of the work of this thesis, an attempt to circumvent some of these problems was made by developing another form of analysis, one which uses a chi-squared minimization, but finds the minimum as a function of frequency²¹. That is, holding the frequency fixed at some value, the minimum in the chi-squared with respect to the other parameters is found. By "stepping through" a range of frequencies, a table of these parameters and the chi-squared is generated as a function of frequency. This has some of the appearance of a Fourier transform, but strictly speaking it is not²². The correct statistical weighting procedure is followed, and there are also no side-lobes. Another advantage of WSFT is that if some parameters are known *a priori*, for example the phase, these can be fixed at the appropriate values, improving the signal-to-noise ratio. Samples of WSFT and FFT are shown in Figure 7, which is taken from the study of hexagonal GeO₂, which will be discussed below. The apparent signal-to-noise is obviously much higher for WSFT than FFT. There are eight clearly visible peaks in the WSFT spectrum, some of which are lost in the FFT. WSFT can, however, produce harmonics of the real frequencies, and its resolution tends to be poor. The

¹⁹ Apodization is simply the multiplication of the signal by a function which varies in time.

²⁰ The approximate function is $e^{-t/2\tau}$ [Brewer 82], which assumes that the background B is negligible, an assumption which is increasingly invalid at longer times.

²¹ An earlier form of this technique was developed independently by Nagamiya et al. [75] to look for weak μ SR signals from negative muons.

²² For a range from, say, zero to fifty megahertz in steps of 0.05 megahertz, some one thousand chi-squared minimizations must be done. This takes rather a long time, perhaps six hours of CPU time on a VAX 11/780, hence it has been dubbed World's Slowest Fourier Transform or WSFT.

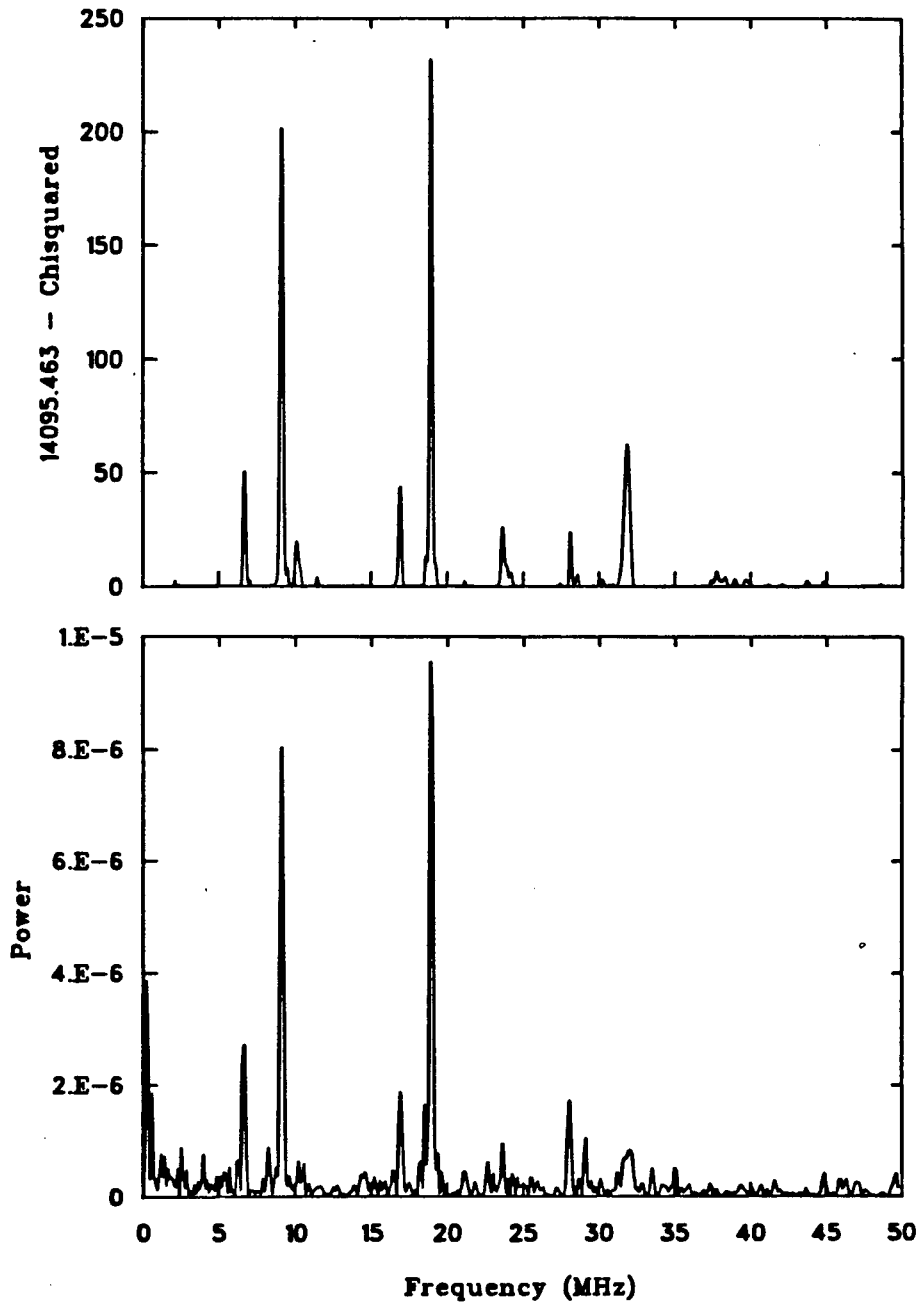


Figure 7

Comparison of WSFT (top) and FFT. Note the enhancement of the signal-to-noise ratio of the WSFT spectrum over the FFT spectrum. For convenience, the chisquared was subtracted from the maximum observed value.

harmonics may be intrinsic to the method, while it may be possible to improve the resolution.

4. EAGLE: A STANDARD SURFACE MUON APPARATUS

Most of the experimental work in this thesis was carried out in an apparatus known as "Eagle", the name being an allusion to both a fancied resemblance to the first lunar lander, and to its American origin at the University of California at Berkeley. It is discussed in [Clawson 82]. Figure 8 shows the interior arrangement of this apparatus.

The vacuum chamber is mounted between a pair of large coils in a modified Helmholtz configuration. A cryostat capable of providing temperatures from 3 to 300K can be placed in the center of this apparatus. At present the apparatus is suitable only for surface muons as there is a single thin muon counter²³. The eight positron counters are used to define four telescopes, which correspond to four histograms for the data. The collimator and muon counter are between the two counters of the Backward telescope so that a positron emitted by a muon stopping in the collimator or muon counter cannot trigger an event in that telescope — it is very unlikely that a positron could go through one counter and scatter backwards to go through the other. Further, any positron from the collimator or muon counter would have to pass through and fire counter B 1 in order to trigger any of the other telescopes. Hence, if the counter B 1 is put in anti-coincidence with the other telescopes, no events of this sort should be observed.

One problem with the apparatus is that the vacuum chamber has nine holes for the light pipes to the counters, two holes for the muon degrader support²⁴, one hole for the collimator, one hole for a removable sample support rod, four large ports, and approximately eight kilograms of graphite, all of which lead to considerable vacuum problems.

Originally the collimator was fixed in place and the entire vacuum chamber — including that of the cryostat — had to be vented in order to change it. This operation could take as long as

²³The very different ranges and energy deposition rates for surface and conventional muons necessitate very different thicknesses of counters, so generally a counter suitable for one type is not at all suitable for the other. Surface muons require a thin counter and all the muons which hit the target stop, so a veto counter is not used.

²⁴ Even with surface muons, it is possible to have a target too thin to stop all the muons, so thin plastic film may be inserted in front of the target.

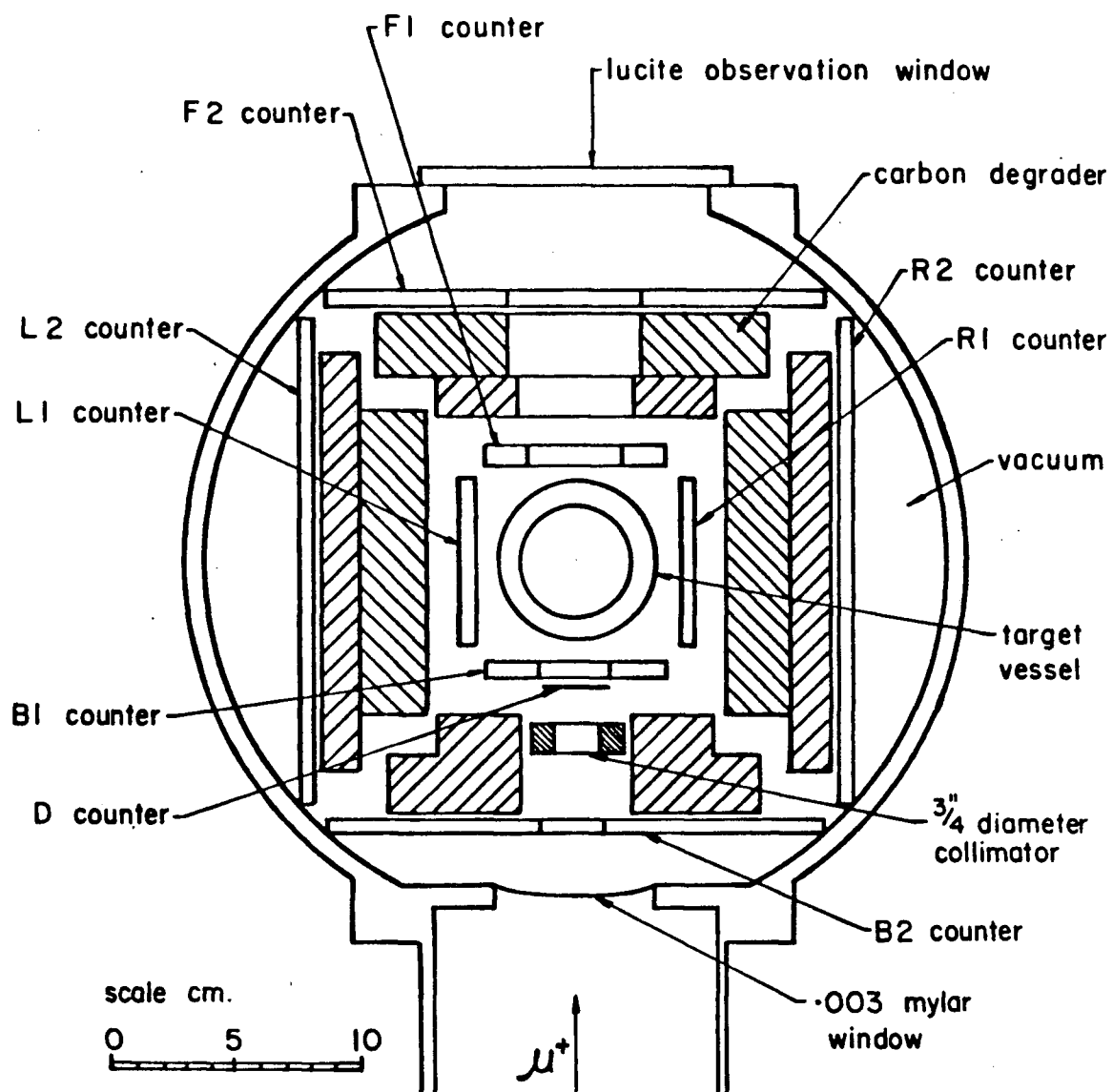


Figure 8

Interior of Eagle. The D (defining) counter is the muon counter and L, R, F, B (for Left, Right, Backward, Forward) are the positron telescopes.

12 hours until the cryostat was operational again, an unacceptable delay given the premium placed on beam time (there is fierce, although rarely bloody, conflict for the limited amount of time available). Needless to say, the collimator was not changed very often under these circumstances. In fact, once.

The variation in the area of samples studied in this present work, from 0.5 cm² to 5.0 cm², made a more easily variable collimator was clearly desirable. Accordingly, a brass bar with four circular threaded apertures was mounted on a rod which was put through a vacuum seal in the bottom plate (see Figure 9). The collimator to be used was chosen by simply varying the height of the pipe. The apertures are threaded for two reasons:

1. Smaller collimators could be installed ahead of time, perhaps even non-circular ones²⁵ ;
2. Threaded holes are believed to cause less scattering of the muons than unthreaded ones, or at least, those muons which would have been scattered are stopped in the threads instead.

5. SOME CONSIDERATIONS IN APPARATUS DESIGN

In designing and choosing apparatuses for this thesis study, there were several criteria that had to be considered. This discussion will be largely restricted to the use of surface muons. These criteria are:

1. the muon must be detected;
2. the muon must stop in the target; and
3. its decay positron must be detected.

1) The muon is detected by a counter, the active part of which is plastic scintillator, typically either 0.013 cm or 0.026 cm thick²⁶. The energy deposited must provide enough light to allow easy detection of the muon. Since the collimator is immediately ahead of, and somewhat smaller than, the active area of the counter, no muons should be able to get into the target without

²⁵ This is of limited utility as scattering from the counter, windows, etc., will blur any sharply defined spot. The tendency is towards a nearly Gaussian shape in two dimensions.

²⁶ Plastic scintillator is manufactured to round numbers in Imperial units, 5 mil (0.005") or 10 mil being the example here.

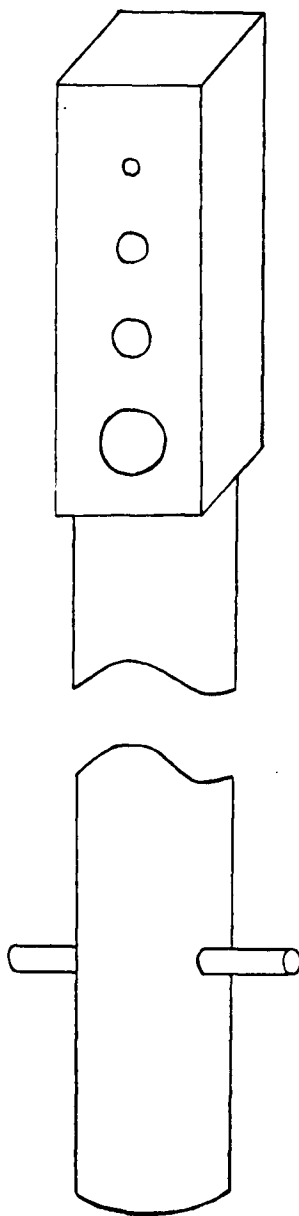


Figure 9

Sketch of the variable collimator. The pipe passes through a vacuum seal and the handle at the bottom allows the operator to adjust the height to choose the size of the collimator. A friction collar is then tightened to hold it in place.

being detected. The only way a muon might be missed is if two muons come within the recovery time of the counter, which is about one hundred nanoseconds.

2) Since surface muons have a short range, it is quite easy to stop them in condensed matter targets. Instead, the problem is to ensure that they do not stop before they get to the target. This necessitates minimizing the total thickness of the beam windows, counter, cryostat windows, heat shield, and magnetic shielding. For example in one run it was observed that 36% of the muons stopped in the 0.005 cm thick (40 mg/cm^2) magnetic shielding before entering the target; however, close to one hundred percent of the muons passed through the 0.0025 cm (20 mg/cm^2) magnetic shielding which was substituted²⁷. Strictly speaking, one should not add the thicknesses of different materials in such a simple-minded way, but it was adequate for present purposes. The range can be determined more accurately from the Bethe-Bloch equation [Evans 55].

Another problem, particularly with surface muons, is multiple scattering by the beamline windows, etc., a pronounced effect due to the low energy of these muons. For example, changing the D.C. Separator windows from 0.0025 cm to 0.0008 cm thickness increases the luminosity (muons/sec/cm^2) of the incident beam by a factor of about three. The material in front of the counter reduces the number of muons entering the apparatus, but the counter itself and the material between it and the target scatter the muons, so that some of them miss the target and stop in the target holder, the walls of the cryostat, or elsewhere. For example, a 0.030 cm thick counter scatters muons through a mean half-angle of 6° . Since the counter is 5 cm far away from the target, the beam spot is at least 1.0 cm from scattering alone. By contrast, a 0.013 cm thick counter scatters them only 2.5° , for a minimum beam spot of 0.4 cm. For small targets then, a thinner counter is much preferred²⁸.

The final consideration is that the muons follow a curved path in the applied magnetic field. This is particularly bad for surface muons which have an energy of typically 3.1 MeV (25.9

²⁷ The dilemma was that if insufficient shielding were used, the magnetic field would not be low enough and the experiment would fail no matter how many muons stopped in the target. The necessity for the use of zero field will be explained later.

²⁸ If the counter is too thin, insufficient light is produced and counter efficiency declines, resulting in a reduced signal and an increased background.

MeV/c) after passing through the thin counter. The radius of curvature of such a muon can be calculated from $H\rho = 86 \text{ KGauss-cm}$ [Trower 65]. For example, this means that in an applied field of 480 Gauss, the radius of curvature (ρ) would be 176 cm, and if the distance from the thin counter to the target were 10 cm, the beam would be laterally displaced by about 5.7 mm. If the target is only 1 cm in diameter, this can be a serious problem. This applies only when the field is transverse to the muon momentum. As mentioned above, a D.C. Separator may also be able to rotate the muon spin relative to its momentum. If the spin is rotated 90 degrees this results in transversely polarized muons, which will precess in an applied magnetic field which is parallel to the muon momentum direction. This allows the use of surface muons in higher fields than might otherwise be feasible.

3) There are two considerations in detecting the decay positrons, the number detected and the asymmetry they show. As a consequence of the weak interaction, positrons emitted with different energies also give different asymmetries. This behaviour is given by the simplified equations [Garner 79, Sachs 75]:

$$\begin{aligned} \frac{dR(x, \theta)}{dx d\Omega} &= \frac{x^2}{2\pi} [(3-2x) - P(1-2x)\cos\theta] \\ &= \frac{n}{2\pi} [1 + aP\cos\theta] \end{aligned} \quad (\text{II.7})$$

where:

$$n = x^2 (3 - 2x) \quad (\text{II.8})$$

$$a = \frac{2x - 1}{3 - 2x} \quad (\text{II.9})$$

and where:

R is the probability of a positron being emitted at an energy x in a direction θ from the muon spin direction;

n is the number of positrons emitted at a certain energy;

a is the asymmetry of those positrons emitted at a certain energy;

P is the muon polarization at the time of decay; and

x is the energy/maximum energy of 52.8 MeV.

The equations for n and a are plotted in Figure 10. The major point here is to note that the higher energy positrons also reflect a higher asymmetry.

The quantity of interest is A^2N ²⁹, where A is the asymmetry, and N the number of positrons detected of all energies.

$$A = \frac{\int a n \, dx}{\int n \, dx} \qquad N = \int n \, dx \qquad (\text{II.10})$$

The A_i defined earlier in eq. II.3 as the amplitude of the i th signal is closely related to this A , with only some small corrections for counter geometries and efficiencies being necessary. In practice, the standard sample A_{max} is used as an empirical measure for this correction, simultaneously taking into account the fact that the muons may not be 100% polarized. The quality of signal is actually proportional to $A\sqrt{N}$, but usually the square is taken for convenience; also, the time it takes to do the experiment is proportional to A^2N , so it is a useful quantity. This dependence can be simply justified by noting that AN is the signal and since Poisson statistics apply, the error in the number of counts is just the square root of that number, therefore

$$\text{signal/noise} = \frac{AN}{\sqrt{N}} = A\sqrt{N} \qquad (\text{II.11})$$

Now consider the effect of rejecting all positrons below some certain energy E_c . From Figure 10 it can be seen that this would, of course, decrease the number of events detected, N , but would also increase A , the observed signal amplitude. By combining equations (eq. II.5) it is possible to calculate A^2N as a function of E_c

$$A^2N = \frac{(f-1)(3f^3+f^2+f+1)^2}{9(f^3-f^2-f-1)} \qquad (\text{II.12})$$

where $f =$ the lower energy cutoff/52.8 MeV, the maximum decay energy. This function is plotted in Figure 11. The maximum is at $f = 0.73$ (38.8) MeV, and is 1.7 times that observed with no energy cut.

²⁹ This does not necessarily apply when comparing different signals as a relaxing signal should not be treated in the same fashion.

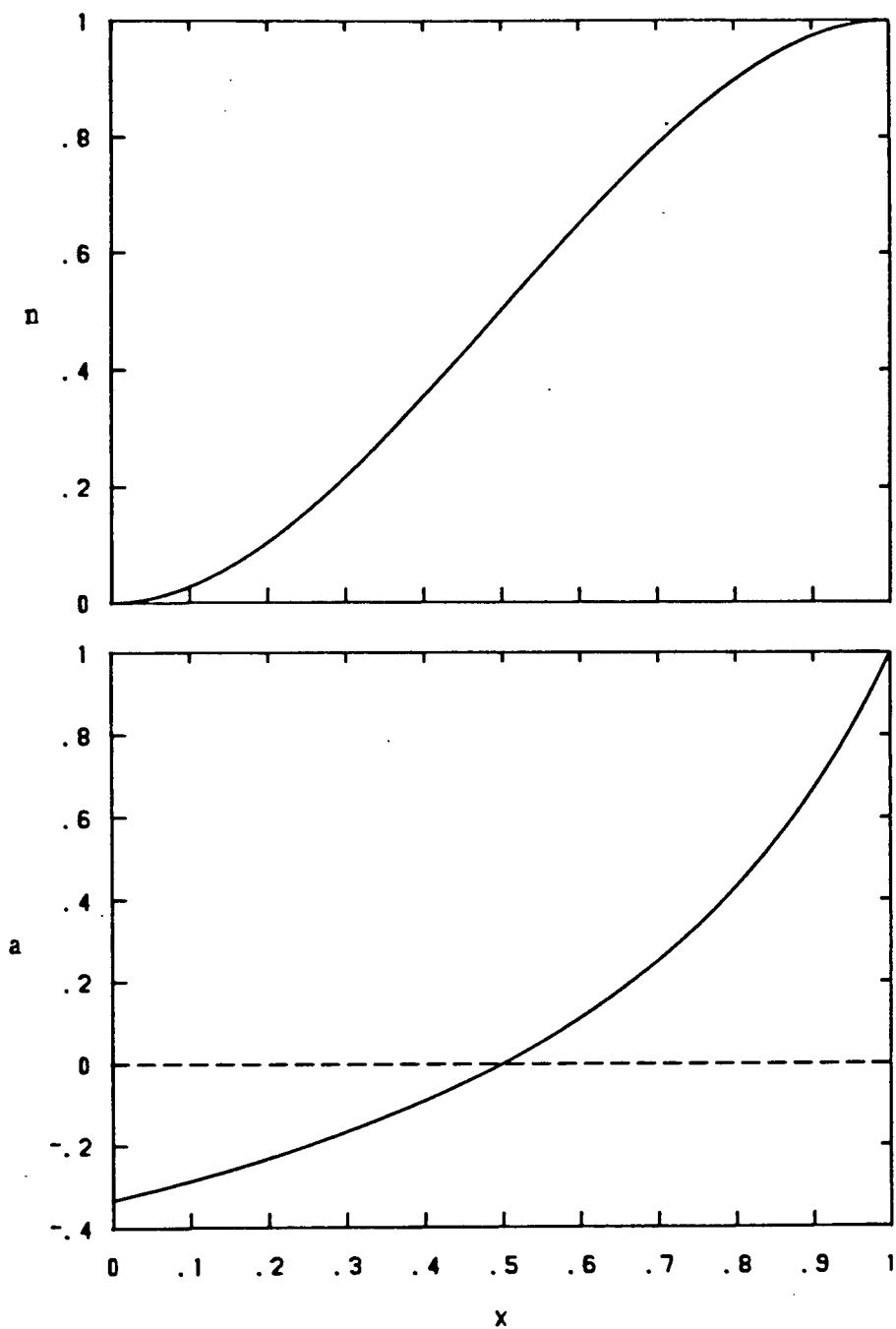


Figure 10

Number n (top) and asymmetry a of the emitted positrons as a function of energy. $x = \text{energy}/52.8 \text{ MeV}$.

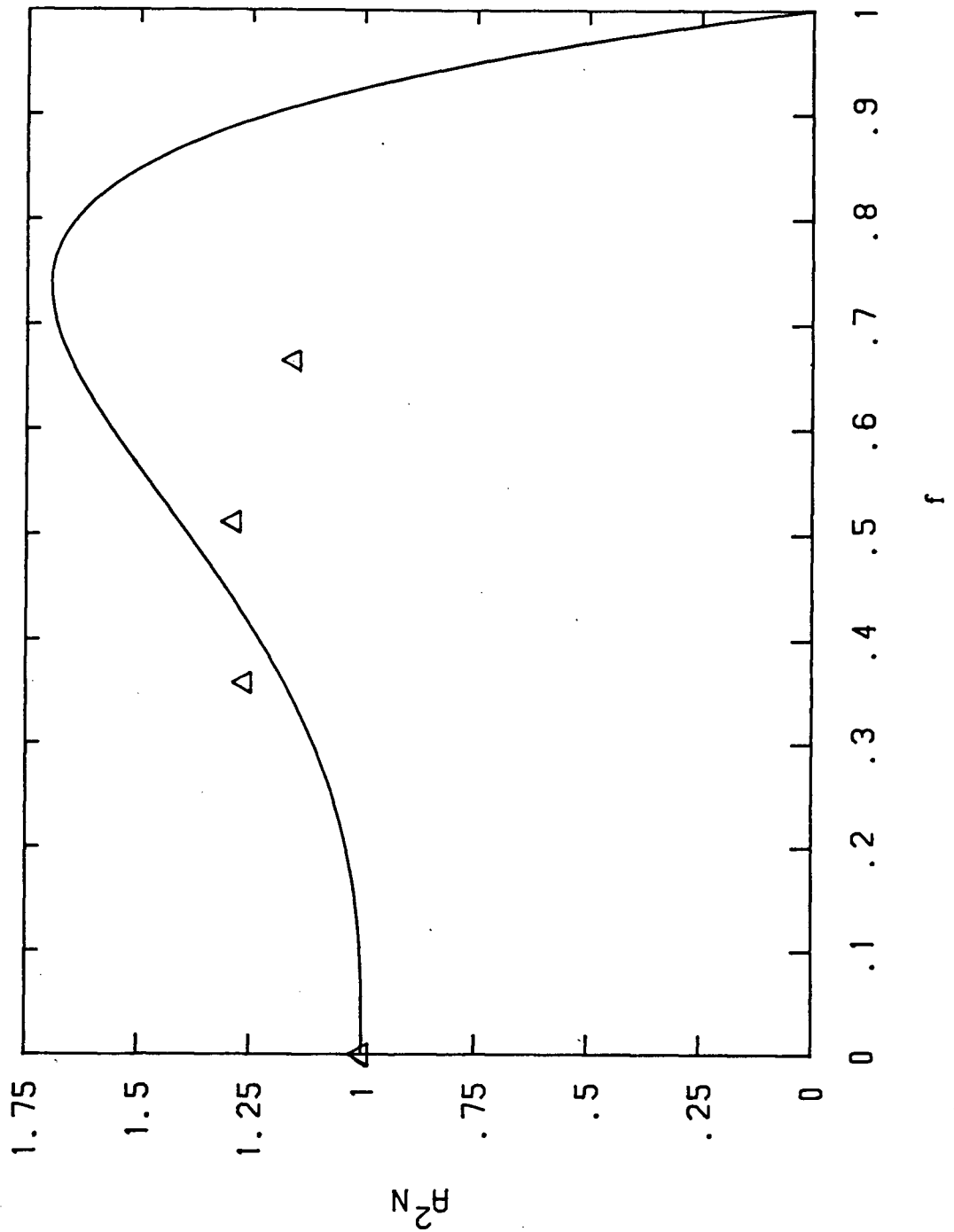


Figure 11

Theoretical plot of the square of the asymmetry times the number observed integrated from a lower limit to the maximum allowed energy, plotted as a function of the lower limit. The points are from a Monte Carlo simulation showing the effect of scattering. Note the decrease in $A^2 N$.

In practice, the simplest way to make such a cut is to place some "absorber" or "degrader" in the positron telescope as in Figure 8. By choosing a suitable thickness it is possible, in principle, to "range out" the lower energy, undesirable positrons. Due to restrictions of geometry and cost, the material of choice is carbon in the form of sheet graphite. It can be calculated from range tables [Berger 64, 66] that 18.4 grams/cm² of carbon is required to eliminate positrons below 38.8 MeV. This is all very well, but one is not interested in the total distance a positron travels, which is what range tables give, but how far in a particular direction the positron travels. Due to scattering, this distance will be less than the expected range so the absorber thickness must be reduced correspondingly, but more importantly the range is blurred by the random nature of the scattering process. Thus, a particular lower-energy positron might escape an absorber which a particular higher-energy one did not. Also, the higher-energy positrons are more likely to undergo energy loss by Bremsstrahlung which can be a catastrophic process, whereas the range tables use only an average value for Bremsstrahlung effects.

A Monte Carlo calculation was done some years ago by Leiss et al. [57] for exactly this interaction. They calculated the probability of electrons escaping a thick carbon absorber in a particular direction. Some of the resulting effects on A²N are plotted in Figure 11. Comparing the points to the line, it can be seen that the maximum corrected gain in A²N of 1.25 is much less than the maximum expected gain of 1.7. The maximum occurs at about 13 grams/cm² rather than the 18 expected. A measurement was done with 7 grams/cm² of carbon, all that would fit in the available space in Eagle, which was found to increase the asymmetry by 30%, whereas the increase calculated from Leiss et al. is only about 25%. This unexpectedly high value is probably due to the sample thickness, as discussed below.

For higher Z (atomic number) materials these "blurring" effects are even worse, and lower Z materials are not cheaply available in sufficiently dense forms, so graphite remains the optimum choice.

As an historical note, perhaps the chief reason for the use of degrader in the positron telescope with surface muons was to prevent the scattered beam positrons from triggering the

positron telescope, thereby increasing the background. Since the beam momentum, 29.8 MeV/c, is less than the momentum of the desired decay positrons, they can be partially ranged out along with those decay positrons reflecting lower asymmetry. With the advent of clean, separated beams, this practice should no longer be necessary.

One of the side-effects of the dependence of the asymmetry on energy is the dependence, in some circumstances, of the signal amplitude on the sample thickness. This makes it more difficult to compare samples of different materials as almost invariably they are different sizes, densities and chemical composition³⁰. Consequently, the most reliable telescope in Eagle for asymmetry measurements is the Backward one (see Figure 8), as in this case the decay positron need only penetrate the small thickness that the muon itself travelled, thus reducing the unwanted sample dependence.

Occasionally it is necessary to have zero applied magnetic field. Since the ambient field at TRIUMF is one to three Gauss, in virtually any direction, to obtain a reasonably good (less than 50 mG) zero field it is necessary to cancel this field. There are two ways to do this: use magnetic shielding material; or use a triaxial coil arrangement.

A disadvantage of the former is that the limited range of the surface muons means that little or no mass must be in the path of the beam. In the restricted space available it was not possible to use a cylinder with an open end toward the beam, so a thin magnetic shield had to be placed in the path of the muon. The commercially available shielding obtained had a thickness of .005 cm, or 40 mg/cm², which as mentioned in Section II.5, stopped some of the muon beam. Thus it was necessary to make the shield thinner. It was found that the material, a nickel alloy, could be etched by a hot acid solution, reducing the thickness to 0.0025 cm, or 20 mg/cm², which was thin enough. Another disadvantage of magnetic shielding is that while the shield is in place, no external magnetic field can be applied. It is sometimes desirable to turn on a small magnetic field to normalize asymmetries, for example.

³⁰ Chemical composition may be important as the influence of Bremsstrahlung is strongly Z-dependent.

The disadvantage of the coil method is that this ambient field changes with time. It is then necessary to monitor the ambient field, a task rendered difficult in Eagle as the sample is in a cryostat, an unsuitable environment for a temperature sensitive probe, and a large vacuum tank surrounds that, so any monitoring probe must be quite far from the sample. In any future apparatus, such as the Omni apparatus currently in the final stages of construction at TRIUMF, a provision should be made for a triaxial, temperature controlled, magnetic field probe.

C. CHAPTER III: MUONIUM HYPERFINE INTERACTIONS

1. SPIN-HAMILTONIAN I: ISOTROPIC HYPERFINE INTERACTION

The first studies of the hyperfine states of muonium were done by Hughes et al. [60] who were interested in measuring the muonium hyperfine frequency ν_0 in vacuum as a test of Quantum Electrodynamics (QED). They did this by using high-pressure argon gas which both stopped their conventional muon beam and served as the medium for muonium formation. By measuring the frequency as a function of pressure, they were able to extrapolate to get a value of ν_0 for muonium in a vacuum. In such studies muonium is, of course, in an isotropic environment.

The isotropic hyperfine interaction is by far the most commonly observed in μ SR, and will not be pursued much here, as it is well treated elsewhere [Brewer 75, Fleming 79]. The Hamiltonian describing it is:

$$H = g_e \mu_B \underline{S} \cdot \underline{B} - g_\mu \mu_\mu \underline{I} \cdot \underline{B} + A_0 \underline{I} \cdot \underline{S} \quad (\text{III.1})$$

where g_e, g_μ are the electron and muon g-factors, respectively;

μ_B, μ_μ are the Bohr (or electron) and muon magnetons;

$\underline{S}, \underline{I}$ are the electron and muon spin operators;

\underline{B} is the applied field; and

$A_0 = h\nu_0$ is the contact hyperfine interaction.

In vacuum, $\nu_0 = 4463$ MHz as given in Table I; the corresponding value for the hydrogen atom is 1420 MHz or 507 G, a unit more natural to EPR. In this work all energies will be given in frequency units.

The solution of this Hamiltonian yields the familiar Breit-Rabi diagram shown in Figure 12. When the electron spin is initially parallel to the muon spin, muonium is in a triplet state, but when the electron spin is initially anti-parallel to the muon spin, the state is a mixture of singlet and triplet in which the muon spin oscillates at the hyperfine frequency. Of six possible transitions, only four are allowed in a transverse magnetic field by angular momentum

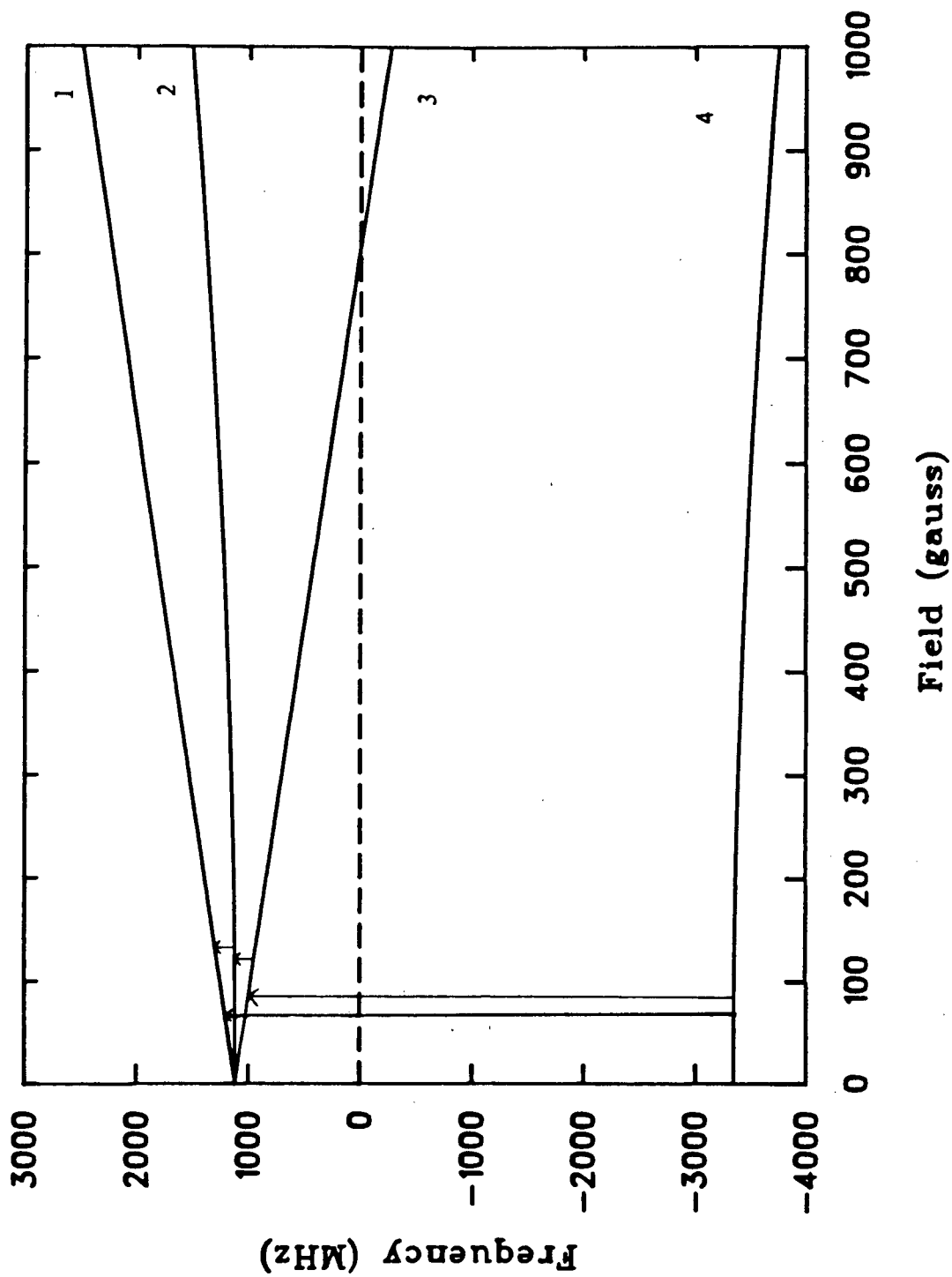


Figure 12

Breit-Rabi diagram for the isotropic hyperfine interaction. The arrows indicate the allowed transitions. The numbers are the labels used in the text.

considerations. These four are indicated on Figure 12. If the field is in the z direction, the observed muon precession can be written [Percival 82]:

$$\begin{aligned} P_{xy} &= P_x + iP_y \\ &= \frac{1}{2}c^2 e^{i\omega_{12}t} + \frac{1}{2}s^2 e^{i\omega_{23}t} \end{aligned} \quad (\text{III.2})$$

where the two precession frequencies $\omega_{ij} = 2\pi\nu_{ij}$ are:

$$\omega_{12} = \omega_- - \Omega \quad (\text{III.3})$$

$$\omega_{23} = \omega_- + \Omega, \text{ with} \quad (\text{III.4})$$

$$\omega_{\pm} = \frac{1}{2}(\omega_e \pm \omega_{\mu}), \text{ where} \quad (\text{III.5})$$

$$\omega_e = g_e \mu_B B, \quad \text{the Larmor precession frequency of an electron}$$

$$\omega_{\mu} = g_{\mu} \mu_{\mu} B, \quad \text{the Larmor precession frequency of a muon}$$

$$\begin{aligned} \Omega &= \frac{1}{2}\{[\omega_0^2 + \omega_+^2]^{1/2} - \omega_0\} \\ &\approx \frac{(\omega_{12} + \omega_{23})^2}{4\omega_0} \end{aligned} \quad (\text{III.6})$$

$$c^2 = \frac{1}{2} \left[1 + \frac{\omega_+}{[\omega_+^2 + \omega_0^2]^{1/2}} \right] \quad (\text{III.7})$$

$$s^2 = 1 - c^2 \quad (\text{III.8})$$

In the low-field limit, $s^2 = c^2 = \frac{1}{2}$ and ω_0 is the hyperfine frequency, $A_0 = \omega_0/2\pi$.

The well-known results are given in reports by Garner [79], and by Brewer [75], and will not be derived in detail here. For present purposes, the important features to note are:

1. two components oscillate at or near the hyperfine frequency ν_0 and are difficult to observe directly, although this has been achieved with high time resolution [Holzschuh 81];
2. in zero applied field, the two low frequency transitions degenerate to one, with a frequency of zero, meaning the signal is constant in time, barring relaxation;
3. for low fields (<20 Gauss)³¹ this degeneracy still holds within the typical experimental frequency resolution and a single characteristic low-frequency muonium signal can be observed, as exhibited in Figure 3, whose frequency is given by 1.39 MHz/Gauss times the

³¹The field regimes assume the hyperfine constant is similar to that for muonium in vacuum.

applied field³²;

4. for medium fields ($20 < B < 150$ Gauss) the degeneracy breaks down and two signals are observed. The average value of their frequencies, $\nu_- = 2\pi\omega_-$, is again 1.39 MHz/G times the applied field; and their splitting, 2Ω , varies as the square of the applied field. This effect is usually referred to as the quadratic Zeeman effect. The measurement of Ω is the standard method of determining ω_0 , since

$$\begin{aligned}\omega_0 &= \frac{-4\Omega^2 + (\omega_{12} + \omega_{23} + 2\omega_\mu)^2}{4\Omega} \\ &\approx \frac{(\omega_{12} + \omega_{23})^2}{4\Omega} \\ &= \frac{\omega_-^2}{\Omega}\end{aligned}\tag{III.9}$$

2. SPIN-HAMILTONIAN II: AXIALLY SYMMETRIC HYPERFINE INTERACTION

In the case of an axially symmetric anisotropy, the Hamiltonian can be conveniently expressed as [Brewer 79b]:

$$H = g_e \mu_B \underline{S} \cdot \underline{B} - g_\mu \mu_\mu \underline{I} \cdot \underline{B} + A_0 \underline{I} \cdot \underline{S} + \Delta A \underline{I}_z \underline{S}_z\tag{III.10}$$

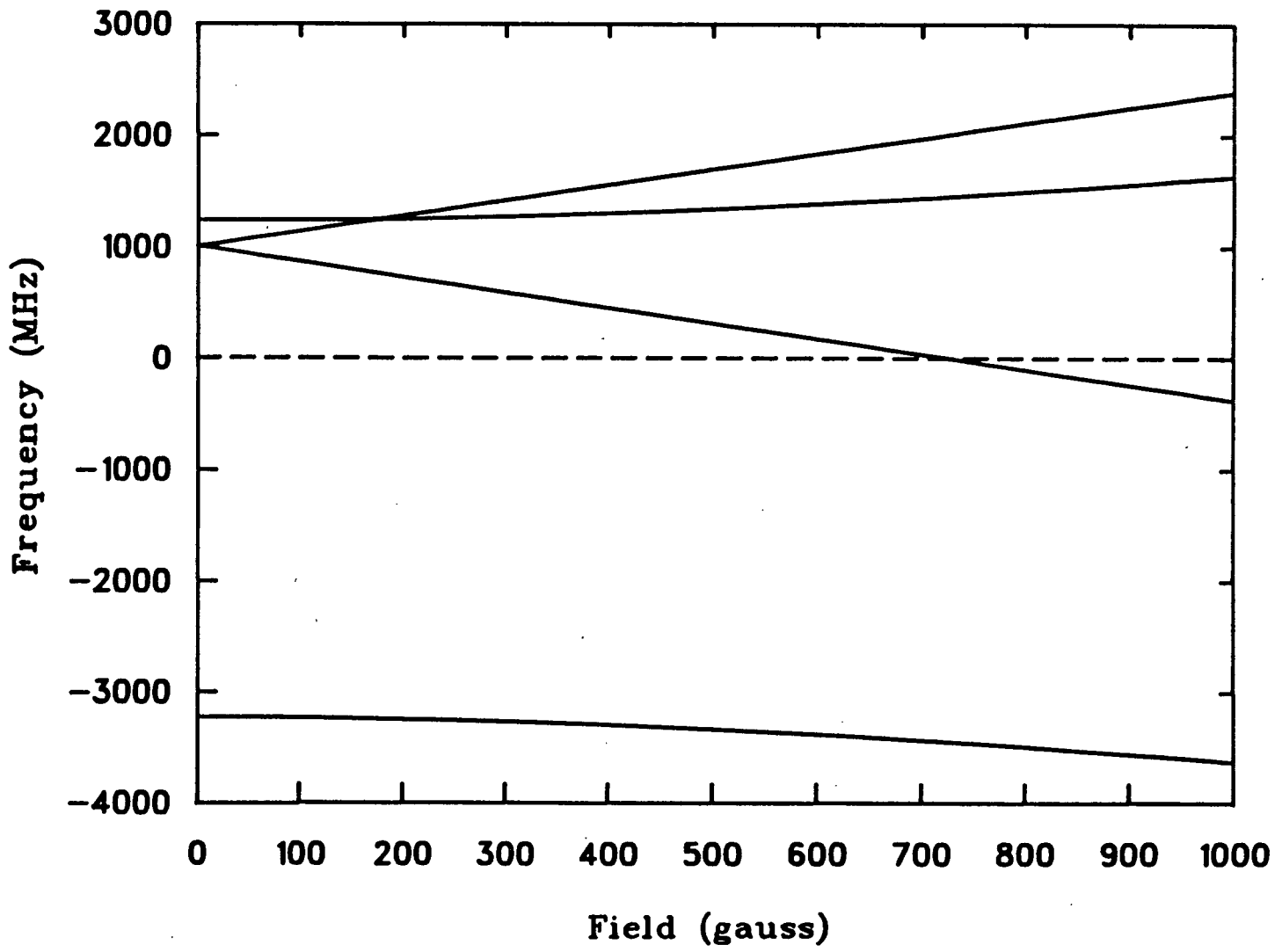
where the symbols are defined as before, with ΔA the deviation from isotropy in the z (symmetry) direction, and the subindex z indicating the z component.

The solutions of this Hamiltonian are given in detail by Patterson et al. [78], and the approximate solutions for small B are given in papers by Beder [80], Baryshevsky et al. [78] and Percival et al. [82]. The resulting energy level diagram is shown in Figure 13. The details are dependent on the angle between the applied magnetic field and the z-axis. The observed muon polarization is still given by equation III.2, but now with the precession frequencies

$$\omega_{12} = \omega_- - \Omega + \frac{1}{2}\delta\omega\tag{III.11}$$

³²The occurrence of this low-frequency signal is the signature for isotropic muonium, and much of the work of this thesis consisted of searching for it.

Figure 13
Breit-Rabi diagram for the cylindrically anisotropic hyperfine interaction.



$$\omega_{23} = \omega_{\perp} + \Omega - \frac{1}{2}\delta\omega, \text{ where} \quad (\text{III.12})$$

$$\delta\omega/2\pi = \frac{1}{2}\Delta A(3\cos^2\theta - 1) \quad (\text{III.13})$$

with Ω and c defined as before, but with ω_0 replaced by ω_{\perp} , where

$$\omega_{\perp}/2\pi = A_0 + \frac{1}{2}\Delta A\sin^2\theta \quad (\text{III.14})$$

This expression is only valid for $\omega_{\perp} > \frac{1}{2}\delta\omega$. For zero magnetic field $\omega_{\perp} = 0$,

$$\nu_{12} = \nu_{23} = \frac{1}{2}\Delta A \quad (\text{III.15})$$

and the intensity I of this transition in the direction parallel to the initial spin of the muon is

$$I = \frac{1}{2}\sin^2\phi \quad (\text{III.16})$$

where ϕ is the angle between the z axis and the initial spin of the muon. The intensity in a direction perpendicular to the initial spin of the muon is $\cos\psi\cos\phi$ where ψ is the angle between the direction of observation and the initial spin. The two main consequences of this Hamiltonian are:

1. the observation of a low-frequency muonium oscillation in zero applied magnetic field, $\frac{1}{2}\Delta A$, whose amplitude is orientation dependent, but whose frequency is orientation independent; and
2. a splitting of the two transitions in low applied fields $\delta\omega$ which is field independent in the low field regime, but strongly angle dependent, This splitting is in addition to the usual splitting seen in medium fields for isotropic muonium. Thus

$$\omega_{23} - \omega_{12} = 2\Omega - \delta\omega \quad (\text{III.17})$$

This allows the determination of the sign of ΔA , which otherwise would be difficult to determine.

3. SPIN-HAMILTONIAN III: COMPLETELY ANISOTROPIC HYPERFINE INTERACTION

Arguably, this section should be first, as the axially anisotropic and isotropic Hamiltonians are but special cases. However, the order chosen reflects the increasing complexity as well as historical sequence of observation. The appropriate Hamiltonian is:

$$H = g_e \mu_B \underline{S} \cdot \underline{B} - g_\mu \mu \underline{I} \cdot \underline{B} + \underline{I} \cdot \underline{A} \cdot \underline{S} \quad (\text{III.18})$$

where \underline{A} is now a tensor. Although more physically realistic, g_e is not taken as a tensor here, since none of the systems studied in this thesis had a sufficiently anisotropic g_e for this complication to be necessary at the low fields used.

If the axes are chosen such that \underline{A} is diagonal,

$$H = g_e \mu_B \underline{S} \cdot \underline{B} - g_\mu \mu \underline{I} \cdot \underline{B} + A_{xx} I_x S_x + A_{yy} I_y S_y + A_{zz} I_z S_z \quad (\text{III.19})$$

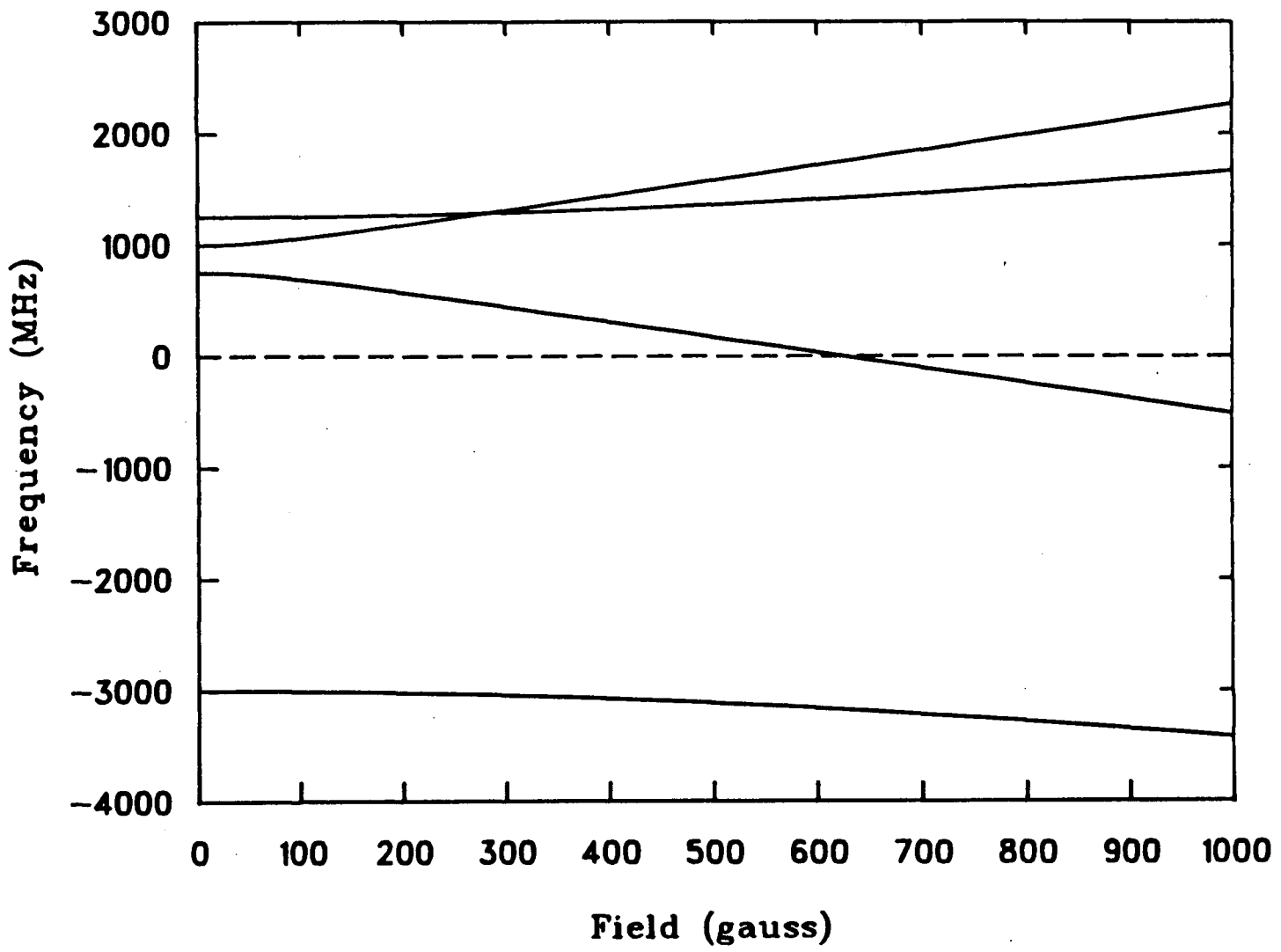
from which it is clear that equation III.1 can be derived by setting $A_{xx} = A_{yy} = A_{zz} = A_0$, and equation III.2 by setting $A_{xx} = A_{yy}$, with $A_0 = A_{xx}$, and $\Delta A = A_{zz} - A_{xx}$.

The eigenvalues and eigenvectors of this Hamiltonian can be found in Appendix 2, and the energy level diagram is plotted in Figure 14. The low field behaviour depends strongly on the orientation of the applied field relative to the principal axes of the tensor. The major new features are:

1. With zero applied field, three frequencies are observable, given by $\frac{1}{2}(A_{xx} - A_{yy})$, $\frac{1}{2}(A_{yy} - A_{zz})$ and $\frac{1}{2}(A_{zz} - A_{xx})$ as shown in Section A2.1, eq. A2.15. The signs are not observables in zero field. A useful feature is that these frequencies have a "sum rule"; that is, the sum of two of them equals the third. Since the signs are not observed, the two lowest observed frequencies sum to the highest observed. This can be a helpful clue³³. The three resulting frequencies will be called a "triple".
2. In zero field, the intensity pattern of these frequencies is strongly angle dependent, but the frequencies themselves are orientation independent. Orientation is with respect to the initial muon polarization, as for the cylindrically symmetric case with zero applied field. This orientation dependence can, in principle, be used to determine the orientation of the principal axes of the tensor with respect to the crystal axes.

³³ When the first experiment on low-temperature α -quartz was done, the anisotropic Hamiltonian was completely unexpected, and this feature was one of the first things noticed.

Figure 14
Breit-Rabi diagram for the completely anisotropic hyperfine interaction.



3. In an applied field, the spectrum becomes much more complex, with as many as nine frequencies. This case is not considered further here, since no experimental work was done on it, but more theory may be found in Appendix 2.

As shown in Section A2.3.c, taking the initial muon polarization as the z' direction in the lab frame, and if the site x axis is parallel to z' , the only frequency observed will be $\nu_{yz} = \frac{1}{2}(A_{yy} - A_{zz})$, and the intensity of this frequency *in the direction of the initial muon polarization* will be $1/2$. That is, the amplitude of the signal at this frequency will be 0.5, just that seen for muonium in a transverse field for an isotropic hyperfine interaction. On the other hand, if the angle between x and z' is $\gamma_{xz'}$, then the intensity of the ν_{yz} frequency will be $\frac{1}{2}\cos^2\gamma_{xz'}$. This is just the same as it was in the case of the axially symmetric hyperfine interaction, the difference being that there are now three such frequencies, each varying as the square of the direction cosine between the site axes and the z' axis. That is, $I(\nu_{xy}) = \frac{1}{2}\cos^2\gamma_{zz'}$, $I(\nu_{xz}) = \frac{1}{2}\cos^2\gamma_{yz'}$, and $I(\nu_{yz}) = \frac{1}{2}\cos^2\gamma_{xz'}$. These intensities are all in the direction of the initial muon polarization. If there is more than one equivalent site present, it can be much more complicated, as shown in Section A2.3.b. It should be noted that the expression for intensities given in the paper by Brewer et al. [81] is incorrect.

4. SUPERHYPERFINE SPIN-HAMILTONIAN

The superhyperfine interaction occurs when another nucleus interacts with the electron of the muonium atom. The Hamiltonian describing the superhyperfine interaction is:

$$H = g_e \mu_B \underline{S} \cdot \underline{B} - g_\mu \mu_\mu \underline{I} \cdot \underline{B} + \underline{I} \cdot \underline{A} \cdot \underline{S} + \underline{J} \cdot \underline{A}^N \cdot \underline{S} \quad (\text{III.20})$$

where \underline{A} and \underline{A}^N are both tensors and \underline{J} is the spin operator of the nucleus. For a spin one-half nucleus in zero magnetic field, neglecting the states corresponding to singlet muonium, this Hamiltonian gives rise to a six-by-six matrix, as shown in Appendix 3. This treatment is completely independent of that carried out by Beck et al.[75] for the specific case of muonium in alkali halides.

The intensity behaviour is now tensorial in nature, this tensor being different for each of the three observable frequencies. This is far more complex than for the case with just the anisotropic hyperfine, where there was one tensor which described the intensities of all three frequencies simultaneously. It should be noted that the sum rule for triples holds for the superhyperfine interaction just as it did for the anisotropic hyperfine.

A numerical example should illustrate, taking the observed values for the anisotropic hyperfine and the superhyperfine determined by Isoya et al. [83], for hydrogen in quartz. The reason for this choice will become apparent later. At 80 K, the principal values of the hyperfine tensor are, 51.9483, 51.7505 and 51.6981 mT, with the corresponding values of the ^{29}Si superhyperfine tensor being 0.068, 0.134 and 0.130. The tensors will be assumed to be coaxial. Substituting these into eq. A3.2, Appendix 3, gives the resulting transition energies: 0.0290, 0.1263 and 0.1553 mT. As noted, the intensity of each frequency is given by a tensor, defined by:

$$I_{ij} = \underline{u} \cdot \underline{I} \cdot \underline{u} \quad (\text{III.21})$$

where \underline{u} is the direction of the initial muon spin, also assumed to be the direction of observation. If the polarization makes an angle 114° from the x axis, 24° from the y axis, and 90° from the z axis of the tensor, the corresponding intensities are: $I_{12} = 0.0064$, $I_{13} = 0.1456$ and $I_{23} = 0.0535$, where an intensity of 0.25 corresponds to a fully allowed transition.

D. CHAPTER IV: A BRIEF SURVEY OF MUONIUM FORMATION AND RELAXATION

Muonium's ionization energy of 13.6 eV is higher than that of almost all materials. It also has considerable kinetic energy available during its slowing down. Perhaps the question should not be "Why does muonium form?", but rather, "Why doesn't it always form?"

It must be noted that the term "relaxation" of the muonium (muon) signal is used to mean three very different processes:

1. muonium (muon) may react chemically to form a diamagnetic (paramagnetic) compound in which the muon precesses at a vastly different frequency. The muonium (muon) is thus effectively removed from the ensemble in an irreversible manner.
2. muonium (muon) may be dephased, that is, different members of the ensemble may precess at slightly different frequencies, or the frequencies may change as a function of time, but there is no chemical change. The result is, though, a loss of signal amplitude. In principle this is a reversible process.
3. if the muonium electron undergoes spin exchange with some other electron, the signal will be lost, irreversibly.

The first mechanism can easily be distinguished from the last two. In zero applied field, any muonium that reacts to form a diamagnetic compound causes *no* loss of polarization, whereas spin exchange or local magnetic moments *will* cause a loss of polarization. The application of a strong longitudinal field, however, can be used to quench this loss of polarization [Brewer 75].

Although the work in this thesis is concerned almost exclusively with solids, most of the existing work on muonium formation has been done in gases and liquids, so this work will be briefly reviewed. Ultimately it is hoped that an understanding of muonium formation in gases, the simplest systems, will help lead to an understanding of muonium formation in liquids and hence in solids.

1. GASES

Of the three phases of matter, gases are usually the easiest to understand. This is true for muonium studies as well. In the gas phase the muon goes through a number of charge exchange cycles where it captures and loses an electron as it slows from its initial energy of approximately 3 MeV³⁴ down to thermal energies. The amount of muonium formed is thus the result of the energy dependence of the relative cross-sections for these charge exchange processes [Fleming 82]. There are other considerations, including the possibility of hot atom reactions [Arseneau 84], but they are less important. In all gases thus far examined only two, helium and neon, do not show large muonium fractions.

The relaxation of muonium in gases, either pure gases or with added impurities, is due to the three processes mentioned above. Chemical and spin exchange reactions of muonium are the subject of considerable current interest [Senba 84, Fleming 82], with the lower limit on the rates of reaction being due to line broadening from inhomogeneous magnetic fields. This is much more troublesome for gas phase than for condensed phase work as the muons have a broad stopping distribution, since:

1. they have a high initial energy and hence travel a long distance (approximately fifty centimetres) before stopping in the gas;
2. the energy loss process has a statistical fluctuation; and
3. the beam has an initial spread in energies due to the momentum acceptance of the channel.

The magnetic field produced by any finite set of coils varies spatially. This means that muons stopping in different regions will be in slightly different magnetic fields, hence precess at slightly different frequencies and the signal is dephased. This effect can be reduced by the use of large coils to produce a homogeneous field over a sufficiently large volume. For example, the coils presently used by the gas chemistry group at TRIUMF have a diameter of 150 cm. The diamagnetic muon signal in gases will also relax due to magnetic field inhomogeneities, although about one hundred times more slowly than muonium. Other possible sources of muon relaxation

³⁴Although surface muons have an energy of 4.1 MeV, the windows and counter reduce the energy to about 3 MeV.

include thermal muonium formation or processes involving μ^+ molecular ions [Fleming 83].

2. LIQUIDS

In liquids, the situation is much more complicated due to the collective processes. It is sufficiently complex to have been the subject of considerable debate in the literature [Percival 84, Walker 81] as well as in conferences, group meetings and the hallways of TRIUMF. Two main differences are observed for muonium and diamagnetic muon fractions between gases and liquids: a much lower muonium fraction and a much higher diamagnetic fraction are observed in liquids than in most gases; and there is frequently a missing fraction, of the order of 20% in water for example, whereas such a missing fraction is almost never observed in the gas phase [Arseneau 84].

The earliest model attempting to explain muonium formation was the "hot atom" model which observed that

"At a kinetic energy of 200 eV, practically all the muons are in the muonium state.",
[Brewer 75]

from which they slow down; but due to their high energy, they may participate in epithermal reactions which would be forbidden for thermal muonium. The observable fractions of muonium and diamagnetic muon would then depend on charge exchange processes, as in the gas phase, followed by possible chemical reactions before the muon or muonium had finished thermalizing. Such processes are relatively unimportant in the gas phase [Arseneau 84] but the large diamagnetic fractions seen in liquids relative to those in vapors suggests that they may dominate in condensed media.

In 1978 a new model, the "spur" model, was developed [Percival 78] in analogy with the model proposed by Mogensen [74] for positronium formation. Positronium is an atom consisting of a positron and an electron in a bound state. This model is based on the premise that in its slowing-down process the muon creates spurs consisting of electrons and radicals typical of the particular solvent. It would then be possible to form muonium by a thermalized muon picking up

one of these electrons, in contrast to the cyclic charge exchange process which takes place at higher energies.

One of the big continuing mysteries in μ SR is the origin of the missing fraction, P_L . This is zero to a fair degree of precision in many materials, particularly in metals and gases at modest pressures [Arseneau 84], but in many cases it is not; indeed in some extreme cases neither muon nor muonium signals are observed at all! The reasons for this loss of polarization have been the subject of considerable speculation. One advantage of the spur model was that it gives a plausible explanation in terms of the radiolytic species formed in the spur, such as solvated electrons, which would be expected to depolarize muonium by spin exchange or chemical reaction [Percival 84]. No model which does not involve muonium or muonium-like states has yet been proposed as a mechanism for the creation of the missing fraction.

For the moment the debate of hot-atom versus spur in muonium formation remains unsettled. As an explanation for the missing fraction the spur model is very attractive, although difficult to test conclusively. The hot-atom model is even harder to test.

Relaxation processes in liquids are similar to those in gases except the stopping distribution is much narrower, so that field inhomogeneities are less important. The most important difference between gases and liquids comes from the possibility that radiation-induced spurs contribute significantly to the muonium formation process in liquids.

3. SOLIDS

a. Muonium Formation

The mechanism of formation of muonium in solids is even cloudier than in liquids. Again the muon has enough ionization energy to forcibly seize an electron from most materials. Although muonium is not observed in metals due to the conduction electrons present, which screen the muon charge, it is observed in some insulators and some semiconductors; but often, as in liquids, there is a large missing fraction. If the spur model works for liquids, then perhaps it holds for solids as well. One might speculate that if the

missing fraction is due to muonium spin exchanging with a spur electron, then materials which allowed the electrons to diffuse rapidly away might, therefore have low missing fractions. α -quartz has large channels which might permit such diffusion, and it has no missing fraction. Ice, on the other hand, also has large channels, but it does have a missing fraction [Percival 85]. A more sophisticated approach along these lines might be profitable. Typical results prior to the present work may be found in a paper by Brewer et al. [75] and are mentioned in Chapter I. In some cases, this missing fraction is easily explained as being due to muonium being relaxed by nearby nuclear spins. For example in CaF_2 the superhyperfine couplings between the muon's electron and the local ^{19}F spin 1/2 nuclei would produce such a large number of different frequencies that the result would look like a fast relaxing muonium signal, or even, since the first few nanoseconds are not readily observed, no muonium would be seen at all, and a missing fraction would result. The superhyperfine interaction has long been the bane of workers in this field as the majority of nuclei have magnetic moments, but recently at SIN the use of strong magnetic fields to quench the superhyperfine interaction has begun to conquer this problem [Kiefl 85]. Missing fractions are still observed in their work, however, so that mysteries yet remain.

That the systems in which muonium is observed are not at thermodynamic equilibrium is clear from the fact that muon and muonium signals are present simultaneously. It is very unlikely that an equilibrium would give observable quantities of both muonium and diamagnetic muon signals in so many different solids. Further, it is known [Isoya 83] that hydrogen atoms are not observed in crystalline quartz, for example, when it is at equilibrium at room temperature, whereas muonium can be observed, so muonium cannot be at equilibrium.

b. Muonium Relaxation

Relaxation is a much more complex topic in solids than in gases or liquids. In addition to the sources of relaxation already mentioned, there are two more: nearby nuclei with magnetic moments; and the anisotropic hyperfine interaction, or AHI.

The former is the most common, these nuclei acting as local magnetic dipoles, producing what is termed random local magnetic fields, or RLMF³⁵. This can be described in a simple-minded way as the magnetic moments adding to the applied field at the muon or muonium, causing the muon spin to precess at a different frequency than another muon near a different magnetic moment. The superhyperfine interaction also occurs in the presence of nuclear moments, but rather than acting like random dipoles, a very strong coupling takes place. A great deal of work has been done on the importance of RLMF on the relaxation of muons in metals [Gygax 84, Celio 84]. The relaxation, λ in eq.II.3, if caused by RLMF is related to the square root of the second moment [Abragam 61]

$$\langle \Delta \nu^2 \rangle \propto \mu_N^2 \frac{J+1}{J} f \quad (\text{IV.1})$$

adapted from a paper by Schenck [76], where μ_N is the nuclear moment, J is the nuclear spin and f is the concentration of nuclei with spins. This assumes just one type of nucleus with spins, but it may be easily generalized.

The AHI, discussed in Section III.3, is more unusual; indeed, the work presented herein is the first muonium study to have correctly identified relaxation due to AHI. That is, earlier studies in crystalline quartz [Myasishcheva 68] and ice [Percival 78] had relaxations caused by AHI, but this was not recognized at the time.

Relaxation of the muonium signal by AHI can be caused either by:

1. Static muonium atoms in a large number of sites with different values for the hyperfine parameters; or
2. Muonium which is not static, but moves among different sites which are not perfectly equivalent.

In the first case, the relaxation envelope will indicate something of the width and strength of the anisotropies present. The detailed theory of this is not yet known, but work is in progress [Turner 85]. Qualitatively, if members of an ensemble are in sites with different principal values of the hyperfine tensor, then they will precess at different frequencies,

³⁵ RLMF may be present, of course, in liquids and gases, but in these systems the rapid motions of the molecules average these fields to zero.

resulting in a dephasing. This is true in both zero and transverse fields. The larger the variation among the sites, the greater the width of the distribution, then the faster the relaxation will be.

In the second case, if the muon spin evolves in time in one of the n sites for a time Δt , then "hops" to one of the other $n-1$ sites, the intensities of the three frequencies will be different. This, repeated for many muons, with random Δt 's and possibly more than one hop, results in a dephasing of the signal. Such a dephasing will occur even if all sites have the same principal hyperfine values, so long as there is a difference in relative orientation, whereas such sites would not cause dephasing for static muonium. This is because it is essential to consider the amplitudes of the different frequencies not as they are observed, which is necessarily an ensemble average, but rather on a single site basis since the relative orientations of the sites must be considered. From looking at the transformation given in eq. A2.63, it is clear that, generally, the transition probabilities are different in two different sites. Therefore, if a muonium atom spends some time in one site, then "hops" to another, the result will be a dephasing of the muonium signal. Typically, the model of diffusion used herein will assume that the time spent between sites is much less than the time spent in each site.

To see this more clearly, consider a simple example in which there are two sites which have the same principal values for their axially symmetric hyperfine tensors, but one of which has its z axis parallel to the initial muon polarization, and the other its z axis perpendicular to the initial muon polarization. In each of these sites two of the three possible frequencies collapse to one with frequency ν , and the remaining frequency has a value of zero. In site 1, the zero frequency transition has all the intensity, as shown by eq. A2.62, and in site 2 all the intensity goes to the frequency ν . The spin of a muon of muonium in site 1 will not change with time whereas in site 2 it will oscillate with a frequency ν . So long as there is no hopping, the spectrum will consist of two sharp lines, one at 0, and one at ν . However, if the muonium atom hops from one site to the other, that spin which was constant will now oscillate, and that spin which oscillated will become constant *at whatever value it had when it hopped*. An

ensemble, each member undergoing hopping at random times, will undergo dephasing. This is true even in zero magnetic field, and for fields of a few gauss, the relaxation may be even faster. Qualitatively, one can see that the shortest possible time for the signal amplitude to fall to $1/e$ of its initial value is of the order of one-quarter of the period of the fastest oscillation. Hence the relaxation rate

$$\lambda \approx 4f \quad (\text{IV.2})$$

where f is the highest frequency signal observed in the static case.

If the rate of hopping increases sufficiently, the average of the tensors will be observed. For example, if a three-fold axis is present, the result will be just the average of the three tensors after they are rotated to the common crystal axis system. The final result is that an anisotropic hyperfine Hamiltonian becomes an axially symmetric one, with the unique axis parallel to the symmetry axis.

E. CHAPTER V: RESULTS AND DISCUSSION

The particular samples were chosen by the criteria given in Section I.4. Briefly, samples had to be insulators with few or no nuclear moments and single crystals were preferred. This excludes most available materials, all the hydrides, halides, and alkali metal compounds, but still leaves a significant number from which to choose. The original motivation for the study of quartz was its natural helicity. The motivation changed to a study of the effects of anisotropic hyperfine interactions. Germanium dioxide was studied due to its close analogy to quartz, and beryl and zircon were chosen because they are silicates like quartz. Rutile and magnesium oxide were chosen because they are simple oxides, and hydrogen atoms have been observed in CaO [Henderson 72], which is very similar to MgO, and strontium titanate was chosen for its ferroelectric properties. Diamond does not fit into this group, but rather it was chosen due to the intense interest in μ SR studies of semiconductors [Yamazaki 84]. The results on all these materials are summarized in Table II., with their sources and impurities given in Table III. All the samples used were synthetic, unless otherwise noted.

1. QUARTZ

Quartz has a three-fold screw axis, the \hat{c} or z axis, and there are two sets of three two-fold axes, \hat{a} and \hat{b} . In this work the usual coordinate system [Nuttall 81] will be used, in which the x axis is parallel to an \hat{a} axis, and the y axis is not an axis of symmetry, but is orthogonal to x and z .

a. Asymmetry of Life

Quartz in its fused and crystalline forms forms the backbone of this thesis. Quartz has been studied with μ SR for rather a long time; in fact it was one of the first solids in which muonium was directly observed [Myasishcheva 68]. In the present work, it was initially used because it occurs in right- and left-handed crystalline forms. This early study was inspired by the two observations that life on earth uses essentially only L-amino acids, and that spatial parity is violated by the weak interaction. Soon after the discovery of parity

Table II

Summary of results in a variety of solids

Sample	T (K)	muon fraction (%)	muon relaxation (μs^{-1})	muonium fraction (%)	muonium relaxation (μs^{-1})	missing fraction (%)
α -quartz	4-295	35 \pm 5		65 \pm 5		0 \pm 7
Fused SiO ₂	4-295	30 \pm 5		70 \pm 5		0 \pm 7
Tetragonal GeO ₂	8-295	70 \pm 5		<5		30 \pm 5
Fused GeO ₂	295	76 \pm 3	.07 \pm .02	10 \pm 4	2.8 \pm 1.8	14 \pm 5
	60	36 \pm 2	.02 \pm .01	16 \pm 6	8.6 \pm 2.4	48 \pm 6
	6			9 \pm 4	4.4 \pm 1.0	
Hexagonal GeO ₂	295	61 \pm 3		<2		39 \pm 4
	90	48 \pm 3	.16 \pm .02	13 \pm 6	.35 \pm .06	39 \pm 7
MgO	6	40 \pm 2	.09 \pm .01	30 \pm 10	5.7 \pm 1.3	30 \pm 10
SrTiO ₃	80	100 \pm 3				
	32	52 \pm 3		<5		48 \pm 6
TiO ₂	4-295	60-70				
Be ₃ Al ₂ Si ₆ O ₁₈	295	16 \pm 5		<10		84 \pm 15
ZrSiO ₄	295	40 \pm 5		<5		60 \pm 10
Diamond	295	48 \pm 2	.05 \pm .01	33 \pm 4	1.807 \pm .042	19 \pm 4
	6	21 \pm 30	.12 \pm .03	26 \pm 5	7.2 \pm 1.0	53 \pm 30

Table III Purities of materials used

Material	Manufacturer	Impurities
α - quartz	Sawyer Research Products Inc.	<0.01 ppm Fe, <0.3 ppm Mn, 1-5 ppm Na, 5-20 ppm H, 0.2-0.5 ppm Al, 0.5-1.0 ppm Li
TiO ₂	Adolf Meller Co.	<50 ppm Fe, Si, Ni, Mo, Cr, <30 ppm Co, B, <10 ppm Cu, Te, Mn, Mg, Be, Bi, 40-64 ppm Al
SrTiO ₃	Adolf Meller Co.	<50 ppm Fe, Si, Ni, Mo, Cr, <30 ppm Co, B, <10 ppm Cu, Te, Mn, Mg, Be, Bi, 40-64 ppm Al
MgO	Adolf Meller Co.	110-140 ppm Fe, 3-20 ppm Mn
tetragonal GeO ₂	John W. Goodrum	40 ppm Fe, 30 ppm Cr, 80 ppm Al
hexagonal GeO ₂	John W. Goodrum	50 ppm W, 20 ppm Na

violation, it was suggested [Vester 57] that there might be some connection between these two observations. A large number of experiments have failed to produce conclusive evidence of such a connection, but the present work was begun at a time when Garay [74] apparently had found one.

The attempts to find a link have taken two routes. One is to attempt through heavy bombardment with particles of only one handedness, for example longitudinally polarized electrons, to differentially decompose a racemic mixture [Bonner 76]. The other is to use, say, the positron, which is created in β -decay with a handedness, as a direct probe, looking directly, on an individual basis, at the interactions of the polarized particles with the medium. This discussion will be restricted to the latter approach. An excellent collection of work on the subject of the origins of optical activity in nature has been edited by Walker [79].

Garay did an experiment looking at positronium formation. The positron acts much like the muon in that it captures an electron whose spin is either parallel or anti-parallel to its own, forming the e^+e^- bound state called positronium (Ps). The two are called ortho (o-Ps) and para (p-Ps) positronium, respectively. A positron undergoes mutual annihilation with an electron to produce gamma rays. If the positronium is unperturbed the annihilation will be between the bound positron and electron; p-Ps having a shorter lifetime ($\tau = 1.2 \times 10^{-10}$ s) than o-Ps ($\tau = 1.4 \times 10^{-7}$ s) producing two gamma rays, whereas o-Ps produces three gamma rays. In condensed matter, o-Ps usually transforms to p-Ps, which then decays, but this still takes longer than the direct decay, and so the initial quantities of p-Ps and o-Ps can in principle be measured from the observed lifetimes [Mogensen 74]. Garay attempted to measure the relative amounts of p- and o- Ps in single crystals of the L and D forms of some amino acids, and claimed the ratio of p- to o- Ps was different in the two isomers.

Garay suggested an explanation of this difference in terms of a "helical electron gas" model which said that electrons travelling in a handed molecule would tend to have their spins aligned in one way, say parallel to their motion. In the same molecule, but of the opposite handedness, the spins would be anti-parallel to their momentum. Thus the electrons would

show positive helicity in molecules of one hand and negative helicity in the other. Since a positron or a muon will tend to capture electrons whose velocity is parallel to their own³⁶, if these electrons have helicity then the ratio of p- to o- Ps in the case of the positron, or triplet to mixed muonium in the case of the muon, normally expected to be one, would be different from one and would be different for the two molecular hands.

The muon should be more sensitive than the positron to any such effect because:

1. its polarization (helicity) can be reversed by changing from surface or forward muons to backward muons, thus providing a check on systematic errors;
2. its greater mass means its direction at the time of capture will be more likely to be the original direction than for the lighter positron. That is, at lower energies they retain their helicity better than positrons.

At the time it was not possible to observe muonium in amino acids or sugars, as they have many nuclear moments, so quartz was chosen as it was known from previous work that it exhibited a large muonium fraction. An additional feature of quartz is that its optical handedness is reversed for the secondary optic axes relative to the principal optic axis.

A high statistics experiment was performed to measure the muonium amplitude in a weak transverse magnetic field using forward and backward muons in left- and right-handed quartz, parallel and perpendicular to the principal optic axis. The final result is a difference in amplitudes of $(1.08 \pm 0.86)\%$ where the error is, as usual in this thesis work, one standard deviation. This number gives no particular confidence in saying that it is not consistent with zero. A more detailed discussion can be found in [Spencer 79].

At about the same time other experimenters [Jean 79] repeated Garay's work with positrons and got a null result to better precision than his experiment. They stated that his results could be explained by the presence of defects in his samples.

³⁶The energy difference will be smaller and the time in which they are close is longer.

b. Asymmetry of Muonium (in Quartz)

i. Room Temperature: Axial Hyperfine

As is said to happen so often in science, serendipity took a hand, yielding results unconnected with the original intent of the experiment. When the first test runs were performed, the muonium signal was observed, as in Figure 15, to have a distinct beat frequency of 0.4 MHz, whereas that expected from the quadratic Zeeman effect in the applied field of 6.3 G is only 0.018 MHz. The initial explanation of this phenomenon was that it was due to the intrinsic quadrupole moment [Baryshevsky 78, Beder 78]³⁷ of the triplet muonium atom interacting with an axially symmetric crystal field gradient [Brewer 79]. This can be described by the cylindrically symmetric anisotropic Hamiltonian described in Section III.2.

The first work of this thesis was to test the predictions of this model as given in Section III.2. One prediction was that the splitting which produces the beat should equal $\frac{1}{2}(3\cos^2\theta - 1)\Delta A$ (eq. III.13), where θ is the angle between the electric field gradient and the magnetic field. This splitting should be independent of the strength of the applied field up to the region where the quadratic Zeeman term begins to contribute. That this is true can be seen in Figure 16. The model also predicted that in zero magnetic field there would be an oscillation at a frequency $\frac{\Delta A}{2}$ whose amplitude would be orientation dependent. This can be seen in Figure 17, which shows two orientations, one in which the \hat{c} axis is parallel to the initial muon polarization, which shows no oscillation, and one in which it is perpendicular, which shows an oscillation. With the use of eq. III.16, the symmetry axis of the electric field gradient was found to be parallel to the \hat{c} axis, the highest symmetry axis of the crystal.

It is also possible to use the model to calculate the sign and estimate the amplitude of this splitting [Beder 80]. The sign may be determined by measuring the

³⁷This intrinsic moment arises from a d-orbital admixture in the ground state of the triplet atom.

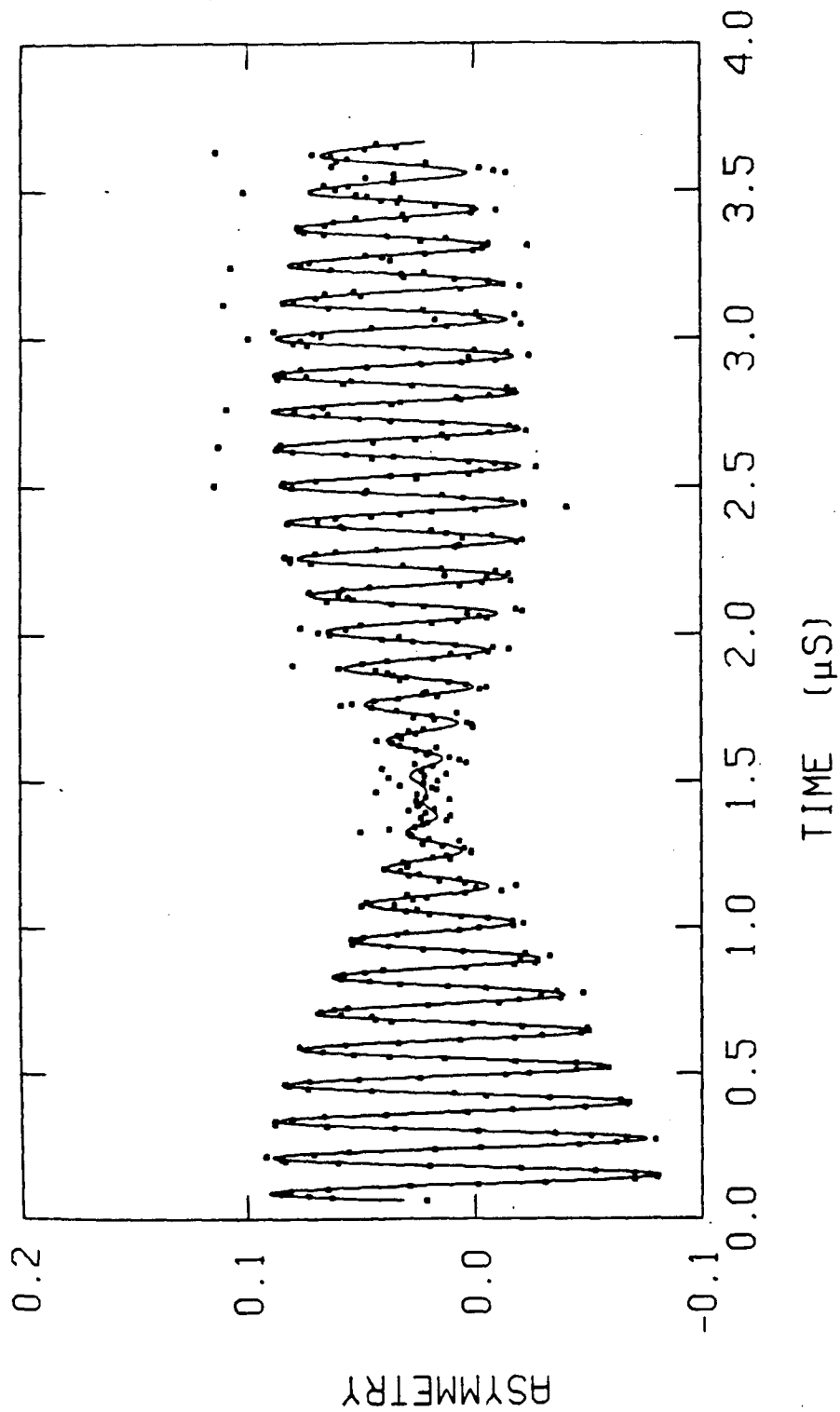


Figure 15
Data showing the distinct beating of the muonium signal in room-temperature crystalline quartz.

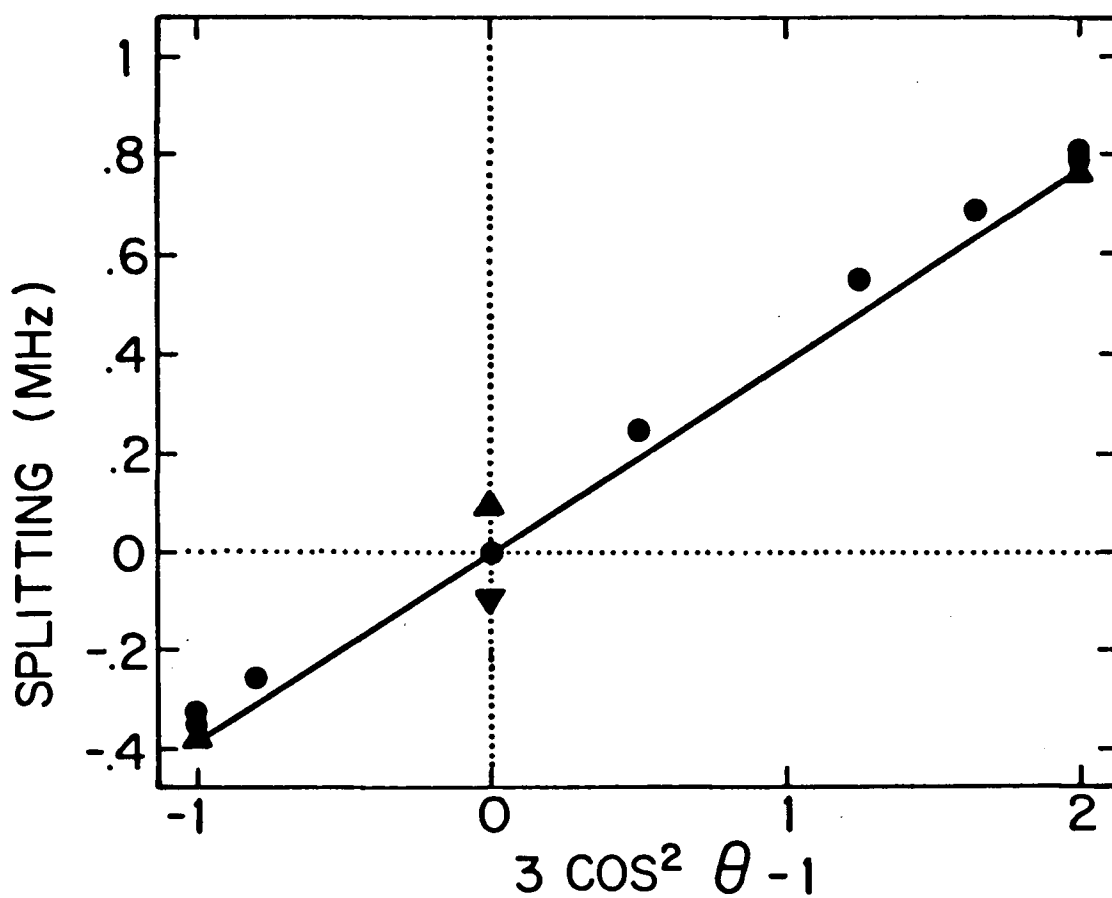


Figure 16

Anisotropy of splitting in α -quartz. θ is the angle between the ϵ -axis of the crystal and the applied magnetic field. The round points are taken at 6.3 Gauss and the triangles at 3.3 Gauss. The error bars are smaller than the points. Two triangles are plotted at $3\cos^2\theta - 1 = 0$ as the sign was not determined.

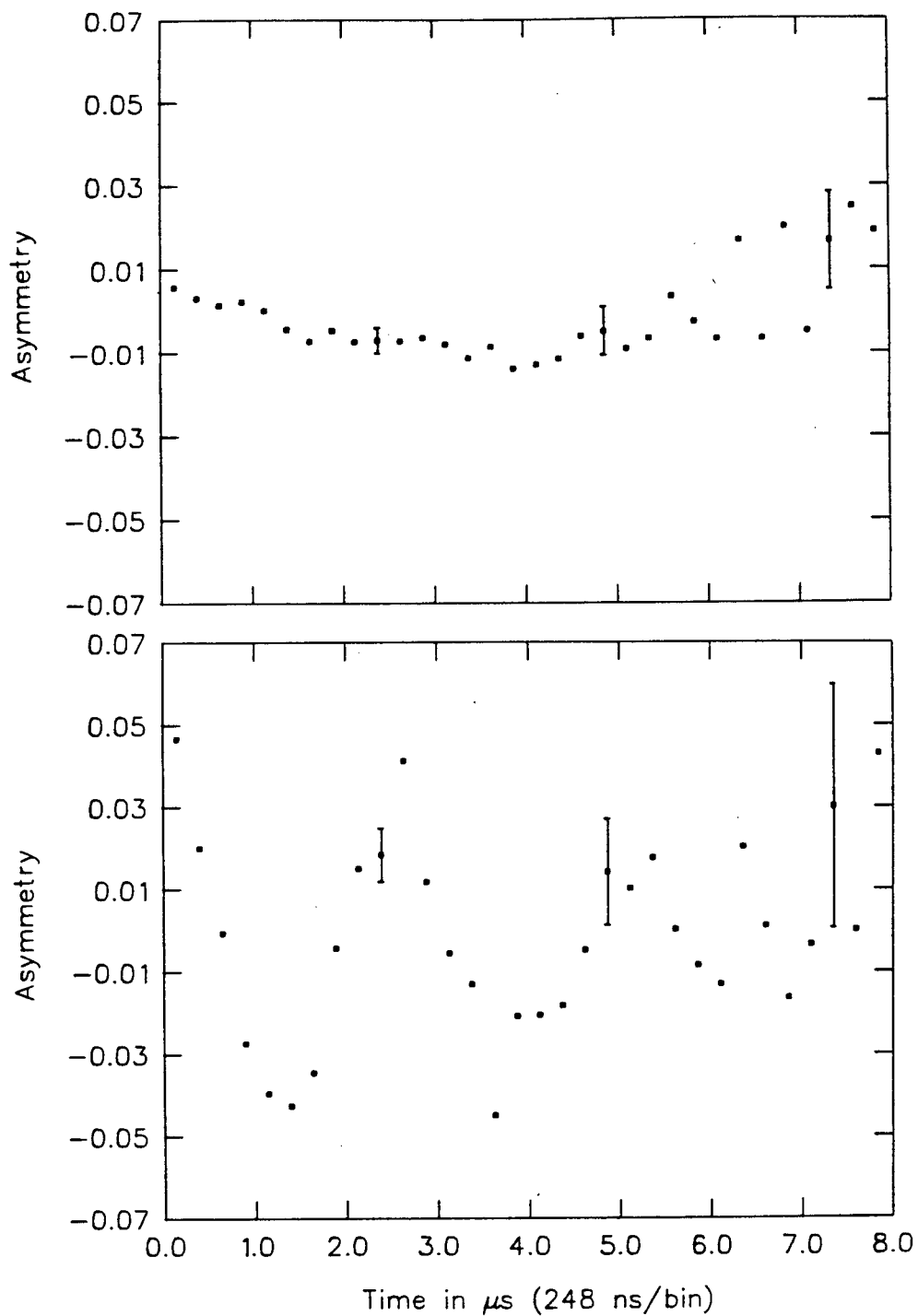


Figure 17

Muonium oscillation in zero field room temperature α -quartz. When the \hat{c} -axis is parallel to the initial polarization of the muon (top), the oscillation has zero amplitude. However, when the \hat{c} -axis is perpendicular to the initial spin, an oscillation occurs (bottom).

total splitting given by eq. III.17, as a function of the applied field. If they are of opposite sign then as the field is increased the splitting will go to zero and then increase again, whereas if they are of the same sign then the splitting will increase monotonically. From the angular dependence it is clear that the sign of the splitting depends on the angle. For $\theta = 0^\circ$ the splitting, and therefore ΔA , was found to be negative. This was confirmed in a measurement by Brown et al. [Brown 80] as well as Barsov et al. [83] who measured the sign of ΔA for $\theta = 90^\circ$. However, the sign predicted by the model is for ΔA to be positive [Beder 80]. It was then concluded that the oscillation was not due to the intrinsic quadrupole moment, but rather a more complex mixture of the intrinsic moment plus effects induced by the lattice [Weil 81b].

All these results are from room-temperature measurements. Since there are large channels along the \hat{c} axis of a -quartz and given the cylindrical symmetry of the gradients about the \hat{c} axis, it was thought that the muonium might be diffusing rapidly in that direction. It would then be interesting to see what happens at a lower temperature, where the muonium might diffuse more slowly.

ii. Low Temperature: Completely Anisotropic Hyperfine

Accordingly, with zero magnetic field, a sample was cooled and a dramatic change took place. Below about 100 K, instead of the single, low-frequency (0.4 MHz) signal seen at room temperature, three higher frequencies at 1.7, 6.2 and 7.9 MHz were seen. The frequencies were independent of sample orientation, but the amplitudes were strongly angle dependent, as shown in Figure 18. The top spectrum shows the intensity pattern for the crystal y axis parallel to the initial muon spin direction, exhibiting the 1.7 and 6.2 MHz signals, and the bottom one shows the spectrum for the \hat{c} axis parallel to the initial muon spin, yielding the 1.7 and 7.9 MHz signals. This latter orientation is the one for which no oscillation could be observed at room temperature. The lower two frequencies sum to the upper. More exact values, as given in Table IV, are: 1.692(11), 6.218(12), 7.899(10), and summing the lower two gives 7.910(16), in excellent agreement with the

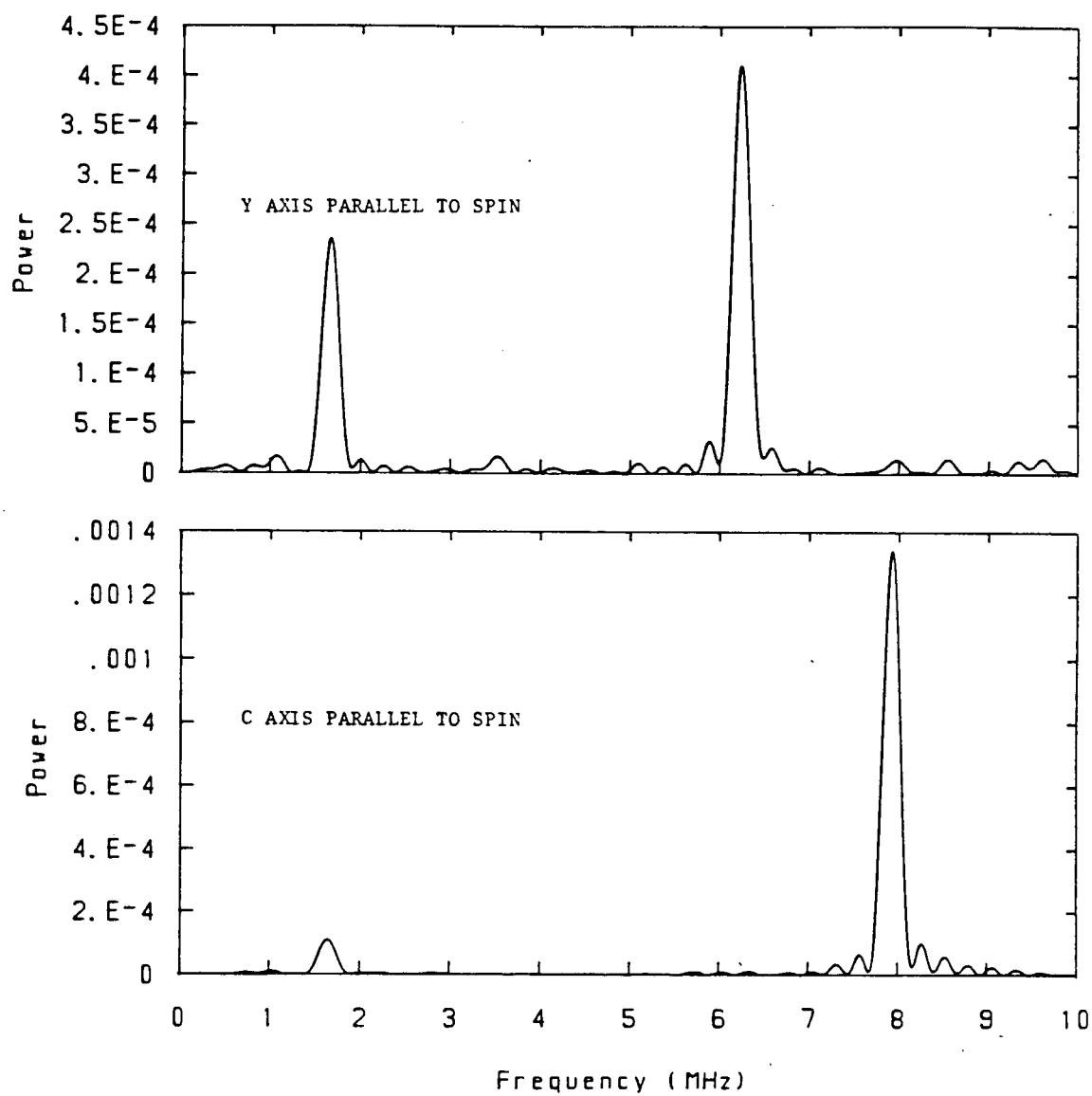


Figure 18
Fourier transforms of 6 K data in α -quartz showing the angular dependence of the signal intensities, with the frequencies constant

Table IV Predicted and Observed Hyperfine and Superhyperfine Transitions for Muonium in α -quartz

Predictions of Muonium Frequencies from Hydrogen EPR Data (MHz) [Isoya 83]	2.26(7)	9.14(6)	11.4(1)
Observed Muonium Frequencies (MHz)	1.692(11)	6.218(12)	7.899(10)
Ratios	1.33(4)	1.47(1)	1.44(1)
Predicted Superhyperfine Frequencies (MHz)	1.9	8.0	9.8
Predicted Intensities	0.026	0.0031	0.071

The observed hyperfine frequency for muonium is 4505.0 MHz at 30 K, [Holzschuh 81] whereas that predicted from hydrogen EPR data is 4561.8.

Angles of the principal axes for hydrogen and muonium, angles in degrees.

Hydrogen	113.75(19)	23.75(19)	90.00
Muonium set 1	118(5)	28(5)	90(5)
Muonium set 2	62(5)	152(5)	90(5)

observed value. This looked like a quadrupole moment in a non-cylindrical field gradient, and is described by the anisotropic Hamiltonian given in Section III.3 where each of the three sites related by the three fold axis has its own hyperfine tensor, with the same principal values. This Hamiltonian has the same form as that observed for hydrogen in α -quartz [Isoya 83].

These measurements represented the first time that a completely anisotropic hyperfine interaction was seen for muonium; and it is of some historical interest to point out that the first time an anisotropic spin Hamiltonian was seen for the hydrogen atom, it was also in quartz [Perlson 74].

If the site seen for muonium were exactly that seen for the hydrogen atom, then the frequencies arising from the anisotropies would be as given in Table IV, which also presents the observed frequencies, as well as the isotropic value of ν_0 measured by Holzschuh et al. [81]. Note that the observed frequencies from the anisotropies are about 1.4 times less than those predicted, and the isotropic term is 1.3% less than that expected based on the hydrogen results. These differences are perhaps due to the increased zero-point motion of muonium versus hydrogen, a trend which is consistent with Isoya et al.'s [83] observation that deuterium shows a larger shift than hydrogen from the vacuum value and also that the anisotropies are larger for deuterium than for hydrogen. The value of ν_0 for both muonium and the hydrogen atom are higher than the vacuum value; 0.9% for muonium, and 2.2% for hydrogen. This suggests that the lattice compresses the atom, as discussed in Isoya et al. [83].

As shown in Section A2.3.c and mentioned above in Section III.3, the observed μ SR intensities can be used to deduce the orientation of the principal axes of the site with respect to the crystal. However, as shown in Section A2.3.d, in zero magnetic field the presence of the three-fold symmetry axis destroys all information about one of the angles, ϕ , that which gives the angle around the \hat{c} axis with respect to the y axis. If a magnetic field is applied, this information should be obtainable, at the cost of a very

messy spectrum with as many as nine muonium signals at different frequencies. The angular information can in principle be extracted from the splitting of these transitions as a function of the angle between the crystal axes and the field. Unfortunately, this was not realized at the time the experiments were done and so it remains as a worthwhile project for future studies. Nevertheless, the angles of the site axes with respect to the \hat{c} axis were determined, and were found to be $118(5)^\circ$, $28(5)^\circ$, and $90(5)^\circ$ at 6 K, which are within error of the hydrogen numbers which are $113.75(19)^\circ$, $23.75(19)^\circ$ and 90.00° at 40 K [Isoya 83]. The hydrogen site is shown in Figure 19 and more details of the hydrogen site can be found in the paper by Isoya [83]. There are two choices of sets of angles due to the fact that it is the square of the cosine which is observed in zero field. These are given in Table IV. One set does agree with the observed hydrogen numbers. This was the first time that muonium was unequivocally shown to behave just like an isotope of hydrogen in the solid phase.

iii Superhyperfine interaction

For hydrogen in quartz, Isoya et al. [83] confirmed their choice of site by observing the coupling of a nearby ^{29}Si nucleus via the superhyperfine interaction. The expected angle the axis between the two nearest neighbour silicons makes with the \hat{c} axis is 112° from the structure [Le Page 80], and the angle found is 116.5° which agrees well enough. An attempt was made to observe this interaction for muonium which would have been the first direct observation with μSR of lines due to a superhyperfine interaction. A broader discussion is available in a paper by Beck et al. [75]. Only 4.7% of the Si nuclei are ^{29}Si , but there are two equivalent silicons in the site, so 9.4% of the sites should have a ^{29}Si and exhibit the superhyperfine coupling. The calculation done in Section III.4 for hydrogen can now be applied to muonium where the crystal z axis is parallel to the initial muon polarization, in zero applied field. It is necessary to scale the H atom values both by the ratio of the magnetic moments and also by the factor 1.4 observed for the anisotropic hyperfine frequencies. The result is three peaks, at 1.9, 8.0,

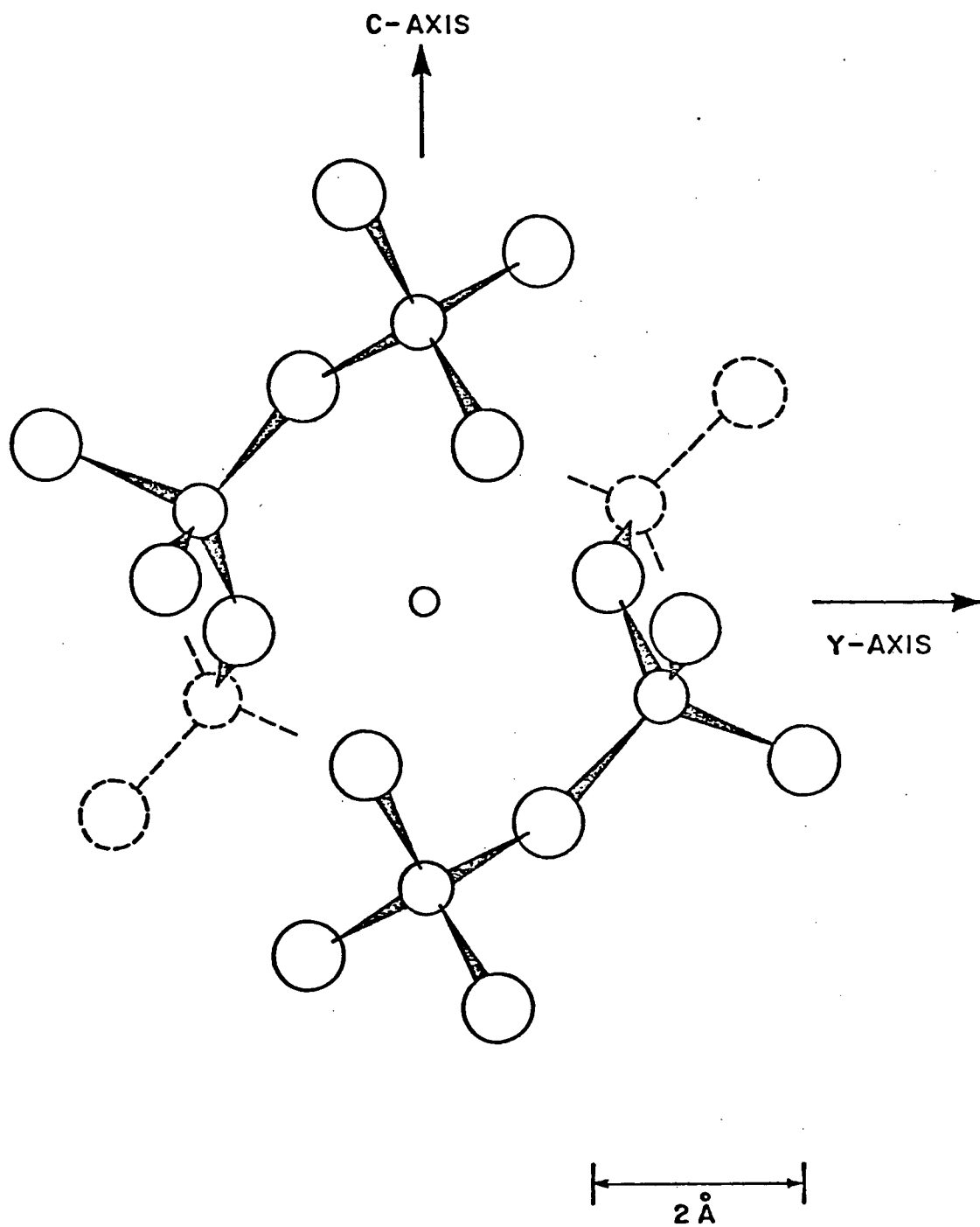


Figure 19

Diagram of the hydrogen site in α -quartz, adapted from Isoya [83].

and 9.8 MHz, given in Table IV, whose intensities with respect to the major anisotropic hyperfine peak at 7.9 MHz, are 0.026, 0.0031, and 0.071 respectively, taking the natural abundance as well as the intensity tensors into account. These peaks are in addition to those normally expected from the anisotropic hyperfine interaction in this orientation at 1.7 and 7.9 MHz. As shown in Section II.5, the quality of a μ SR signal is proportional to A^2N , which means that about 250 times as many events would be required to see the largest of these three additional signals as to see the one at 7.9 MHz.

A series of runs at 6 K were made over a period of about 24 hours and the sum of these, corresponding to 100 million events, is plotted in Figure 20. Unfortunately, when a standard fit to the time histogram was attempted, it was found that the clearly visible relaxation envelope of the normal 1.7 and 7.9 MHz signals did not fit to any of the standard functions, Lorentzian, where the relaxation is $e^{-\lambda t}$, or Gaussian, where the relaxation is $e^{-\sigma^2 t^2}$. This can be seen by inspection. Other functions were tried, at considerable expense of real and CPU time, but none of them proved satisfactory. In spite of this, some fits were tried with an additional frequency to see if the χ^2 improved noticeably. The best fit gave an additional frequency at about 8.5 MHz, and changed the χ^2 from 4246.6/323 degrees of freedom to 3269.8/320 degrees of freedom. It was thought that this improvement might be due to an artifact of fitting a shoulder of the poorly fit main peak, so as a check, the χ^2 for a frequency of 7.3 MHz, an equal distance from the main peak, was found to be 4030.2/320. A rule of thumb [Bevington 69] when adding a parameter is that unless the change in χ^2 exceeds the ratio of the χ^2 to the number of degrees of freedom, it cannot be said to be significant. In the present case the ratio is 13.1. For three parameters, then, the additional parameters may be significant if the change in χ^2 exceeds 39.3. The observed change is 976.8. By comparison, the fit to an assumed peak at 7.3 MHz changed the χ^2 by only 216.4. This latter change is far less than that observed for the 8.5 MHz fit, but by the crude rule used might possibly be significant. This is a good indication that the 8.5 MHz peak is real, but the fit is still

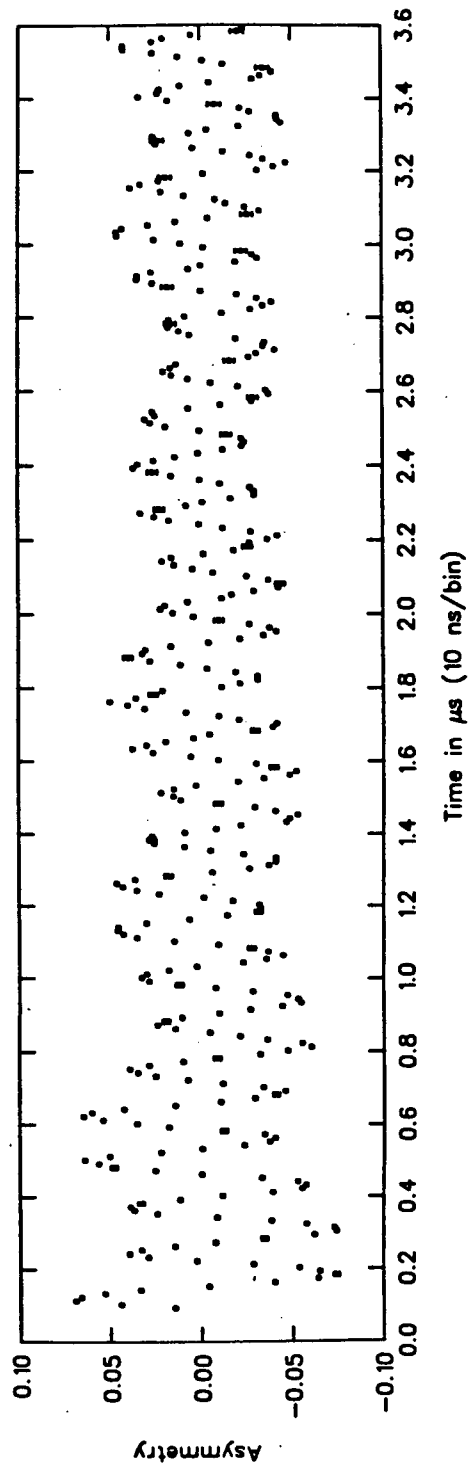


Figure 20

Muonium signal at 6 K. Very high statistics. Note that the relaxation envelope is not Lorentzian nor Gaussian, as the signal relaxes at early times faster than later times.

appallingly bad.

Fast Fourier Transform techniques were also applied to this high statistics data using various apodizations, and the results are shown in Figures 21 and 22. The usual ringing is so intense in both the unapodized and weakly apodized³⁸ spectra in Figure 21, that it would mask any additional frequencies out to 9 MHz. The strongly apodized spectrum (bottom Figure 22) is so broad that it also masks all frequencies out to 9 MHz. The spectrum with medium apodization (top Figure 22) indicates a peak at about 8.6 MHz. That it is only a bump on a larger peak and shows up only under carefully chosen conditions casts doubt upon its reality.

A WSFT analysis was also done, as shown in Figure 23, and it, too, shows a peak at about 8.5 MHz. This WSFT peak looks much more convincing than the FFT peak, but it is still a small bump next to a huge bump, though, so this, too, is not conclusive. Moreover, the WSFT analysis is not truly independent of the normal fitting procedure, so it cannot be said that this 8.5 MHz signal has been seen by three independent methods of data analysis.

That this peak is at lower frequency than the 9.8 MHz predicted by the hydrogen data (Table IV) is surprising, as the coupling is very sensitive ($1/r^3$ [Isoya 83]) to the distance from the muonium electron to the ²⁹Si nucleus. Since the muonium has a larger zero-point motion than hydrogen, $\langle 1/r^3 \rangle$ should increase, shifting the peak to higher frequency. No such peak is observed. Isoya et al. [83] report that the coupling for deuterium is about 10% smaller than for protium, as expected, counter to the result for muonium. The 8.5 MHz peak may be:

1. an artifact of the fitting procedure due to the obscure nature of the relaxation;
2. from a next-nearest or next-next nearest neighbour interaction, as seen by Isoya et al. [83] for hydrogen;

³⁸The apodization functions used are those recommended by Norton and Beer [76] as optimal in their suppression of sidebands relative to the broadening of the central maximum.

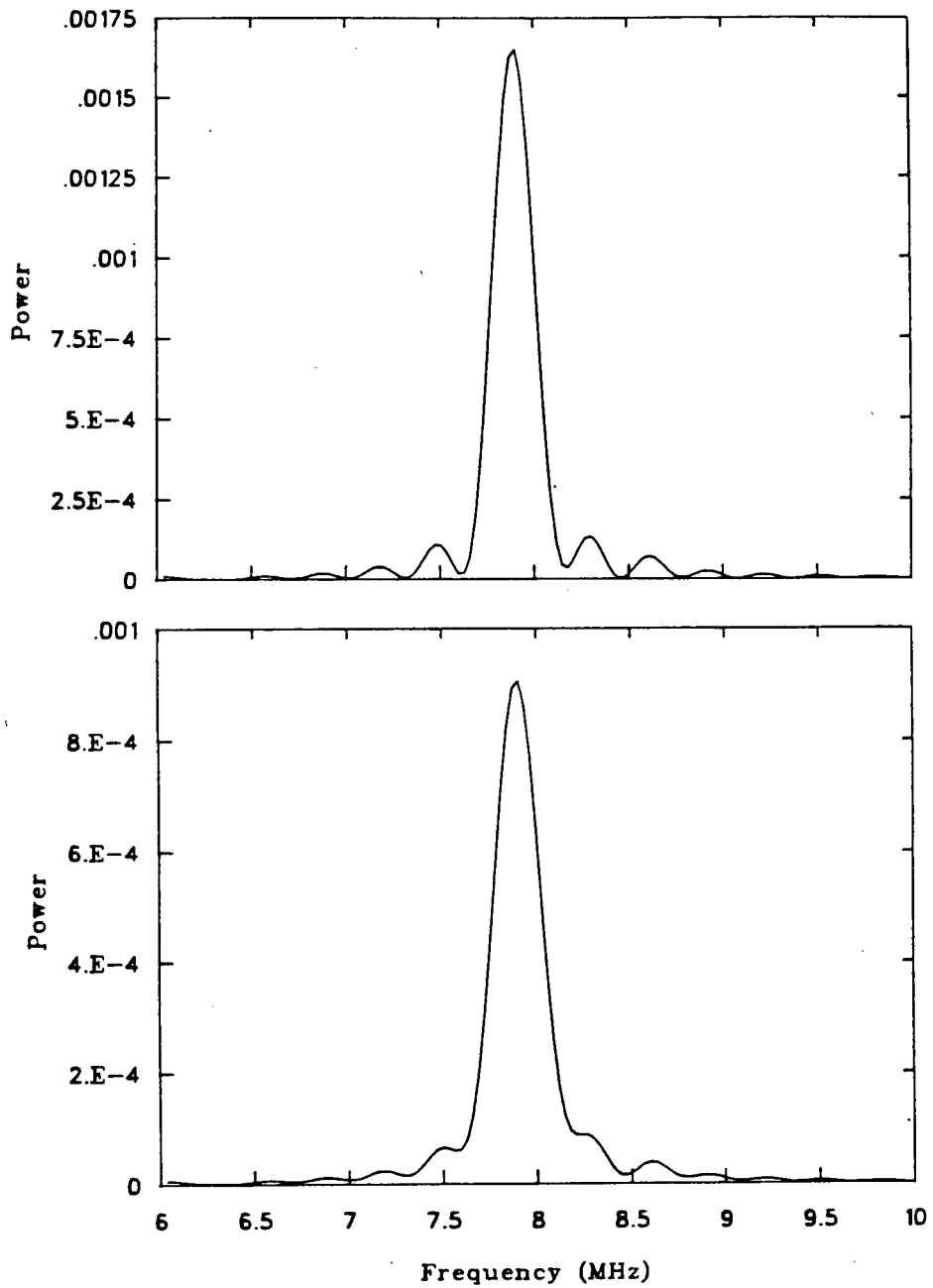


Figure 21

Fourier Transforms of the high statistics 6 K α -quartz data. The unapodized spectrum (top) shows a great deal of ringing, as does the weakly apodized.

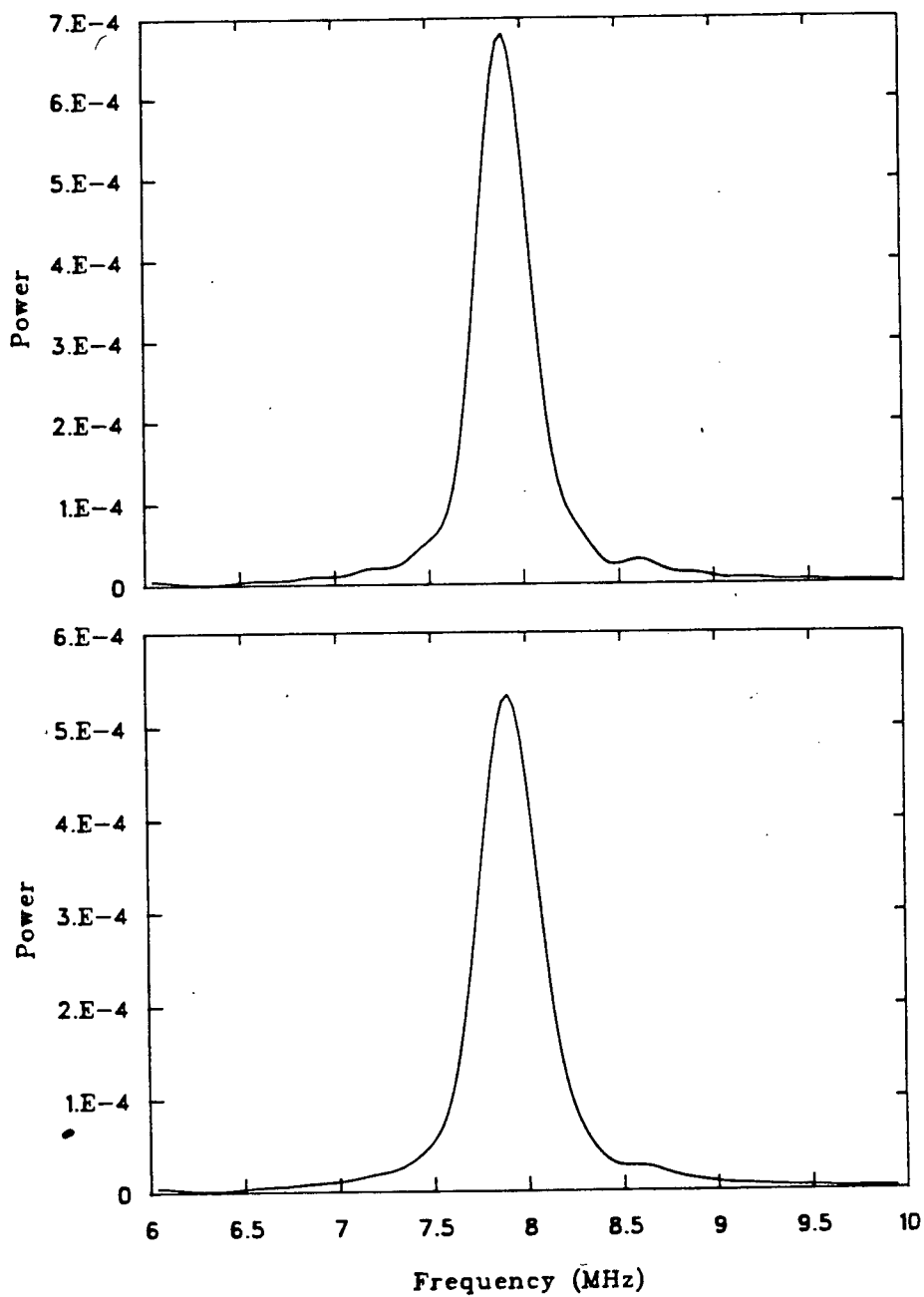


Figure 22

Fourier Transforms of the high statistics 6 K α -quartz data. The strongly apodized spectrum (bottom) is very broad, but the medium apodization gives a hint of a bump at 8.6 MHz.

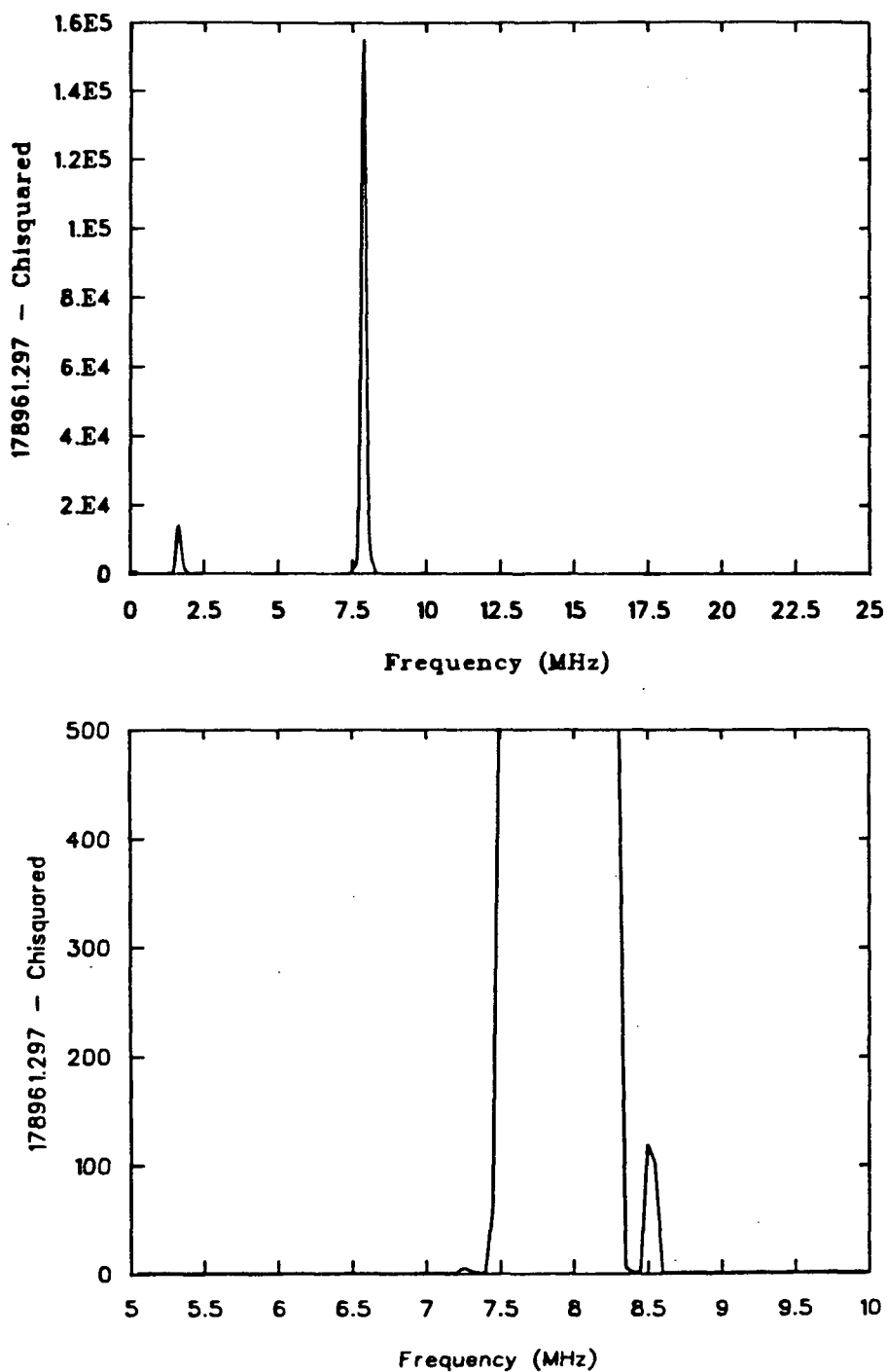


Figure 23

WSFT of the high statistics 6 K α -quartz data. The bottom plot is shown with a greatly expanded scale. For convenience, the chisquared was subtracted from the maximum observed value.

3. from a different type of site from the major peak at 7.9 MHz.

The question would then remain: where is the peak expected from the superhyperfine interaction? The relaxation seen is probably due to the RLMF from the ^{29}Si nuclei. It is perhaps ironic that the difficulty in seeing the ^{29}Si superhyperfine interaction in quartz was due to the presence of the other ^{29}Si nuclei.

It should be noted that the predicted frequencies and intensities are based solely on the data for hydrogen, and are quite sensitive to the values used. For instance, it may be that the 8.5 MHz peak is not that from the 7.9 MHz transition, as expected, but that from the 6.2 MHz transition, which had been expected to be at 8.0 MHz (Table IV). Although this peak was expected to have a much lower intensity, the larger zero-point motion might alter the interaction enough to allow it. This would also then fit with the expected *increase* in the frequency. Due to this aspect of the problem, any further search for a peak from the superhyperfine interaction in quartz must also show the peak or peaks at more than one crystal orientation, allowing all three to be visible, thus making an unambiguous assignment possible. A sample which was isotopically enriched in ^{29}Si would be extremely helpful in any future search. The maximum amplitude for the occurrence of a single ^{29}Si nearest neighbour per site occurs when the abundance is 50%. Since the residual range of surface muons is about 100 mg/cm^2 , for a 1 cm^2 sample, only 100 mg of quartz would be required. Since silicon makes up about 50% of the mass, only 25 mg of ^{29}Si would be required. To make a sample in which changes in orientation were possible would require more material, but if three such thin slices could be grown in the appropriate orientation and arranged as three perpendicular faces of a cube, still only 75 mg of ^{29}Si would be required. Perhaps these could be grown as surfaces on the faces of a cube of unenriched quartz. If a spin rotator, such as that mentioned in Chapter II were available, then the changes of the crystal axis with respect to the muon spin direction could be accomplished by rotating the muon spin, allowing the use of a single thin slice.

iv Intrinsic Quadrupole Moment

Although the picture of an intrinsic quadrupole moment in an electric field gradient is physically appealing, a simple calculation by Beder [80] of where this moment is located shows that fully one-half is located quite far from the nucleus, beyond two Bohr radii. At this radius the electron is certainly interacting strongly with the lattice and the electric field gradient is changing rapidly. Although the Hamiltonian is correct, the physical interpretation is not as clear as for the case of a nuclear quadrupole in an electric field gradient, where the extent of the nuclear charge distribution is small compared to the distances to neighbouring atoms and more fundamentally, the quadrupole moment is not at all influenced by the electric field. A calculation by Weil [81] for hydrogen in quartz suggests that a 2p admixture might be sufficient to account for the observations. However, this is forbidden by the symmetry of the site for a static hydrogen atom. If, however, the atom is moving, even with just the expected zero-point motion, this admixture will be allowed [Isoya 83]. Goshen et al. [83] show that a d-orbital admixture caused by the lattice is a reasonable possibility and would give this result even for a static atom. More detailed calculations of the hyperfine structure for hydrogen-like atoms is given in a paper by Weil [81b], which does not deal with a particular lattice, but rather provides a framework for lattice calculations.

v Relaxation in alpha-quartz

As the temperature is raised the muonium begins to move, "hopping" from site to site. There are three equivalent sites related by a 120° rotation around the three-fold crystal \hat{c} axis. As previewed in Section IV.3.b, all three sites have the same three characteristic frequencies in zero magnetic field, but they give different amplitudes due to the different orientations with respect to the muon polarization at the time the muonium goes to a particular site. The result is a relaxation, and the observed rate as a function of temperature is plotted in Figure 24. As the temperature increases further the hop rate begins to be comparable to the characteristic frequencies themselves, resulting in a peak in

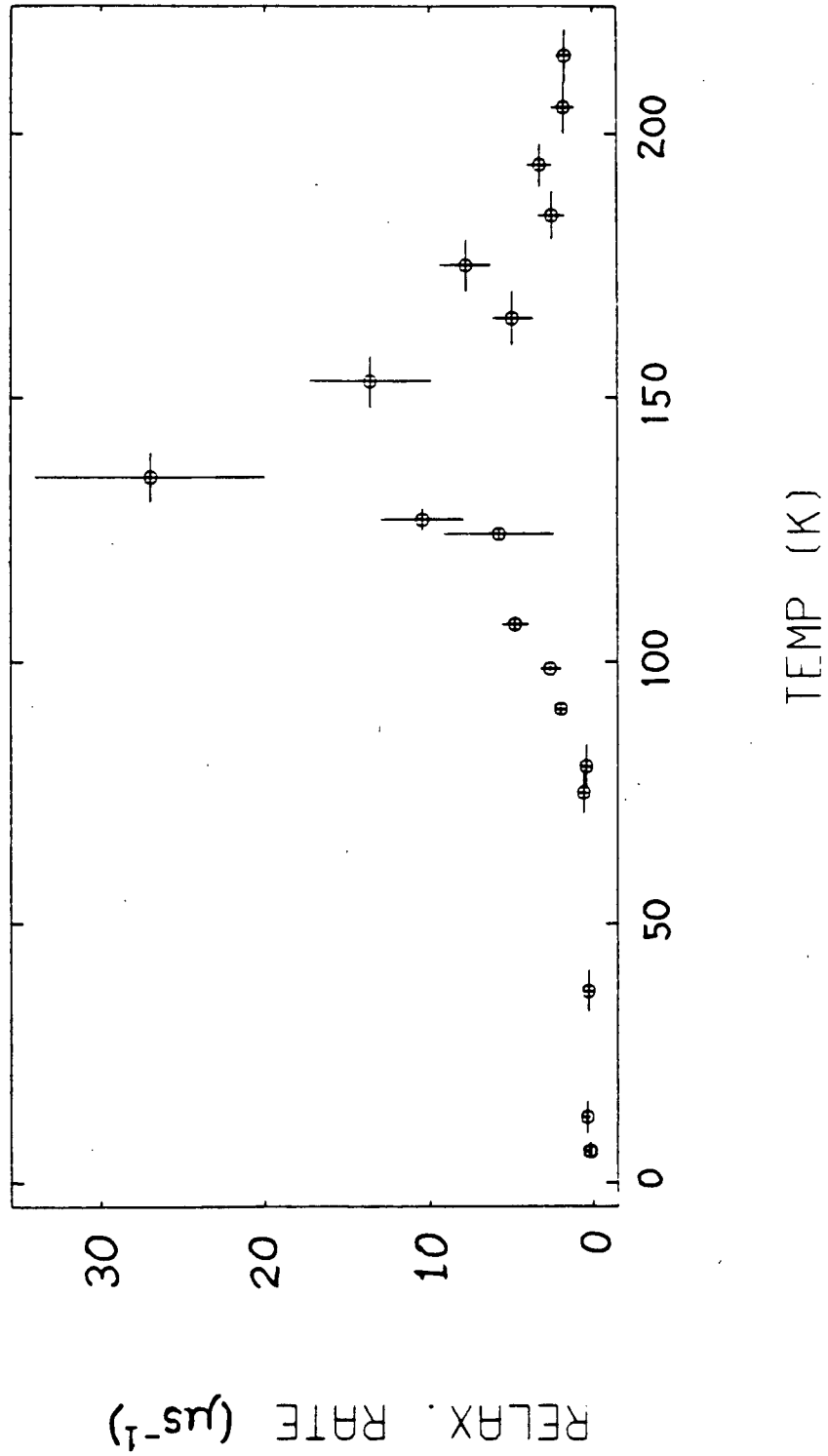


Figure 24
Relaxation rate versus temperature for α -quartz in zero field.

the relaxation at about 140 K. From the rough formula, eq. IV.2, $\lambda = 4f$ gives $32 \mu\text{s}^{-1}$, and the maximum observed rate is $27 \pm 7 \mu\text{s}^{-1}$, in very good agreement, especially since there is no guarantee that the real maximum was observed. Above this temperature, the muonium hops so rapidly that it begins to average the sites resulting in a motional narrowing which reduces the relaxation with increasing temperature, as seen in Figure 24. The result is that the average of these three sites has cylindrical symmetry with the unique axis the three-fold axis. This should sound familiar, as it is the observed room-temperature situation of a slowly relaxing single frequency as in Figure 17.

If the tensors corresponding to the three low-temperature sites are averaged to give the axially symmetric tensor, the result gives $\Delta A = -1.44 \text{ MHz}$, which has the observed sign, but a different magnitude, from the value observed at room temperature of -0.8 MHz . Holzschuh et al. [81] calculate $\Delta A = -5.4 \text{ MHz}$, again with the observed sign but yet another magnitude. That the calculated numbers are different from the observed one is not particularly surprising as the crystal lattice does change slightly with temperature, and as the observed frequencies are small differences between large numbers; extrapolating from 6 to 295K is almost certain to be incorrect. That even the signs agree is probably fortuitous. Isoya et al. [83] have observed changes in the hyperfine parameters for hydrogen, but the EPR spectrum was not reported above 100 K since the hydrogen signal vanishes, at too low a temperature to be useful for extrapolation. Holzschuh et al. [81] report changes in the hyperfine frequency ν_0 at or near room temperature, too high a temperature to compare to the muonium low-temperature results. The μSR results above 100 K and the site determination by EPR together provide a nice example of the complementarity between μSR and EPR.

vi Fused Quartz

Some measurements were also done on fused quartz; even though it had been used many times before in μSR [Brewer 75] due to its large muonium fraction, this was the first study in which the relaxation rate as a function of temperature was studied in

detail. The relaxation rate is shown in Figure 25, where it is seen to decrease monotonically with increasing temperature, in marked contrast to the behaviour seen in crystalline quartz, shown in Figure 24. This fused quartz data was taken in an applied field of 10 G, and a typical plot of the room temperature data is in Figure 3. The model proposed to explain the relaxation is the same as that for crystalline quartz, except that in fused quartz a large number of anisotropic sites exist with different parameters, so each muonium atom precesses in its local environment, each with a different set of frequencies and amplitudes. The result is a relaxation as the phase coherence of the ensemble is lost. Below 50 K, the relaxation rate is no longer temperature dependent, so it is concluded that the muonium is static and so the relaxation rate represents the distribution of frequencies from the anisotropic hyperfine interaction. At higher temperatures the muonium hops and averages these sites which leads to motional narrowing, as was the case for the crystalline phase. In principle it should be possible to calculate the diffusion rate from the observed relaxation rates; however, the theory is not yet sufficiently advanced for this to be possible.

vii Summary of MSR in Quartz

The amplitudes of muonium in fused and crystalline quartz are within error of each other as shown in Table II. Neither exhibits a missing fraction, which is unusual in the solid state. The relaxation rate in fused and crystalline quartz may still be decreasing with increasing temperature at room temperature. The levels of impurities are at about the same levels in the fused and crystalline, so if impurities dominated the relaxation, then they should have the same relaxation rate. This would also be true if the relaxation were due to ^{29}Si nuclear moments. The observed rates are similar, with the fused quartz having a slightly higher rate, $0.30(5) \mu\text{s}^{-1}$ compared to $0.19(2) \mu\text{s}^{-1}$, perhaps due to the random anisotropies not being fully averaged. Measuring the relaxation rates at elevated temperatures might clarify this. A sample of natural quartz did show a faster relaxation, $0.43(3) \mu\text{s}^{-1}$ compared to $0.19(2) \mu\text{s}^{-1}$, than the synthetic one used in these studies,

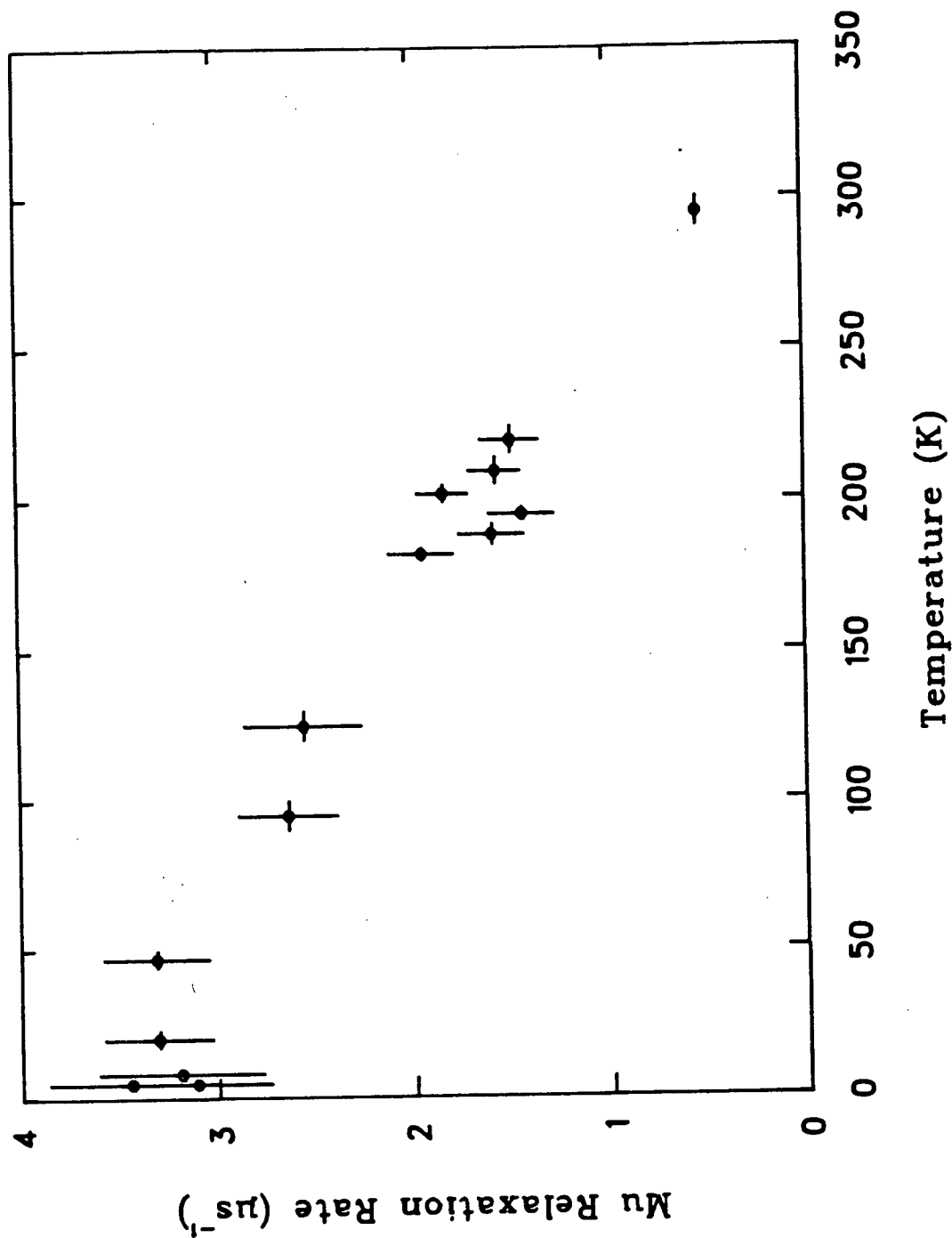


Figure 25

Relaxation of the muonium signal in fused quartz versus temperature.

presumably due to higher concentrations of impurities.

α -quartz undergoes a phase transition at about 845 K [Fron del 62], and studying the muonium frequency and relaxation rate as it goes through this transition might be interesting. It is unfortunate that even at room temperature the muonium is hopping so fast that the direct hyperfine observations of Holzschuh et al. [81] only reveal the average. There are also a number of other forms of SiO_2 , such as cristobalite, tridymite, keatite, coesite and stishovite [Fron del 62] and from the point of view of studying muonium formation it would be interesting to see if these showed a different probability of muonium formation. They are not generally available as large single crystals, though, so that it might be difficult to see muonium if the completely anisotropic hyperfine interaction is present³⁹. Fused silica can be prepared with various amounts of other materials, such as Na_2O present. A series of experiments with various mixtures, as suggested by A. M. Stoneham [84], might be revealing as to the mechanism of formation of muonium in solids, much as mixtures of liquids have done for the study of the formation of muonium in liquids and to belabour the point, mixtures of gases have done for muonium in gases.

As shown in Section A2.3.c, an anisotropy in the hyperfine Hamiltonian can lead to a signal amplitude in the direction perpendicular to the initial muon spin even though there is no applied magnetic field present. This result was surprising to me and so I tested it. The data are plotted in Figure 26, and a signal is clearly visible. For certain orientations of the crystal, in particular that with the principal axis of symmetry parallel to the initial muon spin, this signal will have zero intensity.

Quartz could be considered a laboratory for μSR since it has been used in so many experiments. It was the one of the first solids in which muonium was observed, the first material used in a DEMUR (*Double Electron Muon Resonance*) experiment [Brown 80], the first material in which the completely anisotropic hyperfine interaction was

³⁹For a powder in zero magnetic field this interaction would yield three frequencies with the same intensity.

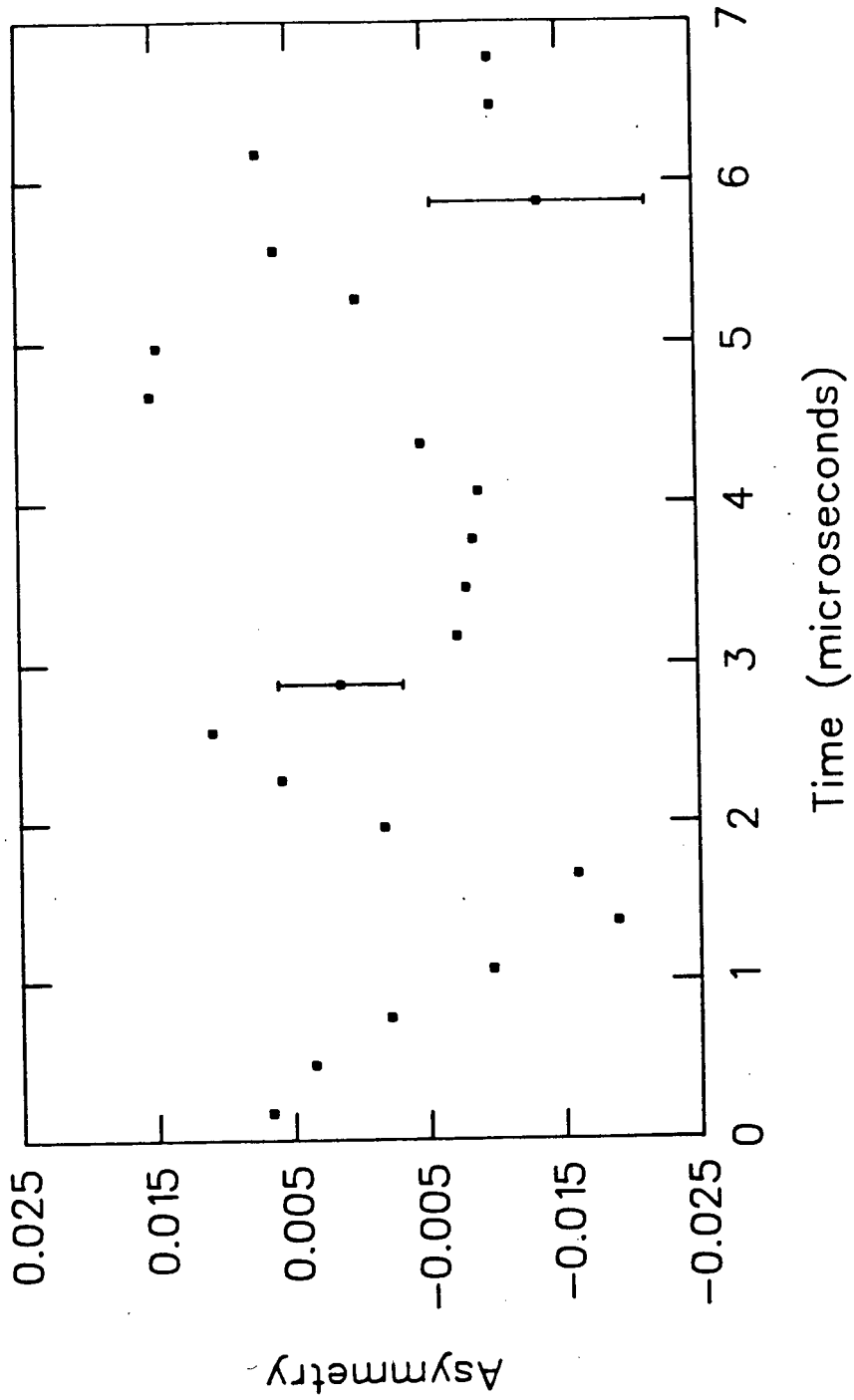


Figure 26

Muonium oscillation in zero applied magnetic field in a direction perpendicular to the initial muon spin.

observed [this thesis] and perhaps the first material in which the superhyperfine interaction was directly observed [this thesis]. This is also in some sense its role in EPR where many different paramagnetic species have been seen, ranging from the atomic hydrogen mentioned frequently in this work, to germanium, lithium, [Weil 71] and aluminum [Weil 75]. An excellent review is given by Weil [84].

2. GERMANIUM DIOXIDE

Germanium dioxide was studied due to its similarities to silicon dioxide. In particular, its hexagonal form is closely analogous to α -quartz [Young 62]. A tetragonal and a fused sample were also studied. The purities of these samples are given in Table III.

The results, however, are somewhat disappointing. As is so annoyingly common, there is a large missing fraction. This cannot be due to nuclear moments, as only 7.8% of the Ge nuclei (^{73}Ge) have nuclear spins compared to the 4.7% ^{29}Si in quartz. One of the problems with the data is that the hexagonal and fused samples were only about one cm in diameter, and the scattering from the thin counter and windows means the beam spot in the Eagle apparatus is necessarily larger than this. This reduces the data rate as many muons miss the target, and increases the background due to stops in other parts of the apparatus⁴⁰. Moreover, the conditions were not necessarily the same for all the runs, so detailed interpretation of the changes in fractions is not possible. The exception to the foregoing is that changes from no muonium observed to some muonium observed is significant.

No muonium was observed in the tetragonal sample, but a diamagnetic signal of 70 % was seen, leaving a missing fraction of 30 %. This sample was so impure as to be distinctly yellow-brown, although translucent. These coloured impurities are believed to involve unpaired electrons [Goodrum 72], so they would be highly depolarizing. Taking the large missing fraction

⁴⁰ Here the term background refers not to the background represented by the B_g term in equation II.3, counts which are independent of time, but rather to the more insidious one of spurious muon and/or muonium signals arising from muons stopping in materials other than the sample. It should be noted that muonium has never been observed in any of the materials used in the construction of this apparatus, so this background acts principally to reduce the sample muon and muonium signal intensities.

as an indication that muonium was formed and depolarized by these impurities implies that it might be fruitful to grow and study a cleaner crystal, if possible. Thermal or other bleaching methods should also be considered.

Only a small amount of muonium was observed in the fused sample which otherwise behaves just like the fused SiO_2 sample, in that the relaxation rate decreases with increasing temperature (Figure 27), although the error bars are much larger. This relaxation can be attributed, as in the case of fused silica, to random anisotropic hyperfine interactions. However, the relaxation rate in fused GeO_2 is higher at all temperatures than it is in fused SiO_2 . If the relaxation is due to the random anisotropic hyperfine interaction, then this would indicate that the deviations from anisotropy were greater by a factor of 2-3 than in fused SiO_2 , which may be related to the frequencies in hexagonal GeO_2 , as mentioned below. The hyperfine frequency ν_0 was measured in a field of 60 G, and found to be 4.0 ± 0.5 GHz, consistent with the vacuum value, and the value found in quartz. The Fourier transform is plotted in Figure 28, where the frequencies ν_{12} and ν_{23} are clearly visible, the value for ν_0 coming from these two frequencies as substituted in eq. III.9

As was expected, the most interesting result is that for the hexagonal GeO_2 , which was polycrystalline, with impurities as in Table III. Due to its structural analogy to α -quartz [Smith 64], it was expected to show similar behaviour, a large muonium signal in a site with a completely anisotropic hyperfine interaction. What was observed was a small muonium signal and a more complex zero-field frequency spectrum than anticipated.

The ordinary Fast Fourier Transform (FFT) of the zero-field spectrum at 6 K showed several frequencies as in Figure 29 (top), but due to the low signal-to-noise ratio, the World's Slowest Fourier Transform (WSFT), as discussed in Section II.3 was invented and applied. The resulting spectrum is also shown in Figure 29 (bottom). The frequencies, amplitudes, and phases of the peaks are given in Table VI. The most dramatic observation is that among the eight largest peaks there are two "triples". For the completely anisotropic hyperfine interaction one expects, as is observed in low-temperature α -quartz, three frequencies where the two lowest sum to the

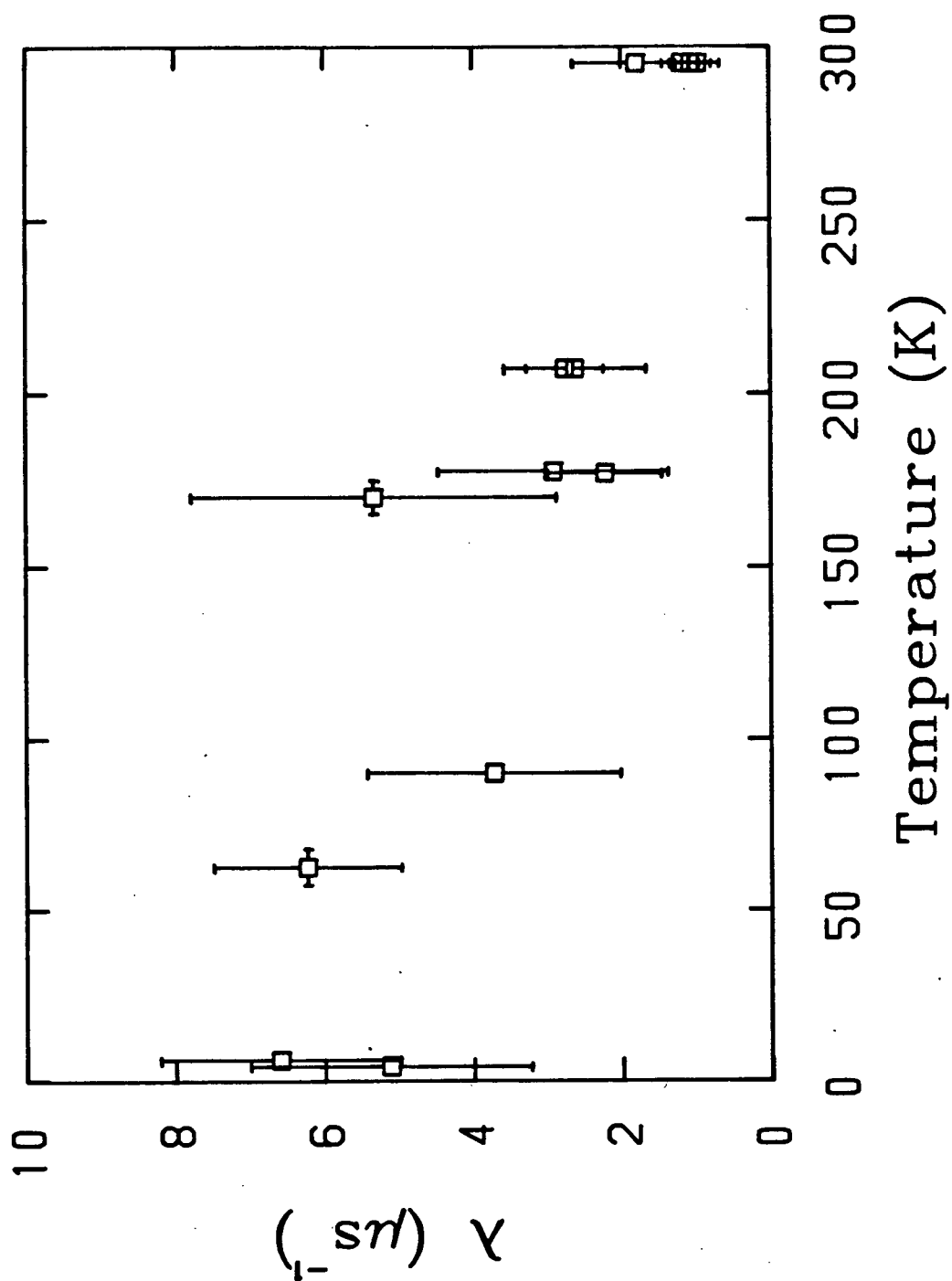


Figure 27

Relaxation of the muonium signal in fused GeO₂, versus temperature. Compare with Figure 25

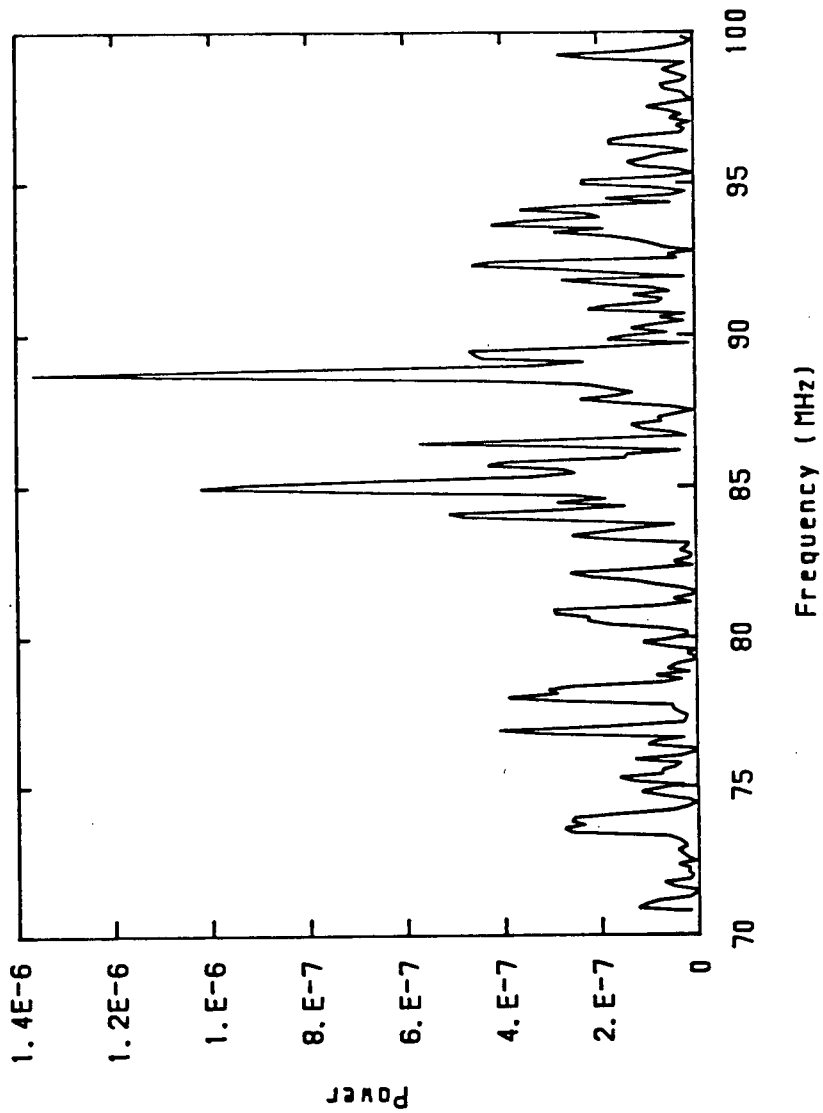


Figure 28

FFT of fused GeO₂ at 60 G, room temperature. Notice the two frequencies, the lower one being ν_{12} and the upper is ν_{23} . The splitting is 2Ω

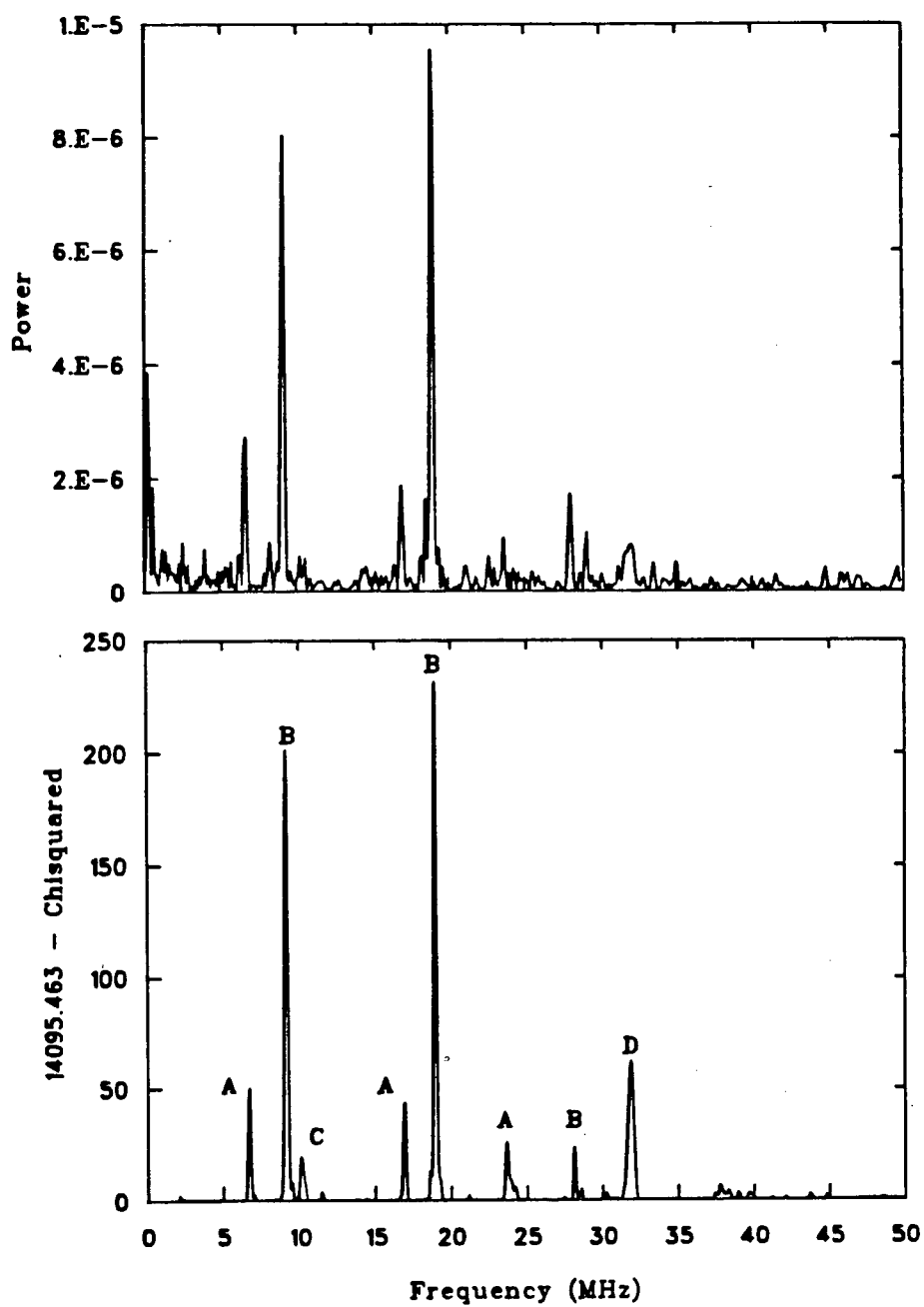


Figure 29

FFT (top) and WSFT of 6 K high statistics hexagonal GeO_2 data. The letters group the eight observed frequencies according to their assignment. See text.

Table V Frequencies observed in GeO₂

A

Frequency (MHz)	6.690(13)	16.947(18)	23.705(24)
100° Amplitude	0.27(4)	0.21(4)	0.18(4)
Relaxation Rate (μs^{-1})	0.28(6)		
Phase (degrees)	31.(5)		

B

Frequency (MHz)	9.148(8)	18.974(7)	28.177(20)
100° Amplitude	0.42(3)	0.43(3)	0.14(3)
Relaxation Rate (μs^{-1})	0.17(3)		
Phase (degrees)	21.(2)		

C

Frequency (MHz)	10.21(4)
100° Amplitude	0.28(5)
Relaxation Rate (μs^{-1})	0.98(26)
Phase (degrees)	13.(11)

D

Frequency (MHz)	31.98(3)
100° Amplitude	0.67(6)
Relaxation Rate (μs^{-1})	1.57(20)
Phase (degrees)	15.(5)

highest. This signature is observed in hexagonal GeO_2 , only there are two such triples. The sets of frequencies are labelled A and B, as shown in Figure 29; there are also two additional peaks labelled C and D. The sum of the two lower type A peaks is 23.64(2) MHz, which is in reasonably good agreement with the frequency of the highest type A peak, 23.71(2) MHz. The sum of the two lower type B peaks is 28.12(1) MHz, which is also in reasonably good agreement with the frequency of the highest type B peak, 28.18(2) MHz. Both of these are slightly outside the error bars, but that the near agreement could be a coincidence is beyond credence. The inference is then that there are two sites with different values for the interaction. If one takes the total intensity for each site, the relative intensity for B:A is 1.5(2):1. Whether this ratio reflects a difference in abundance of the sites, or some sort of thermodynamic equilibrium value is not yet clear. The frequencies seen are about four times higher than those seen in α -quartz, which is consistent with the faster relaxation seen for muonium in fused GeO_2 versus fused SiO_2 .

A least squares fit using MINUIT, as discussed in Section II.3, to all the 8 frequencies independently and simultaneously, gives essentially the same relaxation rate to the six members of the two triples. It is reasonable to suppose that the two triples would have similar relaxation rates, assuming this is due to the ^{73}Ge nuclear moments, as in the case of ^{29}Si nuclear moments in low-temperature α -quartz. The other two large signals, however, show a much higher relaxation rate, but again these two relaxation rates are within error of each other. No temperature dependence measurements were done, as the signals were much too weak. From eq. IV.1, the relaxation expected from the RLMF of ^{73}Ge would be 1.3 times that seen for ^{29}Si . In fact the observed relaxations for the two triples at 6 K are rather a bit less than that seen in α -quartz at the same temperature. Given that the two triples A and B correspond to two distinct sites, what can be said about the other two frequencies C and D? They could also be members of a triple whose third member, at a frequency of 21.77 or 42.19 MHz, is too weak to have been observed. Alternatively, they could be from two different sites, both of which have cylindrical symmetry and so show only one frequency; or if the two sites were more anisotropic, then the other four frequencies are not observed due either to low intensity or too high a frequency. Another

hypothesis is that the two frequencies are for the same cylindrically symmetric site and represent two of the three possible frequencies from a site where the isotropic part is only about 1% of the vacuum value – in analogy to anomalous muonium in Si, Ge, and diamond [Patterson 84], but with an even greater reduction in frequency. In zero-field this last case would be indistinguishable from the first.

It is possible that any of these three or four sites may be associated with an impurity, particularly in view of the very weak signals present. This is a well-known phenomenon in EPR, for example the germanium-hydrogen-lithium site in quartz [Weil 71]. Such an impurity associated site might show a much smaller hyperfine coupling than normal muonium, and if the impurity had a nuclear moment, this might split the line, an unresolved splitting resulting in a broad line.

No determination of the site orientation in GeO_2 was possible, as the sample was not a single crystal. Rather it was polycrystalline with a small number of crystals, so it was also not in the powder limit – in which case all members of a triple would necessarily show the same intensity. Experiments with a large single crystal should give much more information, but if it is not possible to grow such a crystal with sufficiently high purity, a coarse crystalline powder could at least test the hypothesis that triples are present.

3. MAGNESIUM OXIDE

A single crystal of MgO was studied over a temperature range from 6 to 295 K. Muonium was observed at all temperatures. A run at 295 K at 10 G is shown in Figure 30; $P_{\text{Mu}} = 30(10)\%$, $P_{\text{D}} = 40(2)\%$, hence $P_{\text{L}} = 30(10)\%$.

The relaxation rate as a function of temperature, as shown in Figure 31, is not what one might have expected. Any crystal has some impurities which act as depolarizing sites for muonium, or indeed the muon, by being paramagnetic; by being chemically reactive; or by creating a locally anisotropic hyperfine environment. A host site would not be expected to have an anisotropic hyperfine interaction, as the material has cubic symmetry. It is true, however, that the

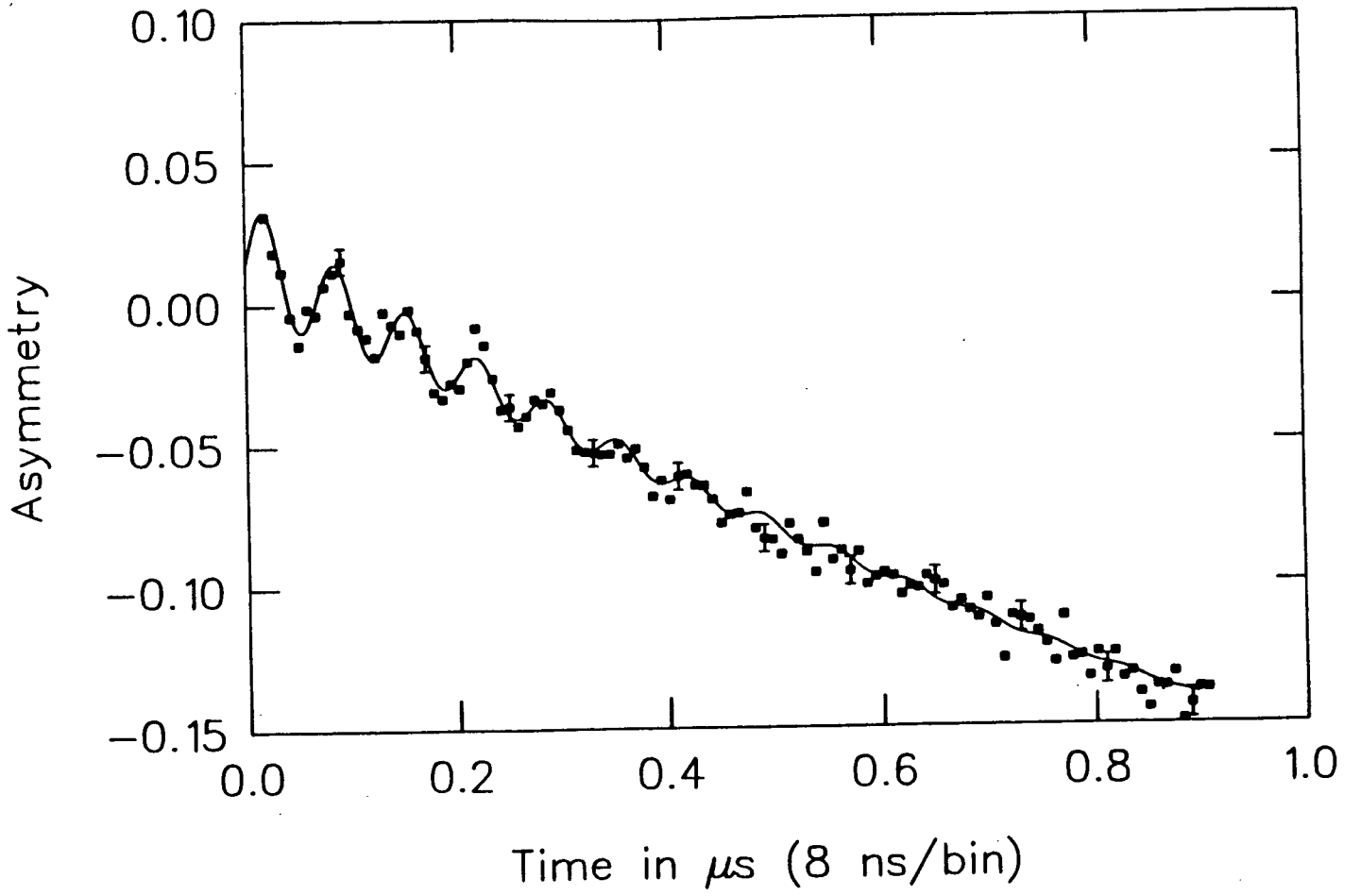


Figure 30
Room temperature signal in MgO at 10 G.

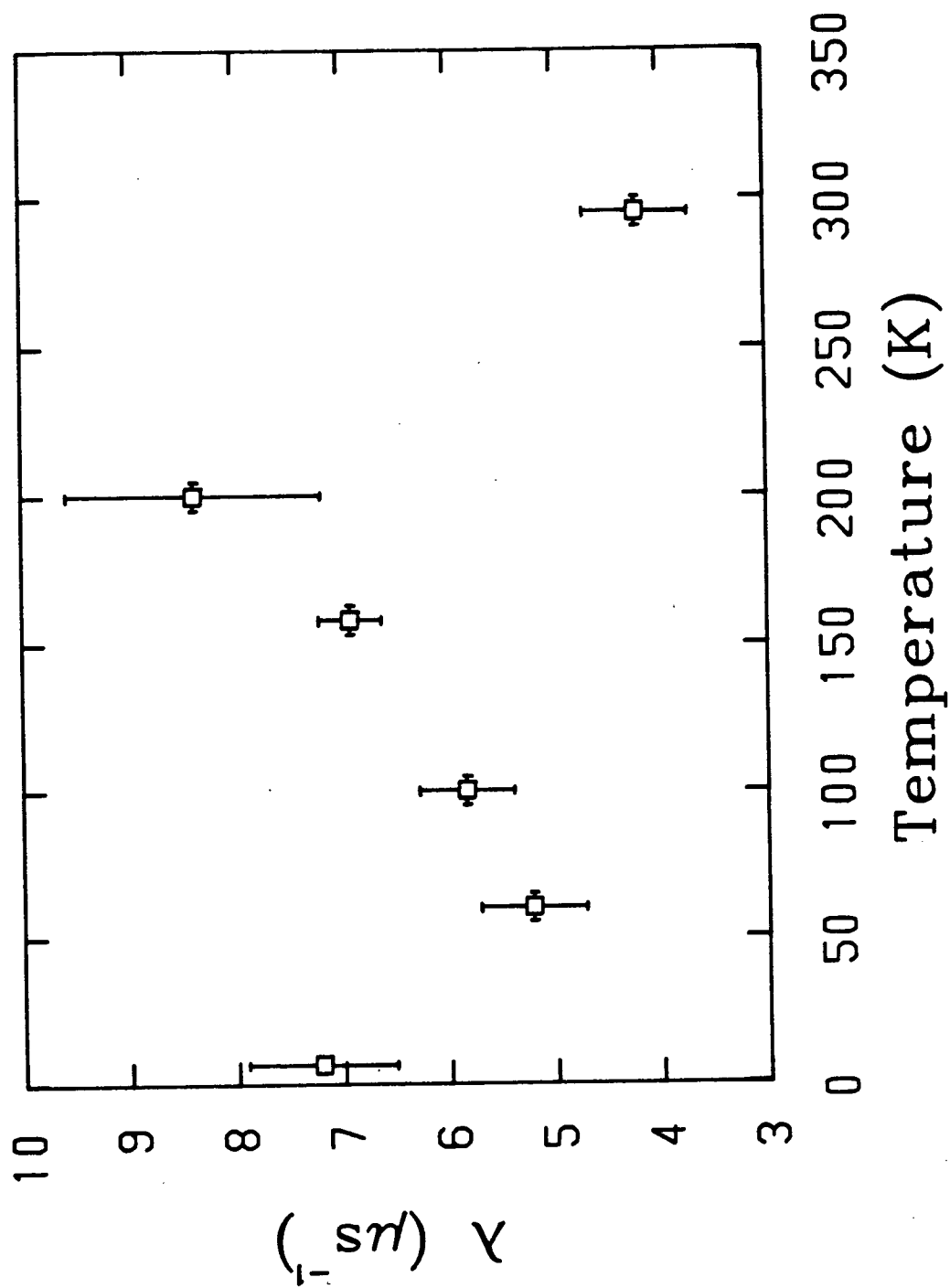


Figure 31
Relaxation of the muonium signal in MgO versus temperature.

local symmetry need not be as high as that of the crystal, as is the case with α -quartz. Any nucleus with a magnetic moment, such as hydrogen, will also depolarize muonium by the superhyperfine interaction or dipole-dipole broadening. The expected temperature behaviour of such a system is for the low-temperature relaxation rate to be low, since the muonium diffuses only slowly and so is unlikely to find a depolarizing site during its lifetime; at higher temperatures the relaxation rate increases as the muonium diffuses faster and so is more likely to find these sites; and then at still higher temperatures the relaxation rate declines again as the muonium is moving past these sites so quickly, or is in them for such a short time, as to avoid being depolarized. In MgO, neither of the two elements has a large percentage of nuclear moments (^{25}Mg 10.1%, ^{17}O 0.037%), and the crystal structure is highly symmetric, so that at low-temperatures, where the muonium is static, relaxation should be slow. The simple scaling from eq. IV.1 predicts a relaxation rate only 1.5 times higher than for α -quartz, about $0.3 \mu\text{s}^{-1}$. No attempt was made to account for the difference in structure, and hence distances from the muonium atom to the nuclei will not be properly accounted for. Also, relative abundances were used rather than concentrations. The relaxation seen is about 20 times faster than this prediction, a surprisingly large disagreement. As the temperature increases, the relaxation rate first falls, then rises to a value comparable to the low-temperature value, at about 200 K, then falls again. That the relaxation rate rises, then falls with increasing temperature is consistent with the expected behaviour due to impurities; what is puzzling is the high relaxation rate at the lowest temperature. This may indicate that even at 6 K muonium is diffusing rapidly and finding a trapping site different from that found at the higher temperature. An exploration of the region below 6 K might be helpful.

The observed hyperfine is considerably reduced from the vacuum value, measured in the same way as for fused GeO_2 , being only 3.4(3)GHz, in agreement with a more recent measurement from SIN, 3849 MHz [Kiefl], a 14% reduction from the vacuum value. This means that the electron wave-function has been expanded by the lattice, the opposite of what is observed in SiO_2 , and to a far greater extent. Such an expansion might suggest that the muonium is in a site

surrounded by Mg^{++} ions, just as the site in α -quartz is surrounded by O^{--} ions, the former being much more ionic than the latter due to some covalency in the Si-O bond, thus accounting for the difference in magnitude of the effect. Since MgO has the same structure as KCl, it is interesting to note that there is also a reduction in the muonium hyperfine constant in KCl of about 5% [Kiefl 84]. If the site is the same for both, this is consistent since the Mg^{++} would attract much more strongly than the K^+ . However, no temperature variation of the muonium amplitude in MgO was observed in this study, such as has been seen in KCl [Kiefl 85]. If this is due to a thermally activated process in KCl, as suggested in the paper by Kiefl et al. [85], then perhaps a wider range of temperatures would show the effect.

The model is then that muonium hops rapidly between equivalent sites even at low temperatures. It would not be difficult to study this material at lower temperatures where this model predicts a decrease in the relaxation rate.

4. STRONTIUM TITANATE

$SrTiO_3$ was chosen as it met the criterion for having a low concentration of nuclear moments (^{87}Sr 7.0%, ^{47}Ti 7.3%, ^{49}Ti 5.5%), and it also shows ferroelectric behaviour [Sakuda 71]. While not a true ferroelectric, nor an antiferroelectric, still its dielectric constant ϵ is a strong function of temperature. It was thought that there might be some connection between muonium formation and the dielectric constant, so this seemed an ideal test case, where ϵ could be varied at will, merely by changing the temperature. A single crystal was used, and the levels of impurities are given in Table III.

Strontium titanate exhibits tantalizing behaviour for the would-be observer of muonium. Generally, a muon signal amplitude is, of course, anti-correlated with a muonium signal amplitude. Naturally, then, the 100% muon signal amplitude observed at room temperature precludes a search for muonium at that temperature. However, the muon signal was measured as a function of temperature from room temperature down to 4 K. The observed amplitude changed dramatically below 60 K, as shown in Figure 32 with a minimum at about 32 K. The muon

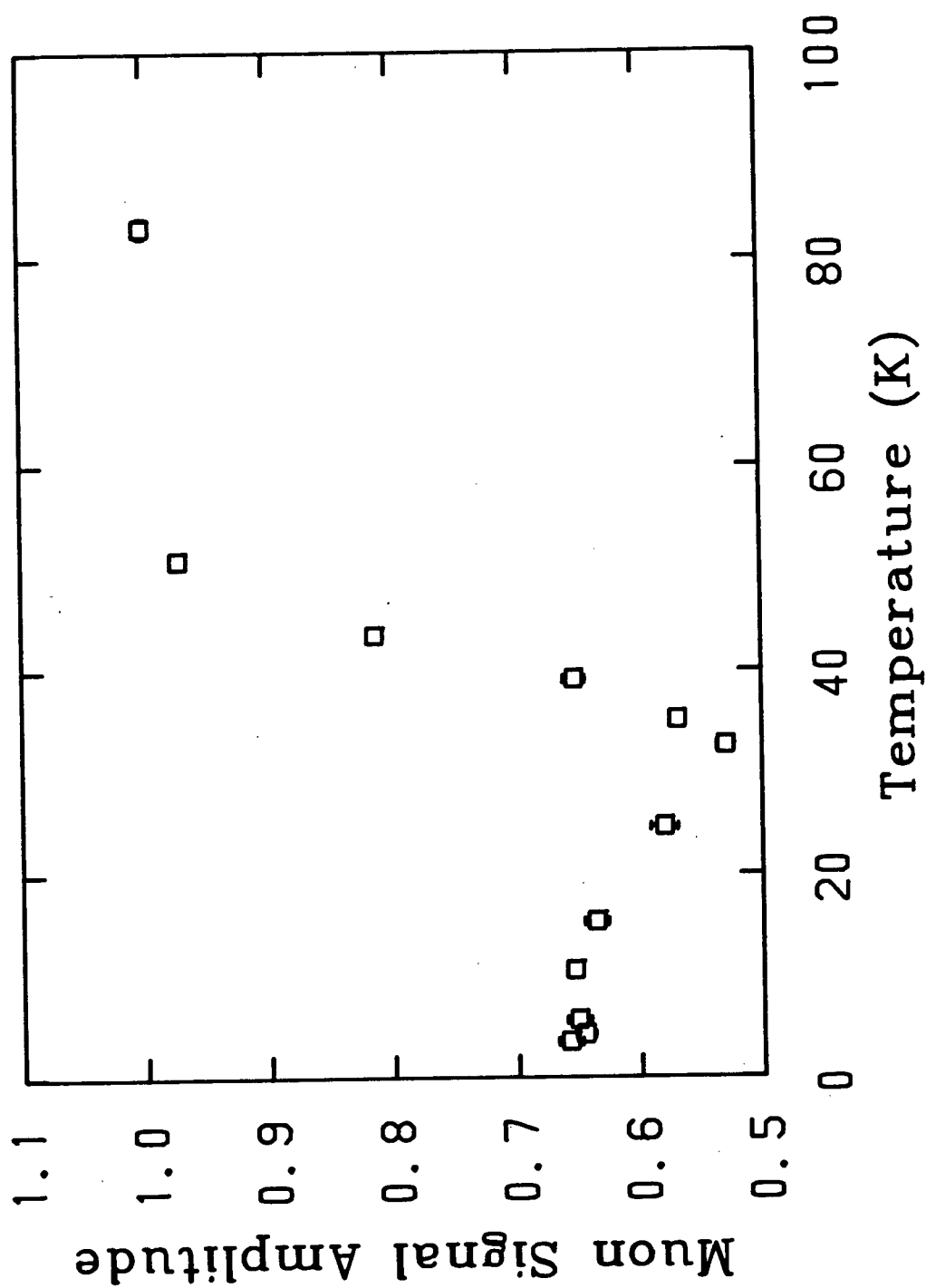


Figure 32

Amplitude of the muon signal in SrTiO₃ versus temperature, normalized to the maximum observed value which is consistent with a 100% muon signal.

relaxation rate is shown in Figure 33, exhibiting a monotonic increase with decreasing temperature with a possible anomaly at 35 K, not at the temperature corresponding to the minimum amplitude.

SrTiO_3 has been studied extensively with other techniques for two reasons: its phase transition at about 105 K [Willemsen 76, Kinase 82], and its ferroelectric behaviour [Sakuda 71]. The muon does not show any remarkable behaviour in the vicinity of the phase transition, although a more accurate measurement of the relaxation might be of interest. At the lower temperatures where the ferroelectric properties of SrTiO_3 become noticeable, the muon fraction declines quite suddenly. Two sets of data were taken under slightly different conditions and they agree in the details of the remarkable structure of the muon amplitude curve. It is interesting to note that the minimum of the curve occurs around 32 K, which has been reported as the ferroelectric transition temperature [Cowley 64]. At any rate, the dielectric constant is a strong function of temperature, increasing monotonically with a decrease in temperature throughout the region where the muon amplitude changes.

As noted before, in a non-magnetic material the only known mechanism for a decrease in the initial muon amplitude is the formation of muonium or muonium-like species. If the muonium is not observed directly, then it has been rapidly depolarized. If muonium is formed, then reacts chemically to form a diamagnetic compound, this can be identified, since the observed muon fraction will depend both on the rate of reaction and the applied field, increasing with the former and decreasing with the latter [Brewer 75]. No such field dependence was observed. A search was made for muonium in SrTiO_3 at several temperatures, particularly at the minimum in the muon amplitude at 32K, but none was observed.

If the loss of muon amplitude is evidence for muonium formation, why then is it a function of temperature? The temperature dependence of the dielectric constant is the most obvious source, but just how could it bring this about? One might naively expect that since the attraction between the muon and electron goes as $1/\epsilon$ (where ϵ is the dielectric constant) muonium would be less likely to form where a high dielectric constant was present; that is, at low temperatures. However, it must be remembered that this ϵ is the bulk ϵ , which does not necessarily apply on a

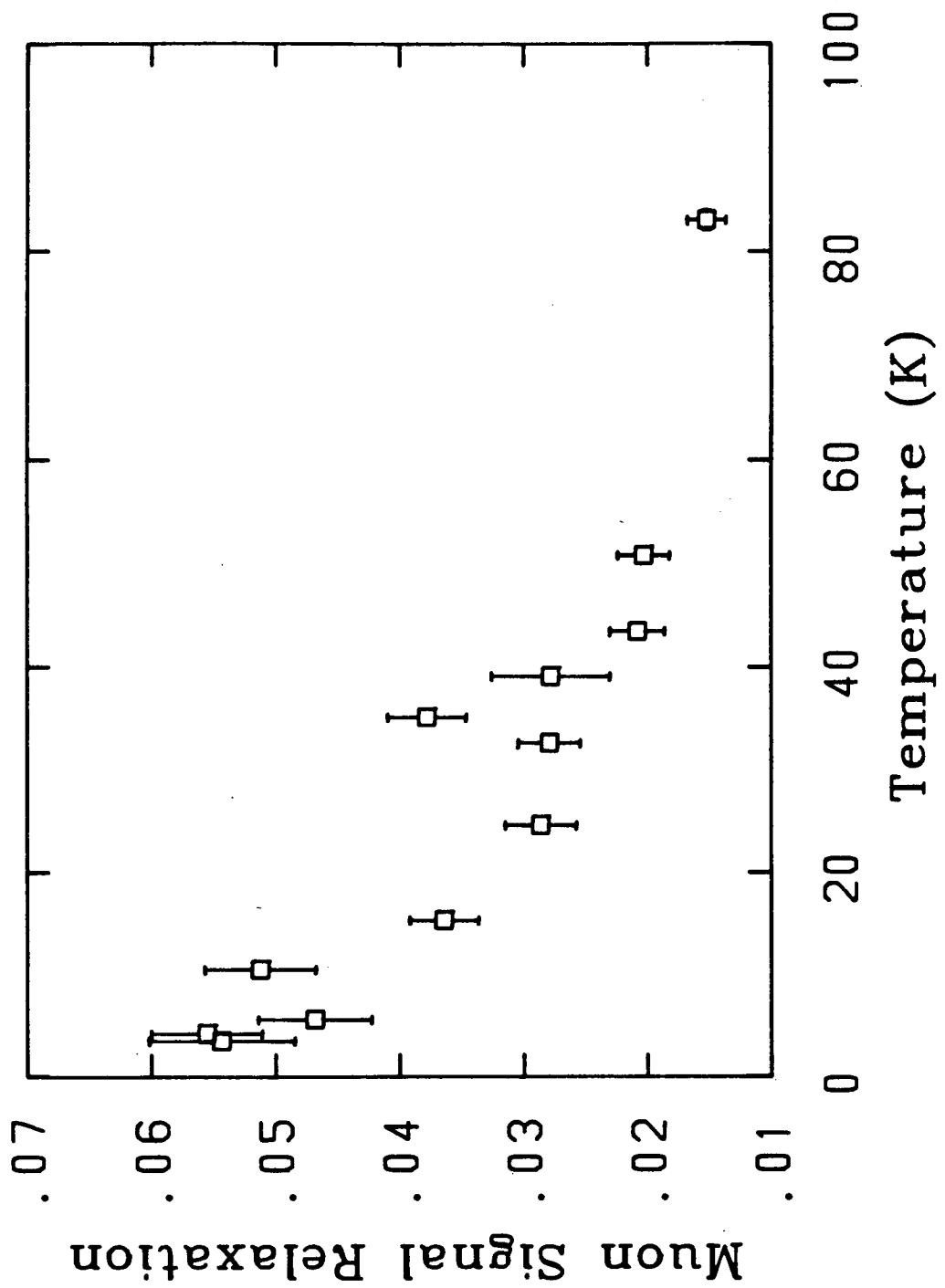


Figure 33
Relaxation of the muon signal in SrTiO₃, versus temperature.

microscopic scale. Moreover, the same reasoning would apply to whatever the muon was seizing the electron from. The ferroelectric transition is associated with a relative shift between the Sr^{++} and the TiO_3^{--} ionic sublattices, so any muonium formation could be associated with this lattice change. Perhaps "holes" are opened up which the muonium atom could occupy.

Since the strontium titanate lattice is much more ionic, the electric field gradients should be far larger than in quartz and germanium dioxide, so any muonium formed might be expected to have a hyperfine constant different from the vacuum value, and highly anisotropic as well. If this were so, then the conventional transverse field search for muonium used frequently in this thesis might well fail, if for no other reason than that the frequency might be split and shifted far from the expected 1.39 MHz/Gauss. If the Forward-Backward spectrum taken at 32 K in a field of 7G shown in Figure 34 is examined closely, a "dip" can be seen at early times (<300 nanoseconds), with an amplitude about half the missing amplitude. This would be consistent with the missing muon polarization being due to muonium formation followed by rapid relaxation of the muonium signal, with two exceptions: its presumed frequency is only half that expected in this field; and it is not seen in the Left-Right spectrum, as expected in a transverse field. The dip is seen in other fields as well, almost unchanged; for example at 0 G (Figure 34) and 25 G (Figure 35). It is not seen in runs of other materials taken before and after these runs, hence it is unlikely to be due to a defect in the data collection system. It is hard to say what this dip could be exactly, but almost certainly it is a remnant of the disappearing muonium. It has been suggested [Brewer 85] that an extremely anisotropic hyperfine interaction might be responsible.

It is worth noting that the recombination time of spurs formed in the slowing down of the muon can be expected to increase with the dielectric constant of the material [Mogensen 74]. If the spur species are thermalized, then lower temperatures would also increase the recombination time. If there were sufficient time to permit an actual buildup of the radiolytic species, this might explain muonium formation and relaxation in SrTiO_3 in much the same way as the spur model does in water, [Percival 84]. The result of a given experiment would then depend on variables like the incident muon rate and the size of the sample. It would be of considerable interest to study other

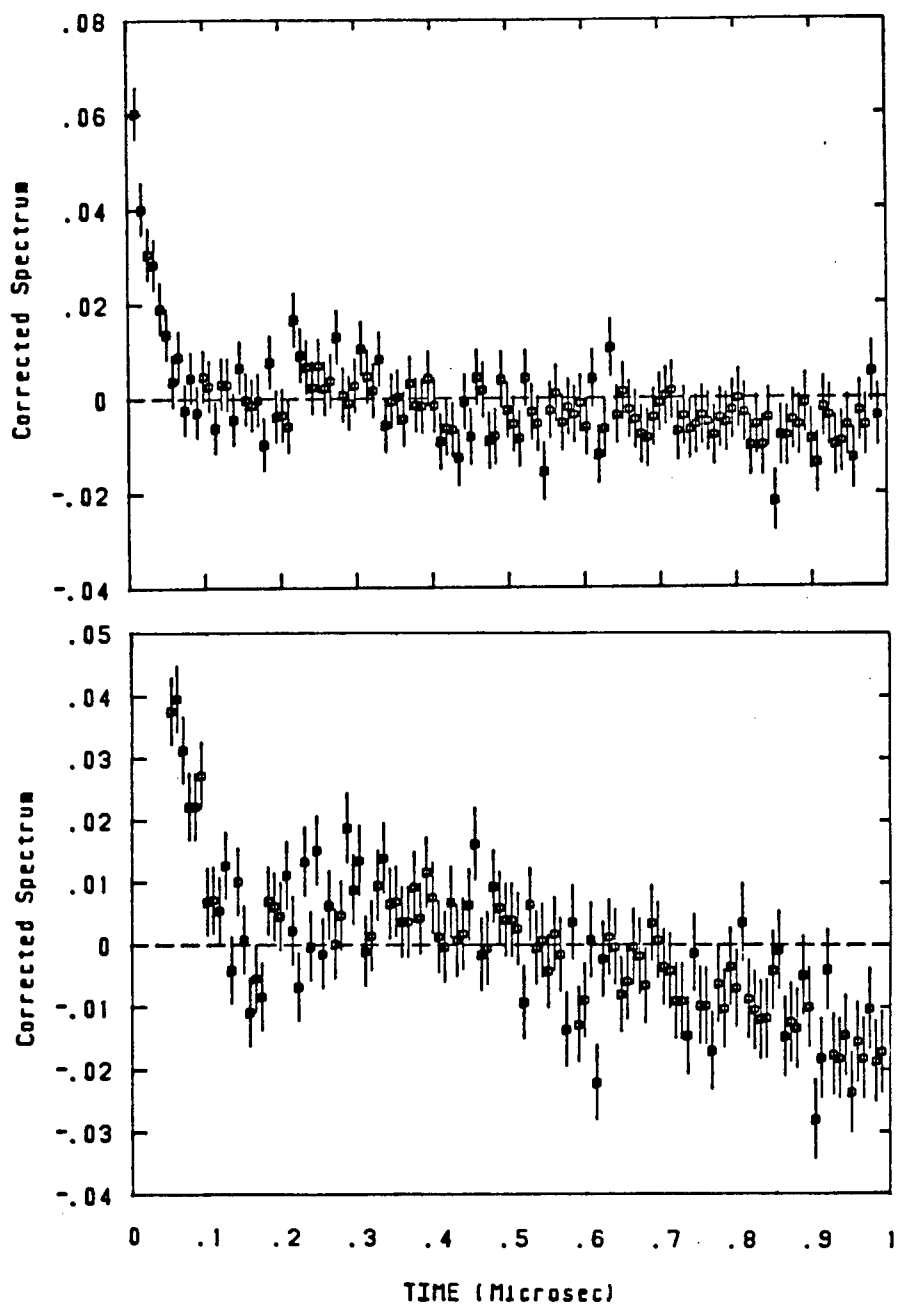


Figure 34

Early time behaviour of the asymmetry in SrTiO_3 , at about 32 K in zero applied magnetic field (top) and 7 Gauss. Note that the anomaly does not change its apparent frequency.

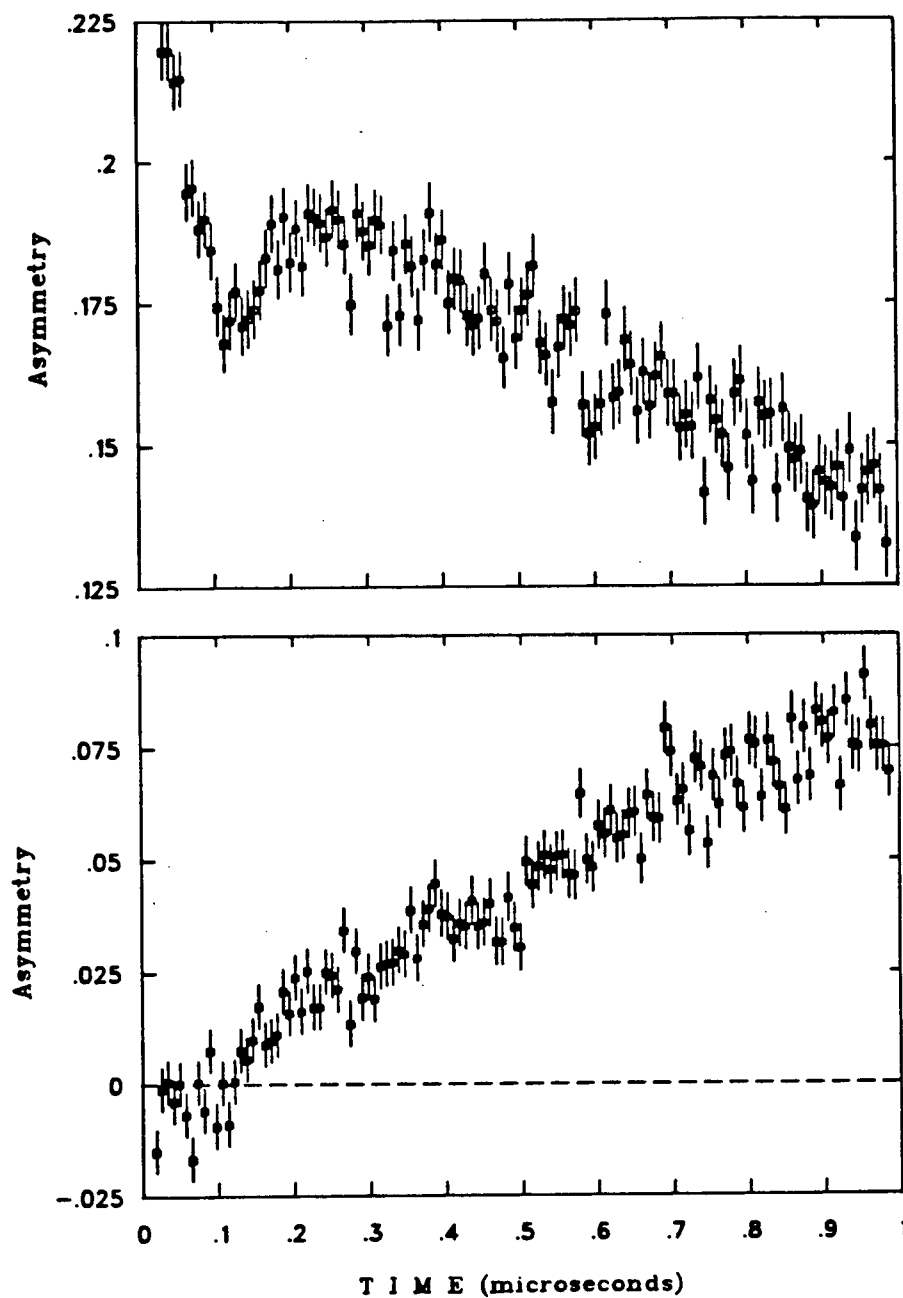


Figure 35

Early time behaviour of the asymmetry in SrTiO₃ at about 32 K in 25 Gauss applied magnetic field. The Backward-Forward spectrum (top) still shows the anomaly at the same frequency as in zero field and seven G, but the Left-Right does not show it at all. Nor did it at 7 Gauss.

ferroelectrics to see if the muon shows similar behaviour to that discussed above. For example, it might be possible to test the hypothesized buildup of radiolytic species by varying the incident muon rate or simultaneously bombarding the sample with other particles, such as electrons.

5. RUTILE

In addition to its small concentration of nuclear moments, rutile (TiO_2) was also studied because hydrogen is a well-known impurity in it [Chen 84]. Accordingly, a single crystal, with impurities as given in Table III, was obtained. Rutile, like strontium titanate, showed interesting behaviour in that the amplitude of the observed muon signal decreased with decreasing temperature as shown in (Figure 36.) However, the effect is much less dramatic, and the small dependence was not apparent when the sample was run, so a search for muonium was made only at the highest temperature, which now seems the least likely place. No muonium was observed. That the dependence of amplitude on temperature is slight can be seen by looking at Figure 37, which presents asymmetry plots at 295 K and 20 K, in a field of 160 G. The data may indicate the formation of muonium which rapidly reacts to form a diamagnetic compound, like the OH^- observed by Bates et al. [79], for example; or perhaps there is a time delay before the Mu atom ionizes to μ^+ , in the same way that Schumacher [80] suggests H atoms in TiO_2 diffuse before ionizing. If the reaction rate is comparable to the triplet precession frequency and if the rate is temperature dependent, the resultant muon amplitude will vary with temperature as well [Brewer 75]. Another signature of this effect is that the amplitude will decrease as the field increases [Percival 78]. However, only one run was done at a different field, the room temperature search for muonium at a lower field. Curiously, rather than showing an increased muon amplitude it shows a decreased amplitude. In principle this could be due to the 160 G field being sufficiently high that the muons are steered away from the target as mentioned in Section II.5. The residual energy of the muons after the thin counter is about 3 MeV which corresponds to a momentum of 25 MeV/c. In the applied field of 160 Gauss, such muons would have a radius of curvature of 500 cm, and so over the 5 cm distance from the thin counter to the target, the muons would "drift" less

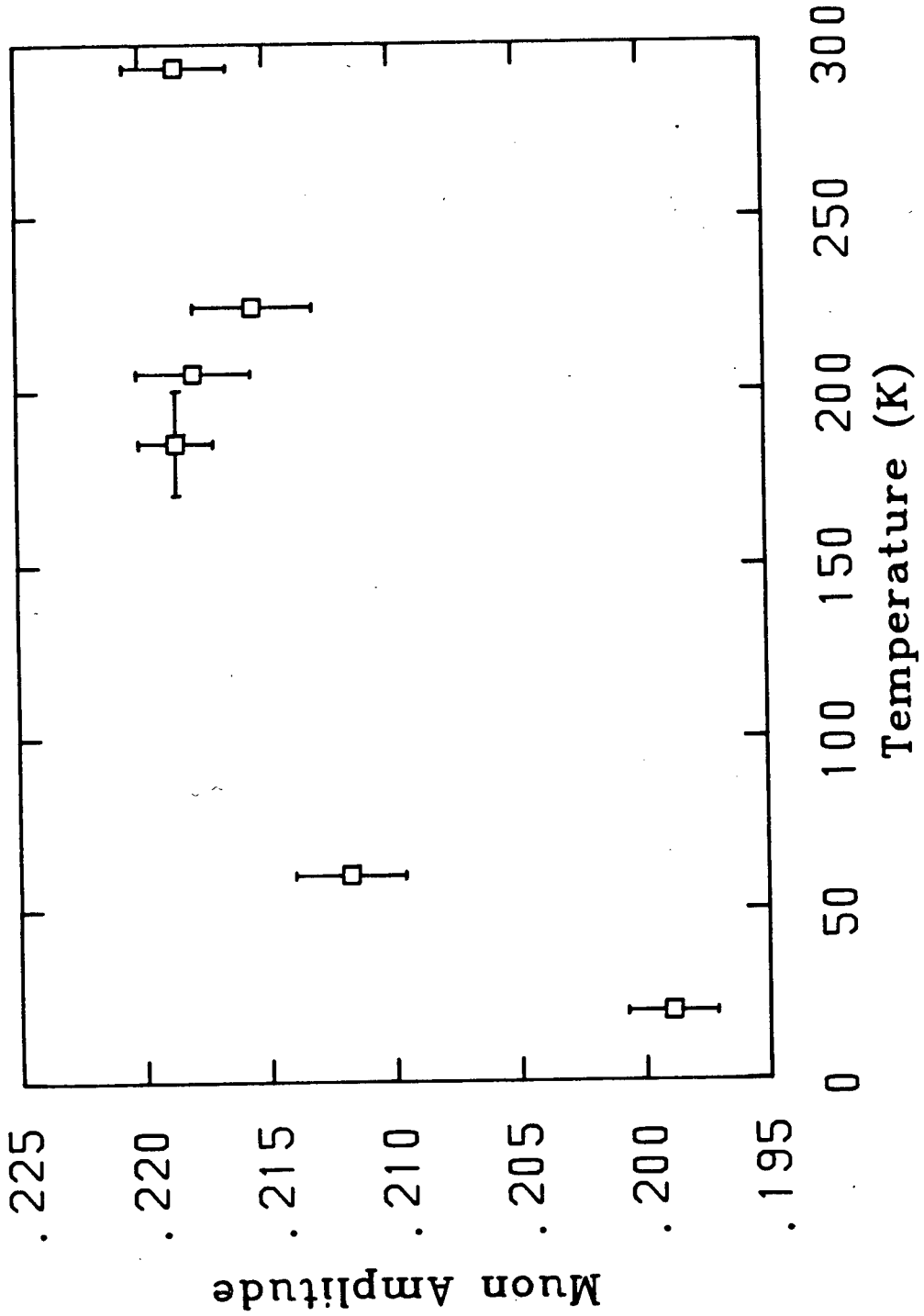


Figure 36

The muon signal amplitude in TiO_2 , plotted as a function of temperature. Note the expanded scale.

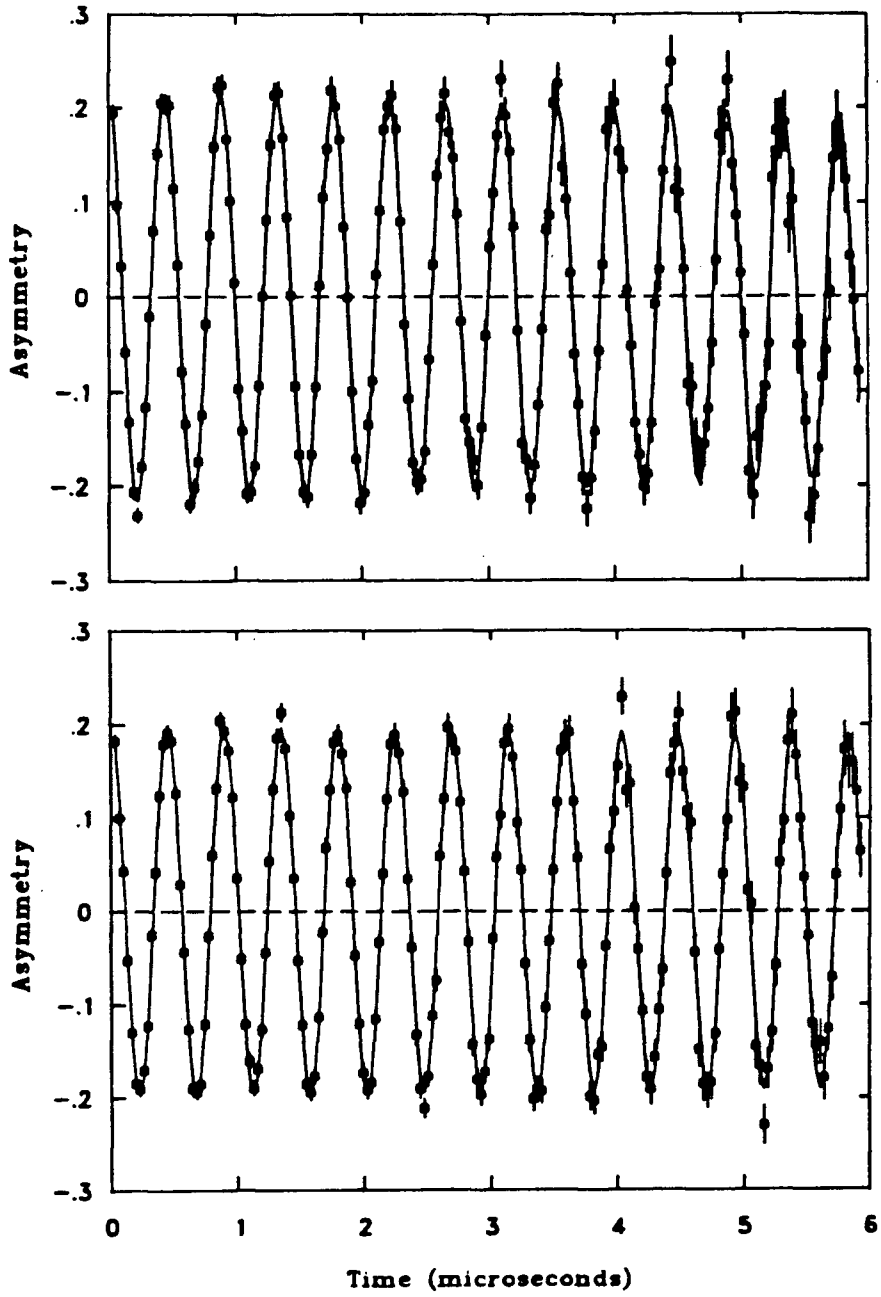


Figure 37

The asymmetry seen in TiO, at 295 K (top), and 20 K. The solid plotted line is a fit to the amplitudes as plotted in Figure 36.

than 1 mm, much less than the size of the crystal, which was a 1.5 cm cube. Thus, this effect seems unlikely to be important.

The missing fraction of about 30% is presumably due to depolarized muonium, although the source of the depolarization is not at all obvious. The only species with significant abundances of nuclear moments are ^{47}Ti at 7.3% abundance, and ^{49}Ti , with an abundance of 5.5%, which, although somewhat higher, are not so much different from quartz as to make the signal utterly vanish.

6. BERYL AND ZIRCON

As part of the survey of materials, $\text{Be}_3\text{Al}_2\text{Si}_6\text{O}_{18}$, or beryl, and ZrSiO_4 or zircon were also studied briefly, beryl as a single crystal and zircon as an assemblage of single crystals. Both were of geological origin. Since both the zircon and the beryl are silicates, it was expected that they would behave somewhat like quartz in their ability to form muonium and perhaps in providing an anisotropic site for it. The EPR of atomic hydrogen has been observed in a geological sample of beryl [Andersson 74] at room temperature where the observed hyperfine interaction has cylindrical symmetry; the hyperfine constant is reduced from the vacuum value by 1%, and the anisotropy is about 0.06%. This is similar to the behaviour of muonium in room-temperature α -quartz.

The beryl shows some sign of muonium, but the time available to study it was too brief to test more carefully, so no P_{Mu} is quoted. The zircon shows a large missing fraction, but no muonium, and so the system may be worth further study with a larger, purer sample. Further pursuit of these two systems with μSR is desirable, if large samples of higher purity become available.

7. DIAMOND

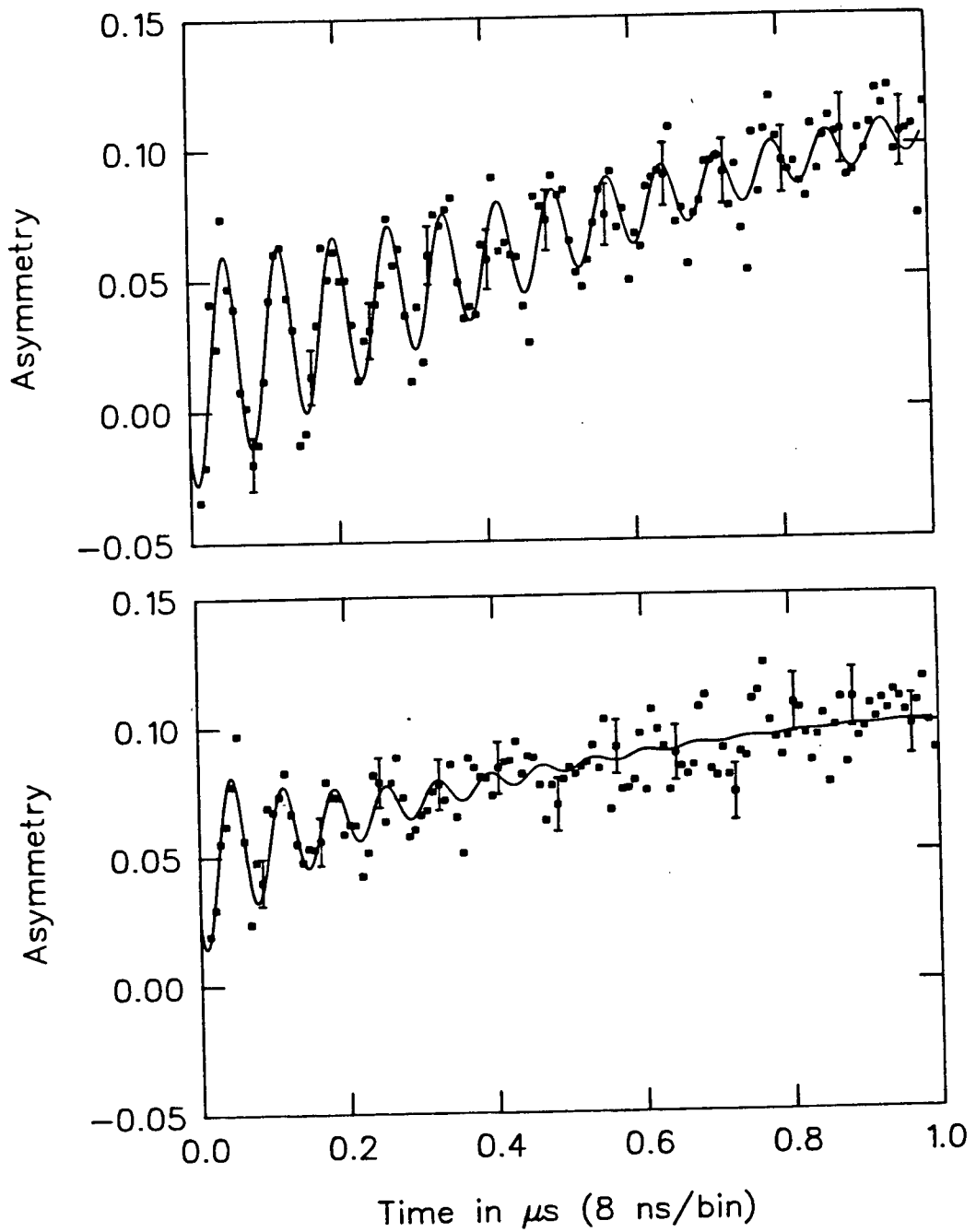
Diamond is a semiconductor like its structural analogues silicon and germanium, although less commonly used for that purpose. Since muonium has been observed in silicon and germanium [Patterson 84], it was hoped that a study of diamond would prove fruitful. As

mentioned earlier, two different species of muonium are observed in silicon and germanium: an isotropic species with a hyperfine frequency reduced by about 50% from the vacuum value, and a species, called anomalous muonium, exhibiting cylindrical symmetry, with a hyperfine frequency greatly reduced from the vacuum value. Anomalous muonium is more difficult to observe in germanium than in silicon due to the ^{73}Ge nuclear moments [Estle 84]. Diamond was very briefly studied by Swanson [58], who saw a reduced initial muon amplitude.

The first sample of diamond studied in this thesis was a large (about $1.5 \times 1.5 \times 3$ cm) very impure intergrowth of crystals of the class known by the inelegant name of bort. It showed absolutely no μSR signal at all, the only non-magnetic material in which that had been observed. A second, smaller (1cm^3) sample of higher purity was also examined but no muonium was seen, and the muon signal was consistent with a muon background in the sample holder. Some time later, a small ($7 \times 7 \times 0.5$ mm), clean, Type IA diamond was obtained from De Beers Diamond Research Laboratory. In the meantime, however, Holzschuh et al. [82] at SIN had studied a somewhat larger diamond (9.2 g versus 80 mg), as well as diamond powder, and saw muonium at low temperatures, their signal vanishing well below room temperature. Naturally, therefore, it was of interest to study the new IA diamond at low temperatures. Again serendipity took a hand: the cryostat was not yet cold when the time came to do the experiment and so the first run was done with the diamond at room temperature. I then made the first observation of muonium in a room temperature semiconductor (Figure 38).

A temperature study down to 6K was also performed and the relaxation rate is plotted in Figure 39, along with those from SIN, which are remarkably different. Both the diamonds are of the same type, with nitrogen as the principal impurity. Their explanation for their results was that muonium was converting to anomalous muonium, this rate increasing with temperature [Patterson 84b].

Patterson et al. saw anomalous muonium up to 1080 K [84b]. No anomalous muonium was observed in the present sample, but in part due to the size and shape of the sample, it was put in in an arbitrary orientation for which there may be as many as eight lines sharing the

**Figure 38**

Asymmetry in diamond. Note that the room temperature (top) muonium signal relaxes much more slowly than the 6 K signal.

polarization; so it is not surprising that anomalous muonium was not observed, and this should not be taken as an observation of absence. The isotropic hyperfine interval was measured to be 3693 ± 83 MHz at room temperature, which is consistent with the SIN result of 3711 ± 21 MHz [Holzschuh 82] measured at 6 K, so it would seem that both experiments are looking at the same type of muonium. It is not at all clear however, how the SIN model, which was also thought to be applicable to silicon and germanium, will mesh with the present thesis data. Both diamonds were of the same type (IA), but these classifications are rather broad and so they could have rather different levels of impurities. It is usual that the sample with the highest relaxation rate has the most impurities; however, since the relaxation rate in the SIN sample is lower at low temperatures and higher at high temperatures than the rate in the TRIUMF sample, as in Figure 39, it is rather difficult to assign this difference to impurities. Looking at the TRIUMF data alone, what can one speculate might be the source of the relaxation? There is only 1.1% ^{13}C present, so nuclear moments seem unlikely to be a source. Looking at Figure 39, a plot of the relaxation rate as a function of temperature, one is most reminded of Figure 25, a plot of the relaxation in fused quartz, over the same temperature range, which was attributed to random hyperfine anisotropies. If the muonium in diamond were not strictly isotropic, but instead showed some anisotropy, perhaps with symmetry along the four $\langle 111 \rangle$ axes, as is true for anomalous muonium [Patterson 84], then the small applied field used would result in a large number of peaks for static muonium, perhaps eight, centered at the normal muonium frequency. An unresolved splitting would give an apparent fast relaxation. If the muonium were diffusing it might average these multiple sites, resulting in motional narrowing. This scenario does seem rather far-fetched, but a zero-field study at low temperature would quickly confirm or deny this model. The most obvious failure of the model is that, in contrast to the SIN model, it "explains" the TRIUMF results but not the SIN results.

The EPR spectrum of hydrogen has been observed in diamond [Karaseva 83], where the species observed is isotropic and has a hyperfine constant only 0.4% less than the vacuum value. Neither of the two species of muonium correspond to this. It has been suggested [Estle 85] that the hydrogen atoms are not in the bulk of the diamond, but rather on the surface. This would

explain the hyperfine constant, but perhaps the spectrum should have resembled that seen for hydrogen on the surface of fused silica [Papp 75], showing a broadening due to anisotropies.

F. CHAPTER VI: SUMMARY AND CONCLUSIONS

The cylindrically symmetric Hamiltonian has now been observed for muonium not only for room-temperature α -quartz, but also for ice [Percival 82], and for anomalous muonium in the semiconductors diamond [Holzschuh 82], silicon [Patterson 78], germanium [Graf 79], gallium arsenide, and gallium phosphide [Kiefl 85]. In the semiconductors, the hyperfine parameter A_0 is sharply different from the vacuum value, and ΔA is comparable to A_0 . The two insulators have values of A_0 comparable to the vacuum value, while ΔA is less than a 0.1% perturbation on A_0 . For both α -quartz and ice, the Hamiltonian z-axis has been shown to correspond to the principal symmetry axis of the crystal, although the signs of ΔA are opposite [Percival 82]. For the semiconductors the axis of symmetry has been shown [Patterson 78] to be the four $\langle 111 \rangle$ axes, which complicates the spectrum even further.

It is important to note that isotropic muonium is also observed in the semiconductors, with a hyperfine constant reduced from the vacuum value by about 50% [Patterson 78, Graf 79]. The observation of two such widely different species at the same time has not, as yet, been satisfactorily explained. The anomalous species is not observed for hydrogen, so it seems that it may be a metastable state, decaying either to the normal atom or to a diamagnetic species. Its presence may be due to impurities or imperfections in the lattice. Sahoo et al. [85] now give fairly convincing calculations to show that anomalous muonium is associated with a doubly positively charged vacancy. Their model works very well for silicon, but not as well for diamond.

In this thesis work, a Hamiltonian new to μ SR was discovered, explained, and observed in two systems, α -quartz and hexagonal germanium dioxide; one with a completely anisotropic hyperfine interaction. This Hamiltonian has not been seen in any other μ SR study, and it is also unusual in hydrogen atom EPR work [Weil 84]. This Hamiltonian allows, in principle, useful geometric information about the site to be extracted from the spectra. Since muonium atoms can be observed in times shorter than those required for hydrogen atom studies, and since muonium may form in materials where hydrogen may not even be present, muonium can be used to provide otherwise unobtainable information about the system and about what the hydrogen atom might do

in such a system, provided it really does act like an isotope of hydrogen. The study of muonium in low-temperature quartz herein provided the first evidence that this is indeed true in a solid.

A summary of representative results obtained in this thesis work is given in Table II. It is now clear that nearly every non-magnetic insulating or semiconducting material shows a reduced muon amplitude due to muonium formation. This agrees with the statement at the beginning of Chapter IV. That muonium is not *directly* observed with conventional techniques is easily explainable for those materials containing nuclei with significant abundances of nuclear moments. That muonium should be unobservable in so many other materials is surprising. It might be suspected that impurities play a role, as they certainly do in the semiconductors silicon [Albert 84], germanium [Clawson 81] and gallium arsenide [Kiefl 85]. In a semiconductor, though, impurities will, due to their effect on electronic properties, have an influence over a much longer range than they would in an insulator. Also, why would quartz, no purer than the other materials, show such a large, long-lived muonium signal? Perhaps muonium in these others diffuses rapidly to depolarizing impurities. Why then is a small, slowly relaxing, signal seen in germanium dioxide? Perhaps the observed muonium is trapped, not in some intrinsic site as it is in low-temperature α -quartz, but at some non-depolarizing impurity. Such a site may have been missed in other materials, such as zircon and rutile, as fewer events were taken. Germanium dioxide was pursued more vigorously due to the expected analogy with quartz. If this hypothetical diffusion were strictly thermally activated, then it might be possible to observe muonium at lower temperatures. This might also be achieved by lowering the level of impurities. Both of these courses could be pursued, perhaps simultaneously.

The nonobservance of muonium in these materials is reflected in the large missing fraction which is found even when some muonium is present. The only exception to this statement is quartz, where there is no missing fraction. In ice, recent analysis shows that there is a missing fraction [Percival 85]. In this case, as for liquid water, it is suggested [Percival 85] that the missing fraction is due to depolarization of muonium by spur electrons. The present results for strontium titanate might be construed as supporting the spur model, but such an interpretation is far from

unequivocal, and it must be stated that a general mechanism for muonium formation and the missing fraction in solids is not yet established. It is likely that no single mechanism is sufficient, in contrast to the situation in gases [Arseneau 84]. The large diamagnetic signals seen in strontium titanate, rutile and magnesium oxide may be related to the formation of MuO^- as suggested in the Fe_2O_3 system by Boekema [84], or the H^- seen in MgO by Gonzalez et al. [81] in MgO, but this provides no information on the missing fractions. The very small muonium signals seen in fused and hexagonal germanium dioxide compared to quartz is perhaps the biggest challenge to any theory attempting to explain the missing fraction. If it had only been one sample that showed this, it might be passed off as a poor sample; since two different samples, a fused sample and a crystalline sample, both have a large missing fraction, it must be explained in some more interesting way.

Several suggestions have been made in the body of this thesis as to future directions for the study of muonium formation. Stoneham [83] has also made some suggestions as to how to pursue the problem. A few of these suggestions are:

1. that the muon fraction may increase in alkaline earth fluorides close to their melting points due to anion Frenkel disorder;
2. that the $P_{\text{Mu}}/P_{\text{D}}$ ratio should show interesting behaviour near the metal-insulator transition in silicon - a study of the metal-nonmetal transition is currently planned for TRIUMF [Noakes 85];
3. and the muonium fraction should increase in materials in which the preferred μ^+ site is blocked by hydrogen, as in the case of CaO with increasing amounts of water added to form $\text{Ca}(\text{OH})_2$, and by sodium ions as in the case of $(\text{Na}_2\text{O})_x(\text{SiO}_2)_y$ where he expects the muonium fraction to increase with increasing amounts of Na.

In the last case, since the muonium fraction is already so high, and since Na will depolarize muonium, as would hydrogen, it might not be feasible. In the case of the CaO study, it is encouraging to note that hydrogen atoms have been observed in this material [Henderson 72].

Stoneham does not address the missing fraction.

The latest weapon in the arsenal of muonium observation is the use of high transverse fields to decouple the superhyperfine interaction [Kiefl 84]. If the depolarizing impurities hypothesized above depolarize via some magnetic coupling, then a sufficiently high transverse field should decouple the muonium and allow its direct observation. If a chemical reaction is responsible for the loss of signal, then the high fields would not help. High fields will also be of no service if the depolarizing mechanism is an anisotropic hyperfine interaction. In fact, if low-temperature α -quartz with an arbitrary orientation were placed in a high transverse field, six lines would be produced rather than the usual two [Kiefl 84] observed for other materials. Given the A^2N rule, this would mean nine times as many events would be required to achieve the same quality of signal. The use of high transverse fields is by no means a panacea, but rather it is complementary to work at low and zero fields. Even in the high fields used to date, 12 KG, there are still missing fractions, although it is more difficult for the fractions to be measured accurately.

Muonium was found to be behaving as an isotope of hydrogen in α -quartz, giving further credence to the use of muonium as a proxy for hydrogen, particularly in systems or temperature regimes where hydrogen is difficult or impossible to study.

The main difficulty in pursuing various of the experiments which have been suggested herein is that every proposed experiment is in competition for beam time not only with other μ SR experiments, but with experiments in more esoteric branches of physics. Hence the proposed "muon magic beamline", as discussed in Appendix 1, which would allow up to five times as many experiments in a given amount of time, would permit the exploration of many new phenomena, including the questions raised in this work, than might otherwise be possible.

G. APPENDIX I: A MUON MAGIC BEAMLINE FOR TRIUMF

1. INTRODUCTION

A magic muon beamline is one which delivers a single muon on demand, whenever demanded, and delivers none at any other time. This cannot, as yet, be done. However, it is possible to turn off a flow of muons either at a pre-determined time or on demand. When turned on, it is merely a matter of waiting until a muon comes along. The term "magic beamline" will be used to mean a beamline which can be switched on and off, with delays for both. It is envisioned as an "add-on" to a present beamline, probably either M15 or M20, associated with the DC separators presently there or possibly upstream. Ideally, the muons rejected by the switch would be sent to an alternate beamline.

2. STATE OF THE ART

Conventional μ SR allows the muons to enter the target at random intervals. The rate limiting factor is the necessity of distinguishing which positron came from which muon, meaning only one muon may be allowed in the target at one time, any "second muon" events must be discarded. The maximum muon rate is, therefore, $N = \frac{1}{2T}$ where T is the length of the data gate used. The resulting maximum good muon rate $N_g = N/e$. That is, at the optimum incident rate, only 1/e (37%) of the muons are acceptable. Therefore, $N_g = \frac{1}{2eT}$. If one had a magic beamline, by turning it off every time a muon entered, and turning it back on at T, the maximum good muon rate would be $N_g = 1/T$. This represents an improvement of a factor of 2e, so a magic beamline could improve the real data rate by a factor of 5.4. In a typical experiment, T=10 microseconds, so the maximum rate would go from 18,000 to 100,000 per second.

3. ALTERNATIVES

At the present time, there are three other major ways of doing μ SR with increased data rates.

1. Pulse μ SR.

Periodically, a pulse containing many muons enters the target and the positrons are detected. One of the problems is that the time of stopping cannot be well defined, another is that due to the large numbers of muons and other particles scattering through the positron counters there can be large distortions at the beginning of the spectra. Probably the biggest single drawback is that one needs a pulsed source of muons – one which has a period longer than the longest time range of interest.

2. Stroboscopic μ SR.

In this method, a transverse magnetic field is applied such that the muon precession frequency is an integer multiple of the frequency of the cyclotron. In principle, an infinite number of muons can be accepted. One major disadvantage are that the magnetic field cannot be varied smoothly, as most cyclotrons are unable to vary their frequency except by, for example, a 1:5 selector. Another is the intrinsic linewidth of $1/\tau_{\mu}$, about 400 kHz, which is much too broad for many experiments. Finally, μ SR experiments in zero applied field are totally excluded⁴¹.

3. Cern wire-chamber technique.

Here, a wire chamber is used to monitor the decay positrons in order to determine their origin. In principle, it is also possible to monitor the incoming muon beam with chambers and determine where in the target they stop. Then, since one can determine where the positrons come from, it should be possible to logically "split" the target into many sub-targets only limited by the resolution of the chambers.

This reduces the second muon problem noted above, as it is less likely that two muons will enter the same small region of the target. The limiting factors are the time required to

⁴¹It might be possible to use a magic beamline to produce a time structure of whatever frequency is desired, thus removing some of the limitations mentioned. As the muons generated while the switch is off are thrown away, while with the regular stroboscopic technique all the muons generated are used, this might not be advantageous.

calculate the positions and the spatial resolution, which is limited by scattering. Perhaps one million muons per second could be tracked, but the spatial resolution might be only 5 millimetres, so a target 5 cm. on a side would be needed to get this high rate. However, many of the interesting solid state targets are about 1 cm or less. Again, though, at this rate, only 37% of the muons would be considered "good", so the good muon rate would be 370,000 per second. Such a technique is not at all suitable for gas-phase work, as the stopping region is quite ill-defined.

Surface muons have only about 140 mg/cm² range and are 100% polarized. For many experiments their use is essential, as in thin solid-state or gaseous targets. Their high polarization means they are preferred for all μ SR experiments. Using any of these 3 techniques with surface muons may not be possible, as they scatter easily reducing the spatial resolution for (3), and their time structure is very broad, broadening the pulse in (1) and making (2) less sensitive.

4. JUSTIFICATION

A magic beamline would work with surface muons for gas, liquid and solid targets in and out of cryostats just as conventional μ SR now operates, but 5 times faster. This makes it much more flexible and much more powerful than any of the other methods for increasing the rate at which experiments can be done. The availability of such a beam line would have greatly facilitated the work done in this thesis. Moreover, by increasing the real data rate by a factor of 5, it will inevitably lead to the performance of experiments which are not presently feasible due to the high statistics required. μ SR at TRIUMF currently does about 2000 runs each year.

Some of the background present in μ SR is due to muons which decay in the collimator or elsewhere. With a magic beamline this source would be shut off and the remaining background muons would then decay with the muon lifetime and not contribute to the background at longer times.

The combination of higher data rates and reduced background would allow the time scale of μ SR to be pushed further out, possibly rendering the measurement of 100 microsecond

relaxation times routine.

If a beamline were split into two legs, and this switch were installed upstream of the split, it may be that rather than use a septum and have one magic leg and one ordinary leg, it might be better to have two magic legs, where experiments take turns. For example, at this increase in data rate, experiments which presently take 1 hour for each run would take only 10 minutes. For some experiments, a change is made to the target for each run, for example, the temperature is changed, or the gas mixture might be slightly altered, meaning that at least 10 minutes downtime will occur. This leads quickly to the conclusion that for a magic beamline to be used to its full potential, it must be part of a two leg beamline. Even if the switch were downstream of a split, during the macroscopic downtime on the magic line, the other side would be an ordinary line.

Of course, an even better scenario is one in which there are two legs which are magic simultaneously (a doubly magic beamline), and the rejected muons are just dumped. Naturally, the next step is to have two legs magic and one leg ordinary If the T of interest is 10 microseconds, and the muon rate is 1,000,000 per second, it would be possible to service as many as 10 ports, all of them magic.

A multiplexed muon beam!

5. DESIGN CONSIDERATIONS

Clearly a magic beamline is desirable. How can one be made? It is necessary to bend the muon beam through an estimated angle of 3 degrees. This can be done by an effective electric field of 400 kV (the potential in volts divided by the gap times the length) or magnetically with 5000 G-cm (the field times the effective length).

Presently, at LAMPF, the TPC has an electrostatic separator for surface muons which can also be used as a switch. It does this by charging the plates of the separator to let the muons through then dumping the charge to steer the muons away. The on and off switches are triggerable, switching in about 100 nanoseconds. The problem in adapting it for a magic beamline is that it can only be used with a frequency of 500 Hz. The application at TRIUMF calls for

100,000 Hz. The limiting factor in the speed of switching and the frequency of switching is dissipating the heat generated. By accepting a slower switching time it would be possible to increase the frequency, so, for example, if more of the charging devices were used, the same technology should work here. This work, including the actual construction, should cost of the order of \$100,000. The present LAMPF device cost \$20–30,000.

Another method is to use a kicker magnet, a well-established technique used elsewhere to do fast switching on high energy proton beams. The main difficulties are that although the momentum of the surface muons is much lower, the required angle is much greater, and the beam envelope of a muon beam is much larger than for a proton beam.

For example, the AGS fast kicker has a rise time of 150 nanoseconds, and generates 100 kG-cm, but the gap is only 0.5 inches vertically and 1.25 inches horizontally. A typical muon beam envelope will be at least 6 inches in diameter. In addition, its repetition rate is only 45 Hz. Fermilab estimates the lifetime of their 250 kG-cm kicker as greater than 10^7 pulses. This lower limit would be reached in 100 seconds of use on a magic beamline. 10^9 pulses would take only 3 hours. However, these fields are much larger than we would require, so perhaps both higher repetition rates and longer lifetimes might be achievable.

A report was commissioned by TRIUMF on the feasibility of using a 43.5 kHz kicker with a rise time of 20 nanoseconds as part of the injection to a kaon factory. The requirements for field and switching time were somewhat different from the application proposed here, but the repetition rate was nearly what is being envisioned. One of the results of the study was that it was predicted the tube would last about seven hours. At perhaps \$40,000 per tube, this is not very attractive. A magic beamline with a switching time of 200 nanoseconds instead of the 20 nanoseconds for the kaon factory might mean the lifetime would increase, but if only to 70 hours, it is still inadequate.

A third method has been suggested by Syd Kreitzman of TRIUMF. He suggests that if 2 sets of saddle coils producing a field normal to the beam were positioned successively along the beam line, each with a circularly polarized RF magnetic field, by suitable choices of their phases it should be possible to transmit the muons (phase= 180°) or bend the muons away (phase= 0°).

That is, a muon passing through the first set would experience a magnetic field bending it upwards, say, then the second set would either bend it downwards if the switch were on, or upwards if the switch were off. Switching is then merely a matter of changing the relative phases of these 2 sets. The switching time should then be very quick, as no energy changes are involved.

A disadvantage of this is that it does not appear that any such device has as yet been tried anywhere. Saddle coils with RF fields are used commonly in NMR, but typically to produce fields over a much smaller volume. In such a large volume as, say 15 cm diameter by 20 cm long, a field of 125 G might be difficult to establish at the 1-50 MHz required.

The actual frequency is not so important, but the lower limit is determined by the switching time required, and the upper limit is set by the requirement that the field not change too much while the muon passes through. Surface muons only travel 8 cm per nanosecond. For example, a coil 20 cm long, with a frequency of 50 MHz would mean the field would change direction by about 46 degrees, reducing the effective field by 15%.

The capital cost is estimated to be less than \$150,000.

An advantage of the first two methods is that they bend the beam in only one direction, so it may be possible to take the rejected muons and send them out an alternate final leg on the same beamline. This would probably require a septum magnet to "amplify" the bend. This is not possible with the third method.

The triggerability and rise/fall times of the switch are important considerations. If it is not triggerable, that is, if the on and off intervals must be preset and only variable macroscopically, this would decrease the efficiency somewhat, perhaps a factor of two less than the triggered version. The rise/fall times must be less than the mean time between muons which should be at most two microseconds (M15 should have a total flux of 1 million muons/second), and preferably they should be kept to of the order of 200 nanoseconds or less. If the mean time between muons is increased, then the rise/fall times could be allowed to be longer, but all this is at the cost of a loss in efficiency. One of the limits as to how fast the muons will stop or start after the switch is flipped off or on is the time-of-flight of the muons. As noted above, their velocity is only 8 cm

per nanosecond, so a switch 8 metres upstream of the experimental target would mean the experiment would not notice the change until 100 nanoseconds later. This is in addition to the time required to tell the switch to flip, and the switching time itself. This gives some motivation for keeping the switch close to the target.

6. CONCLUSIONS

Development of the magic beamline requires work in several areas. All three of the ideas need to be explored, as the DC-type switches are presently used at frequencies 100–1000 times lower than required and the RF-type is untested and may not be feasible, although a bench test of the basic idea should not be too difficult.

Work should be done on the optics of these systems as applied to an existing beamline, either M15 or M20. M15 may be easier due to the better optics design.

Some work should be done to see the effects of the switch on the μ SR spectra, in particular the problem of an incomplete switch, i.e. if the muons are still transmitted at a level of, for example, 10%, what are the consequences to the maximum good muon rate and the background?

A magic muon beamline would increase the real data rate of a typical conventional μ SR experiment by a factor of 5 at a cost far less than that of an ordinary beamline.

H. APPENDIX 2: SOLVING THE ANISOTROPIC HYPERFINE

HAMILTONIAN

The Hamiltonian is given by:

$$H_T = -g_\mu \mu_\mu \underline{I} \cdot \underline{B} + g_e \mu_B \underline{S} \cdot \underline{B} + \underline{I} \cdot \underline{A} \cdot \underline{S} \quad (\text{A2.1})$$

where g_μ and g_e are the muon and electron g-factors respectively,

μ_μ and μ_B are the muon and Bohr (electron) magnetons,

\underline{I} and \underline{S} are the muon and electron spin operators

and \underline{A} is the hyperfine tensor.

It can be split into two pieces,

$$H_T = H_A + H_B \quad (\text{A2.2})$$

where

$$H_A = \underline{I} \cdot \underline{A} \cdot \underline{S} \text{ and} \quad (\text{A2.3})$$

$$H_B = -g_\mu \mu_\mu \underline{I} \cdot \underline{B} + g_e \mu_B \underline{S} \cdot \underline{B} \quad (\text{A2.4})$$

To solve it, first choose as a basis set, where e, μ is the order of labelling,

$$\begin{aligned} |X\rangle &= \frac{1}{\sqrt{2}}(|aa\rangle + |\beta\beta\rangle) \\ |Y\rangle &= \frac{1}{\sqrt{2}}(|aa\rangle - |\beta\beta\rangle) \\ |Z\rangle &= \frac{1}{\sqrt{2}}(|a\beta\rangle + |\beta a\rangle) \\ |0\rangle &= \frac{1}{\sqrt{2}}(|a\beta\rangle - |\beta a\rangle) \end{aligned} \quad (\text{A2.5})$$

Note:

$$\begin{array}{lll} 2I_x |X\rangle = |Z\rangle & 2I_y |X\rangle = i|0\rangle & 2I_z |X\rangle = |Y\rangle \\ 2I_x |Y\rangle = |0\rangle & 2I_y |Y\rangle = i|Z\rangle & 2I_z |Y\rangle = |X\rangle \\ 2I_x |Z\rangle = |X\rangle & 2I_y |Z\rangle = -i|Y\rangle & 2I_z |Z\rangle = -|0\rangle \\ 2I_x |0\rangle = |Y\rangle & 2I_y |0\rangle = -i|X\rangle & 2I_z |0\rangle = -|Z\rangle \end{array}$$

$$\begin{array}{lll}
2S_x |X\rangle = |Z\rangle & 2S_y |X\rangle = -i|0\rangle & 2S_z |X\rangle = |Y\rangle \\
2S_x |Y\rangle = -|0\rangle & 2S_y |Y\rangle = i|Z\rangle & 2S_z |Y\rangle = |X\rangle \\
2S_x |Z\rangle = |X\rangle & 2S_y |Z\rangle = -i|Y\rangle & 2S_z |Z\rangle = |0\rangle \\
2S_x |0\rangle = -|Y\rangle & 2S_y |0\rangle = i|X\rangle & 2S_z |0\rangle = |Z\rangle
\end{array}$$

(A2.6)

$$\begin{aligned}
\mathbf{I} \cdot \mathbf{B} &= I_x B_x + I_y B_y + I_z B_z \\
\mathbf{I} \cdot \mathbf{B} |X\rangle &= \frac{1}{2}(B_x |Z\rangle + iB_y |0\rangle + B_z |Y\rangle) \\
\mathbf{I} \cdot \mathbf{B} |Y\rangle &= \frac{1}{2}(B_x |0\rangle + iB_y |Z\rangle + B_z |X\rangle) \\
\mathbf{I} \cdot \mathbf{B} |Z\rangle &= \frac{1}{2}(B_x |X\rangle - iB_y |Y\rangle - B_z |0\rangle) \\
\mathbf{I} \cdot \mathbf{B} |0\rangle &= \frac{1}{2}(B_x |Y\rangle - iB_y |X\rangle - B_z |Z\rangle)
\end{aligned}$$

(A2.7)

$$\begin{aligned}
\mathbf{S} \cdot \mathbf{B} &= S_x B_x + S_y B_y + S_z B_z \\
\mathbf{S} \cdot \mathbf{B} |X\rangle &= \frac{1}{2}(B_x |Z\rangle - iB_y |0\rangle + B_z |Y\rangle) \\
\mathbf{S} \cdot \mathbf{B} |Y\rangle &= \frac{1}{2}(-B_x |0\rangle + iB_y |Z\rangle + B_z |X\rangle) \\
\mathbf{S} \cdot \mathbf{B} |Z\rangle &= \frac{1}{2}(B_x |X\rangle - iB_y |Y\rangle + B_z |0\rangle) \\
\mathbf{S} \cdot \mathbf{B} |0\rangle &= \frac{1}{2}(-B_x |Y\rangle + iB_y |X\rangle + B_z |Z\rangle)
\end{aligned}$$

(A2.8)

1. SOLVE H_A , THE HYPERFINE PART

In the axis system in which \underline{A} is diagonal

$$H_A = A_{xx} I_x S_x + A_{yy} I_y S_y + A_{zz} I_z S_z \quad (\text{A2.9})$$

Now the matrix elements can easily be worked out:

$$\begin{aligned}
H_A |X\rangle &= \frac{1}{4\sqrt{2}}(A_{xx}|\beta\beta\rangle - A_{yy}|\beta\beta\rangle + A_{zz}|aa\rangle + A_{xx}|aa\rangle - A_{yy}|aa\rangle + A_{zz}|\beta\beta\rangle) \\
&= \frac{1}{4\sqrt{2}}(A_{xx} - A_{yy} + A_{zz})(|\beta\beta\rangle + |aa\rangle) \\
&= \frac{1}{4}(A_{xx} - A_{yy} + A_{zz})|X\rangle \\
&= E_x |X\rangle
\end{aligned} \tag{A2.10}$$

$$\begin{aligned}
H_A |Y\rangle &= \frac{1}{4\sqrt{2}}[(A_{xx} - A_{yy})|\beta\beta\rangle + A_{zz}|aa\rangle - (A_{xx} - A_{yy})|aa\rangle - A_{zz}|\beta\beta\rangle] \\
&= \frac{1}{4\sqrt{2}}(A_{xx} - A_{yy} - A_{zz})(|\beta\beta\rangle - |aa\rangle) \\
&= \frac{1}{4}(-A_{xx} + A_{yy} + A_{zz})|Y\rangle \\
&= E_y |Y\rangle
\end{aligned} \tag{A2.11}$$

$$\begin{aligned}
H_A |Z\rangle &= \frac{1}{4\sqrt{2}}(A_{xx}|\beta a\rangle + A_{yy}|\beta a\rangle - A_{zz}|a\beta\rangle \\
&\quad + A_{xx}|a\beta\rangle + A_{yy}|a\beta\rangle - A_{zz}|\beta a\rangle) \\
&= \frac{1}{4\sqrt{2}}(A_{xx} + A_{yy} - A_{zz})(|\beta a\rangle + |a\beta\rangle) \\
&= \frac{1}{4}(A_{xx} + A_{yy} - A_{zz})|Z\rangle \\
&= E_z |Z\rangle
\end{aligned} \tag{A2.12}$$

$$\begin{aligned}
H_A |0\rangle &= \frac{1}{4\sqrt{2}}(A_{xx}|\beta a\rangle + A_{yy}|\beta a\rangle - A_{zz}|a\beta\rangle - \\
&\quad A_{xx}|a\beta\rangle - A_{yy}|a\beta\rangle + A_{zz}|\beta a\rangle) \\
&= \frac{1}{4\sqrt{2}}(-A_{xx} + A_{yy} - A_{zz})(|a\beta\rangle - |\beta a\rangle) \\
&= \frac{1}{4}(-A_{xx} - A_{yy} - A_{zz})|0\rangle \\
&= E_0 |0\rangle
\end{aligned} \tag{A2.13}$$

which can be written in matrix notation as:

$$H_A =$$

$$\frac{1}{4} \begin{bmatrix} A_{xx} - A_{yy} + A_{zz} & 0 & 0 & 0 \\ 0 & -A_{xx} + A_{yy} + A_{zz} & 0 & 0 \\ 0 & 0 & A_{xx} + A_{yy} - A_{zz} & 0 \\ 0 & 0 & 0 & -A_{xx} - A_{yy} - A_{zz} \end{bmatrix} \quad (\text{A2.14})$$

A lucky choice of basis.

Check - the trace = 0.

Check - let $A_{xx} = A_{yy} = A_{zz} = A_0 \rightarrow$ get three levels

at $\frac{1}{4}A_0$, one at $-\frac{3}{4}A_0$, just as for the isotropic case.

The transition energies are then given by:

$$\begin{aligned} 1. E_x - E_y &= \frac{1}{4}(2A_{xx} - 2A_{yy}) = \frac{1}{2}(A_{xx} - A_{yy}) \\ 2. E_x - E_z &= \frac{1}{4}(-2A_{yy} + 2A_{zz}) = \frac{1}{2}(-A_{yy} + A_{zz}) \\ 3. E_x - E_0 &= \frac{1}{4}(2A_{xx} + 2A_{zz}) = \frac{1}{2}(A_{xx} + A_{zz}) \\ 4. E_y - E_z &= \frac{1}{4}(-2A_{xx} + 2A_{zz}) = \frac{1}{2}(-A_{xx} + A_{zz}) \\ 5. E_y - E_0 &= \frac{1}{4}(2A_{yy} + 2A_{zz}) = \frac{1}{2}(A_{yy} + A_{zz}) \\ 6. E_z - E_0 &= \frac{1}{4}(2A_{xx} + 2A_{yy}) = \frac{1}{2}(A_{xx} + A_{yy}) \end{aligned} \quad (\text{A2.15})$$

2. SOLVE THE ZEEMAN PART H_B

The magnetic field part is given by:

$$H_B = -g_\mu \mu_\mu \underline{I} \cdot \underline{B} + g_e \mu_B \underline{S} \cdot \underline{B} \quad (\text{A2.4})$$

This gives

$$H_B =$$

$$\begin{bmatrix} 0 & \frac{1}{2}B_z(\gamma_e - \gamma_\mu) & \frac{1}{2}B_x(\gamma_e - \gamma_\mu) & \frac{i}{2}B_y(\gamma_e + \gamma_\mu) \\ \frac{1}{2}B_z(\gamma_e - \gamma_\mu) & 0 & -\frac{i}{2}B_y(\gamma_e - \gamma_\mu) & -\frac{1}{2}B_x(\gamma_e + \gamma_\mu) \\ \frac{1}{2}B_x(\gamma_e - \gamma_\mu) & \frac{i}{2}B_y(\gamma_e - \gamma_\mu) & 0 & \frac{1}{2}B_z(\gamma_e + \gamma_\mu) \\ -\frac{i}{2}B_y(\gamma_e + \gamma_\mu) & -\frac{1}{2}B_x(\gamma_e + \gamma_\mu) & \frac{1}{2}B_z(\gamma_e + \gamma_\mu) & 0 \end{bmatrix} \quad (\text{A2.16})$$

where $\gamma_e = g_e \mu_B$ and $\gamma_\mu = g_\mu \mu_\mu$

3. SOLVE THE TOTAL H_T

Substituting eqs. A2.14 and A2.16 into A2.2 and multiplying both sides by 4 for convenience,

$$4H_T =$$

$$\begin{bmatrix} A_{xx} - A_{yy} + A_{zz} & 2B_z(\gamma_e - \gamma_\mu) & 2B_x(\gamma_e - \gamma_\mu) & 2iB_y(\gamma_e + \gamma_\mu) \\ 2B_z(\gamma_e - \gamma_\mu) & -A_{xx} + A_{yy} + A_{zz} & -2iB_y(\gamma_e - \gamma_\mu) & -2B_x(\gamma_e + \gamma_\mu) \\ 2B_x(\gamma_e - \gamma_\mu) & 2iB_y(\gamma_e - \gamma_\mu) & A_{xx} + A_{yy} - A_{zz} & 2B_z(\gamma_e + \gamma_\mu) \\ -2iB_y(\gamma_e + \gamma_\mu) & -2B_x(\gamma_e + \gamma_\mu) & 2B_z(\gamma_e + \gamma_\mu) & -A_{xx} - A_{yy} - A_{zz} \end{bmatrix} \quad (\text{A2.17})$$

which is rather unpleasant, however analytical expressions for the energy can be found easily for certain special cases.

a. Special case: $B_z \neq 0, B_x = B_y = 0$

i. Finding the eigenvalues of H_T

$$4H_T =$$

$$\begin{bmatrix} A_{xx} - A_{yy} + A_{zz} & 2B_z(\gamma_e - \gamma_\mu) & 0 & 0 \\ 2B_z(\gamma_e - \gamma_\mu) & -A_{xx} + A_{yy} + A_{zz} & 0 & 0 \\ 0 & 0 & A_{xx} + A_{yy} - A_{zz} & 2B_z(\gamma_e + \gamma_\mu) \\ 0 & 0 & 2B_z(\gamma_e + \gamma_\mu) & -A_{xx} - A_{yy} - A_{zz} \end{bmatrix} \quad (A2.18)$$

$$\text{To solve, set } |4H_T - \lambda \underline{1}| = 0 \quad (A2.19)$$

One set of solutions is:

$$\begin{aligned} (A_{xx} - A_{yy} + A_{zz} - \lambda)(-A_{xx} + A_{yy} + A_{zz} - \lambda) - 4B_z^2(\gamma_e - \gamma_\mu)^2 &= 0 \\ = \lambda^2 + \lambda(A_{xx} - A_{yy} - A_{zz} - A_{xx} + A_{yy} - A_{zz}) + \\ (A_{xx} - A_{yy} + A_{zz})(-A_{xx} + A_{yy} + A_{zz}) - 4B_z^2(\gamma_e - \gamma_\mu)^2 & \\ = \lambda^2 - 2A_{zz}\lambda + A_{zz}^2 - (A_{xx} - A_{yy})^2 - 4B_z^2(\gamma_e - \gamma_\mu)^2 & \end{aligned}$$

$$\begin{aligned} \lambda &= \frac{1}{2} \{ 2A_{zz} \pm [4A_{zz}^2 - 4A_{zz}^2 + 4(A_{xx} - A_{yy})^2 + 16B_z^2(\gamma_e - \gamma_\mu)^2]^{1/2} \} \\ &= A_{zz} \pm [(A_{xx} - A_{yy})^2 + 4B_z^2(\gamma_e - \gamma_\mu)^2]^{1/2} \end{aligned} \quad (A2.20)$$

which gives the energy levels:

$$\begin{aligned} E_1 &= \frac{1}{4} \{ A_{zz} + [(A_{xx} - A_{yy})^2 + 4B_z^2(\gamma_e - \gamma_\mu)^2]^{1/2} \} \\ E_2 &= \frac{1}{4} \{ A_{zz} - [(A_{xx} - A_{yy})^2 + 4B_z^2(\gamma_e - \gamma_\mu)^2]^{1/2} \} \end{aligned} \quad (A2.21)$$

The other set of solutions is:

$$\begin{aligned} (A_{xx} + A_{yy} - A_{zz} - \lambda)(-A_{xx} - A_{yy} - A_{zz} - \lambda) - 4B_z^2(\gamma_e + \gamma_\mu)^2 &= 0 \\ = \lambda^2 + 2A_{zz}\lambda + A_{zz}^2 - (A_{xx} + A_{yy})^2 - 4B_z^2(\gamma_e + \gamma_\mu)^2 & \end{aligned}$$

$$\begin{aligned}\lambda &= \frac{1}{2}(-2A_{zz} \pm [4A_{zz}^2 - 4A_{zz}^2 + 4(A_{xx} - A_{yy})^2 + 16B_z^2(\gamma_e + \gamma_\mu)^2]^{1/2}) \\ &= -A_{zz} \pm [(A_{xx} + A_{yy})^2 + 4B_z^2(\gamma_e + \gamma_\mu)^2]^{1/2}\end{aligned}\quad (\text{A2.22})$$

$$\begin{aligned}E_3 &= \frac{1}{4}\{-A_{zz} + [(A_{xx} + A_{yy})^2 + 4B_z^2(\gamma_e + \gamma_\mu)^2]^{1/2}\} \\ E_4 &= \frac{1}{4}\{-A_{zz} - [(A_{xx} + A_{yy})^2 + 4B_z^2(\gamma_e + \gamma_\mu)^2]^{1/2}\}\end{aligned}\quad (\text{A2.23})$$

A2.21 and A2.23 lead to the transition energies:

$$\begin{aligned}E_{12} &= E_1 - E_2 \\ &= \frac{1}{2}[(A_{xx} - A_{yy})^2 + 4B_z^2(\gamma_e - \gamma_\mu)^2]^{1/2}\end{aligned}\quad (\text{A2.24})$$

$$\begin{aligned}E_{13} &= E_1 - E_3 \\ &= \frac{1}{4}\{2A_{zz} + [(A_{xx} - A_{yy})^2 + 4B_z^2(\gamma_e - \gamma_\mu)^2]^{1/2} \\ &\quad - [(A_{xx} + A_{yy})^2 + 4B_z^2(\gamma_e + \gamma_\mu)^2]^{1/2}\}\end{aligned}\quad (\text{A2.25})$$

$$\begin{aligned}E_{14} &= E_1 - E_4 \\ &= \frac{1}{4}\{2A_{zz} + [(A_{xx} - A_{yy})^2 + 4B_z^2(\gamma_e - \gamma_\mu)^2]^{1/2} \\ &\quad + [(A_{xx} + A_{yy})^2 + 4B_z^2(\gamma_e + \gamma_\mu)^2]^{1/2}\}\end{aligned}\quad (\text{A2.26})$$

$$\begin{aligned}E_{23} &= E_2 - E_3 \\ &= \frac{1}{4}\{2A_{zz} - [(A_{xx} - A_{yy})^2 + 4B_z^2(\gamma_e - \gamma_\mu)^2]^{1/2} \\ &\quad - [(A_{xx} + A_{yy})^2 + 4B_z^2(\gamma_e + \gamma_\mu)^2]^{1/2}\}\end{aligned}\quad (\text{A2.27})$$

$$\begin{aligned}E_{24} &= E_2 - E_4 \\ &= \frac{1}{4}\{2A_{zz} - [(A_{xx} - A_{yy})^2 + 4B_z^2(\gamma_e - \gamma_\mu)^2]^{1/2} \\ &\quad + [(A_{xx} + A_{yy})^2 + 4B_z^2(\gamma_e + \gamma_\mu)^2]^{1/2}\}\end{aligned}\quad (\text{A2.28})$$

$$\begin{aligned}
 E_{34} &= E_3 - E_4 \\
 &= \frac{1}{2} [(A_{xx} + A_{yy})^2 + 4B_z^2(\gamma_e - \gamma_\mu)^2]^{1/2}
 \end{aligned}
 \tag{A2.29}$$

Check: for $B_z = 0$, these agree with the zero-field expressions.

Now, if the anisotropy is small, A_{xx} , A_{yy} and A_{zz} are approximately equal, and if $B_z(\gamma_e - \gamma_\mu)$ is much smaller than A_{xx} , which of these transitions is "normally" observable, without, for the moment, considering transition intensities? That is, what is the order of magnitude of E_{ij} ? Is it like $A_{xx} - A_{yy}$ or like $A_{xx} + A_{yy}$? E_{12} is clearly small, and therefore should be observable. E_{34} is clearly large, and therefore likely unobservable.

Observable	Unobservable
E_{12}	E_{14}
E_{13}	E_{24}
E_{23}	E_{34}

which is quite a natural grouping, as in zero-field the state 4 corresponds to the singlet and the states 1,2,3 to the triplet.

ii. Find the Transition Intensities

To find the intensity of the E_{12} transition, first find the appropriate eigenvectors.

To find ψ_1 , substitute E_1 into the top line of the secular equations corresponding to A2.18.

$$(A_{xx} - A_{yy} + A_{zz} - A_{zz} - [(A_{xx} - A_{yy})^2 + 4B_z^2(\gamma_e - \gamma_\mu)^2]^{1/2})C_1 + 2B_z(\gamma_e - \gamma_\mu)C_2 = 0 \quad (\text{A2.30})$$

$$C_1 = \frac{-2B}{A_{xx} - A_{yy} - [(A_{xx} - A_{yy})^2 + 4B^2]^{1/2}} C_2 \quad (\text{A2.31})$$

where $B = B_z$. Also, $C_1^2 + C_2^2 = 1$

$$C_2 = \pm \left[\frac{4B^2}{\{A_{xx} - A_{yy} - [(A_{xx} - A_{yy})^2 + 4B^2]^{1/2}\}^2 + 1} \right]^{-1/2} \quad (\text{A2.32})$$

$$C_1 = \mp \left[\frac{2B}{A_{xx} - A_{yy} - [(A_{xx} - A_{yy})^2 + 4B^2]^{1/2}} \right] \times \left[\frac{4B^2}{\{A_{xx} - A_{yy} - [(A_{xx} - A_{yy})^2 + 4B^2]^{1/2}\}^2 + 1} \right]^{-1/2} \quad (\text{A2.33})$$

Look at limits:

as B approaches 0, C_2 approaches 0

C_1 approaches ± 1

as B approaches ∞ , C_2 approaches $\pm \frac{1}{\sqrt{2}}$

C_1 approaches $\mp \frac{1}{\sqrt{2}}$

To find ψ_2 , substitute E_2 from A2.21 into A2.18.

$$2BC_1 + (-A_{xx} + A_{yy} + A_{zz} - A_{zz} + [(A_{xx} - A_{yy})^2 + 4B^2]^{1/2})C_2 = 0$$

$$C_1 = \frac{A_{xx} - A_{yy} - [(A_{xx} - A_{yy})^2 + 4B^2]^{1/2}}{2B} C_2 \quad (\text{A2.34})$$

From the overall normalization,

$$C_2 = \pm \left[\frac{\{A_{xx} - A_{yy} - [(A_{xx} - A_{yy})^2 + 4B^2]^{1/2}\}^2}{4B^2} + 1 \right]^{-1/2} \quad (\text{A2.35})$$

$$C_1 = \pm \left[\frac{A_{xx} - A_{yy} - [(A_{xx} - A_{yy})^2 + B^2]^{1/2}}{2B} \right] \\ \times \left[\frac{A_{xx} - A_{yy} - [(A_{xx} - A_{yy})^2 + 4B^2]^{1/2}}{2B} \right]^2 + 1 \right]^{-1/2} \quad (\text{A2.36})$$

Now, for ψ_2 as

B approaches 0, C_2 approaches ± 1

C_1 approaches 0

B approaches ∞ , C_2 approaches $\pm \frac{1}{\sqrt{2}}$

C_1 approaches $\mp \frac{1}{\sqrt{2}}$

So

for $B=0$, $\sigma_z |1\rangle = |2\rangle$

$\sigma_z |2\rangle = |1\rangle$

(A2.37)

where σ is the Pauli spin matrix.

For $B=\infty$,

$$\begin{aligned} \sigma_z |1\rangle &= \frac{1}{\sqrt{2}}(\sigma_z |X\rangle - \sigma_z |Y\rangle) \\ &= \frac{1}{\sqrt{2}}(|Y\rangle - |X\rangle) \\ &= -|1\rangle \end{aligned}$$

$$\begin{aligned} \sigma_z |2\rangle &= \frac{1}{\sqrt{2}}(\sigma_z |X\rangle + \sigma_z |Y\rangle) \\ &= |2\rangle \end{aligned}$$

(A2.38)

Since there is no matrix element for σ_z to connect levels 1 and 2 for $B=\infty$, and since

σ_x and σ_y cannot connect 1 and 2 for any B_z , the intensity of E_{12} is equal to zero. However, there is an intensity for $B=0$. To generalize, set $\frac{B}{A_{xx} - A_{yy}} = K$.

$$\psi_1 = \left[\frac{4K^2}{\{1 - [1 + 4K^2]^{1/2}\}^2} + 1 \right]^{-1/2} \left[\frac{2K}{1 - [1 + 4K^2]^{1/2}} |X\rangle - |Y\rangle \right] \quad (\text{A2.39})$$

$$\psi_2 = \left[\frac{\{1 - [1 + 4K^2]^{1/2}\}^2}{4K^2} + 1 \right]^{-1/2} \left[\frac{1 - [1 + 4K^2]^{1/2}}{2K} |X\rangle + |Y\rangle \right] \quad (\text{A2.40})$$

Check: does $\langle \psi_2 | \psi_1 \rangle = 0$? Yes, so alright so far.

In general,

$$\begin{aligned} \sigma_z |1\rangle &= N_1 \left[\frac{2K}{1 - [1 + 4K^2]^{1/2}} |Y\rangle - |X\rangle \right] \\ \sigma_z |2\rangle &= N_2 \left[\frac{1 - [1 + 4K^2]^{1/2}}{2K} |Y\rangle + |X\rangle \right] \end{aligned} \quad (\text{A2.41})$$

$$\begin{aligned} \langle 2 | \sigma_z | 1 \rangle &= N_1 N_2 \left[\frac{2K}{1 - [1 + 4K^2]^{1/2}} - \frac{1 - [1 + 4K^2]^{1/2}}{2K} \right] \\ &= N_1 N_2 \left[\frac{4K^2 - 1 - 1 - 4K^2 + 2[1 + 4K^2]^{1/2}}{\{1 - [1 + 4K^2]^{1/2}\} 2K} \right] \\ &= -N_1 N_2 \left[\frac{1 - [1 + 4K^2]^{1/2}}{\{1 - [1 + 4K^2]^{1/2}\} K} \right] \end{aligned}$$

$$= -\frac{N_1 N_2}{K} \quad (\text{A2.42})$$

Now,

$$N_1 N_2 = \left[2 + \frac{4K^2}{\{1-[1+4K^2]^{1/2}\}^2} + \frac{\{1-[1+4K^2]^{1/2}\}^2}{4K^2} \right]^{-1/2}$$

$$\text{aside:} = \left[2 + x + \frac{1}{x} \right]^{-1/2} = \left[\frac{(x+1)^2}{x} \right]^{-1/2} = \frac{x^{1/2}}{x+1}$$

$$N_1 N_2 = \frac{2K}{1-[1+4K^2]^{1/2}} \frac{\{1-[1+4K^2]^{1/2}\}^2}{2+8K^2-2[1+4K^2]^{1/2}}$$

$$N_1 N_2 = \frac{K\{1-[1+4K^2]^{1/2}\}}{1+4K^2-[1+4K^2]^{1/2}}$$

$$\text{aside:} = \frac{1-y}{y^2-y} = \frac{1-y}{-y(1-y)} = -\frac{1}{y}$$

$$N_1 N_2 = -\frac{K}{[1+4K^2]^{1/2}} \quad (\text{A2.43})$$

Substituting A2.43 into A2.42, we get

$$\langle 2 | \sigma_z | 1 \rangle = -\frac{1}{(1+4K^2)^{1/2}} \quad (\text{A2.44})$$

To check,

$$\begin{aligned} \langle 1 | \sigma_z | 2 \rangle &= N_1 N_2 \left[\frac{2K}{1-[1+4K^2]^{1/2}} - \frac{1-[1+4K^2]^{1/2}}{2K} \right] \\ &= -\frac{1}{(1+4K^2)^{1/2}} \end{aligned}$$

To find ψ_4 , substitute E_4 into line 3 of A2.18.

$$[A_{xx} + A_{yy} - A_{zz} - \{-A_{zz} + [(A_{xx} + A_{yy})^2 + 4B_2^2]^{1/2}\}]C_1 + 2B_2C_2 = 0$$

$$= [A_{xx} + A_{yy} + [(A_{xx} + A_{yy})^2 + 4B_2^2]^{1/2}]C_1 + 2B_2C_2 \quad (\text{A2.45})$$

Where $B_2 = B_z(\gamma_e + \gamma_\mu)$.

From the normalization, $C_1^2 + C_2^2 = 1$

$$C_2 = \pm \left[\frac{4B_2^2}{\{A_{xx} + A_{yy} + [(A_{xx} + A_{yy})^2 + 4B_2^2]^{1/2}\}^2} + 1 \right]^{-1/2} \quad (\text{A2.46})$$

$$C_1 = \mp \left[\frac{4B_2^2}{\{A_{xx} + A_{yy} + [(A_{xx} + A_{yy})^2 + 4B_2^2]^{1/2}\}^2} + 1 \right]^{-1/2} \\ \times \left[\frac{2B_2}{A_{xx} + A_{yy} + [(A_{xx} + A_{yy})^2 + 4B_2^2]^{1/2}} \right] \quad (\text{A2.47})$$

$$\psi_4 = \left[\frac{4B_2^2}{\{A_{xx} + A_{yy} + [(A_{xx} + A_{yy})^2 + 4B_2^2]^{1/2}\}^2} + 1 \right]^{-1/2} \\ \times \left[\frac{2B_2}{A_{xx} + A_{yy} + [(A_{xx} + A_{yy})^2 + 4B_2^2]^{1/2}} |z\rangle + |0\rangle \right] \\ = \left[\frac{4K_2^2}{\{1 + [1 + 4K_2^2]^{1/2}\}^2} + 1 \right]^{-1/2} \\ \times \left[\frac{2K_2}{1 + [1 + 4K_2^2]^{1/2}} |z\rangle + |0\rangle \right] \quad (\text{A2.48})$$

where $K_2 = \frac{B_2}{A_{xx} + A_{yy}}$

Similarly,

$$\psi_3 = \left[\frac{\{1 + [1 + 4K_2^2]^{1/2}\}^2}{4K_2^2} + 1 \right]^{-1/2} \left[\frac{1 + [1 + 4K_2^2]^{1/2}}{2K_2} |Z\rangle - |0\rangle \right] \quad (\text{A2.49})$$

Since ψ_1 and ψ_2 are composed only of $|X\rangle$ and $|Y\rangle$, and since the only σ which connects $|X\rangle$ and $|Y\rangle$ is σ_z , it follows that for any magnetic field parallel to the z axis there will never be an E_{12} signal observed in the x or y directions. Since ψ_3 and ψ_4 are only made up of $|Z\rangle$ and $|0\rangle$, and since the only σ which connects them is σ_z , even the high frequency E_{34} signal will have no intensity in the x or y directions.

b. Solve for three sites

So far, only the simple case of a single site has been considered. Now consider what happens if there are three sites related by a one hundred twenty degree rotation around a symmetry axis? The eigenvalues and transition intensities must be calculated for each site separately, then the spectra summed to give the experimentally observed spectrum. To do this, it is useful to take the magnetic field in terms of the external crystal axes, x' , y' and z' , and transform it to the internal axes, x , y and z . There is a

transformation from x', y', z' to x, y, z for each of the three sites, $\underline{D}(0)$, $\underline{D}(+120)$, and $\underline{D}(-120)$. The notation $\underline{D}(n)$ will be used to represent all three cases.

$\underline{D}(n) =$

$$\begin{bmatrix} \cos(\phi+n)\cos\psi & \sin(\phi+n)\cos\psi & \sin\theta\sin\psi \\ -\cos\theta\sin(\phi+n)\sin\psi & +\cos\theta\cos(\phi+n)\sin\psi & \\ -\cos(\phi+n)\sin\psi & -\sin(\phi+n)\sin\psi & \sin\theta\cos\psi \\ -\cos\theta\sin(\phi+n)\cos\psi & +\cos\theta\cos(\phi+n)\cos\psi & \\ \sin\theta\sin(\phi+n) & -\sin\theta\cos(\phi+n) & \cos\theta \end{bmatrix}$$

(A2.50)

θ, ϕ , and ψ are defined conventionally as in Classical Mechanics by Goldstein [50].

What is \underline{B} in terms of \underline{B}' ?

$\underline{B} = \underline{D}\underline{B}'$

$$\begin{bmatrix} B_x \\ B_y \\ B_z \end{bmatrix} = \begin{bmatrix} [\cos(\phi+n)\cos\psi - \cos\theta\sin(\phi+n)\sin\psi]B'_x \\ + [\sin(\phi+n)\cos\psi + \cos\theta\cos(\phi+n)\sin\psi]B'_y \\ + \sin\theta\sin\psi B'_z \\ [-\cos(\phi+n)\sin\psi - \sin\theta\sin(\phi+n)\sin\psi]B'_x \\ + [-\sin(\phi+n)\sin\psi + \cos\theta\cos(\phi+n)\cos\psi]B'_y \\ + \sin\theta\cos\psi B'_z \\ \sin\theta\sin(\phi+n)B'_x - \sin\theta\cos(\phi+n)B'_y + \sin\theta B'_z \end{bmatrix}$$

(A2.51)

One can then substitute these values for the components of \underline{B} into equation A2.17, and get H_T in terms of the external axes.

(A2.52)

$$\begin{aligned}
 \delta H = & \\
 A_{xx} - A_{yy} + A_{zz} & \quad 2(\gamma_e^{-\gamma_\mu}) \{ \sin\theta \sin(\phi+n) B'_x \\
 & \quad - \sin\theta \cos(\phi+n) B'_y + \cos\theta B'_z \} \\
 & \quad 2(\gamma_e^{-\gamma_\mu}) \{ (\cos(\phi+n) \cos\psi \\
 & \quad - \cos\theta \sin(\phi+n) \sin\psi) B'_x \\
 & \quad + [\sin(\phi+n) \cos\psi \\
 & \quad + \cos\theta \cos(\phi+n) \sin\psi] B'_y \\
 & \quad + \sin\theta \cos\psi B'_z \} \\
 & \quad - A_{xx} + A_{yy} + A_{zz} \\
 & \quad -2(\gamma_e^{-\gamma_\mu}) \{ \sin\theta \sin(\phi+n) B'_x \\
 & \quad - \sin\theta \cos(\phi+n) B'_y + \cos\theta B'_z \} \\
 & \quad 2(\gamma_e^{-\gamma_\mu}) \{ (\cos(\phi+n) \cos\psi \\
 & \quad - \cos\theta \sin(\phi+n) \sin\psi) B'_x \\
 & \quad + [\sin(\phi+n) \cos\psi \\
 & \quad + \cos\theta \cos(\phi+n) \sin\psi] B'_y \\
 & \quad + \sin\theta \cos\psi B'_z \} \\
 & \quad -2(\gamma_e^{+\gamma_\mu}) \{ [-\cos(\phi+n) \sin\psi \\
 & \quad - \cos\theta \sin(\phi+n) \cos\psi] B'_x \\
 & \quad + [-\sin(\phi+n) \sin\psi \\
 & \quad + \cos\theta \cos(\phi+n) \cos\psi] B'_y \\
 & \quad + \sin\theta \cos\psi B'_z \} \\
 & \quad A_{xx} + A_{yy} - A_{zz} \\
 & \quad 2(\gamma_e^{-\gamma_\mu}) \{ [-\cos(\phi+n) \sin\psi \\
 & \quad - \cos\theta \sin(\phi+n) \cos\psi] B'_x \\
 & \quad + [-\sin(\phi+n) \sin\psi \\
 & \quad + \cos\theta \cos(\phi+n) \cos\psi] B'_y \\
 & \quad + \sin\theta \cos\psi B'_z \} \\
 & \quad -2(\gamma_e^{+\gamma_\mu}) \{ (\cos(\phi+n) \cos\psi \\
 & \quad - \cos\theta \sin(\phi+n) \sin\psi) B'_x \\
 & \quad + [\sin(\phi+n) \cos\psi \\
 & \quad + \cos\theta \cos(\phi+n) \sin\psi] B'_y \\
 & \quad + \sin\theta \sin\psi B'_z \} \\
 & \quad -A_{xx} - A_{yy} - A_{zz} \\
 & \quad 2(\gamma_e^{+\gamma_\mu}) \{ \sin\theta \sin(\phi+n) B'_x \\
 & \quad - \sin\theta \cos(\phi+n) B'_y + \cos\theta B'_z \}
 \end{aligned}$$

There are three of these corresponding to the three values of n . Each must be solved separately, and the frequencies and intensities calculated. The experimental spectrum will then be the sum of all three. To use it for the purpose of interpreting experimental data would be a daunting task but for the existence of computers. The Hamiltonians can be numerically solved for a given θ , ϕ , ψ , and the experimental spectrum can be predicted. This can be done as an iterative process, driven by the disagreement between the prediction and the observation, eventually resulting in a set of θ , ϕ , ψ which should successfully predict the experimental spectrum.

c. Time dependence of the polarization for a single site

The time dependence of the polarization can be written as:

$$\langle \sigma_{\underline{u}_f} \rangle(t) = \underline{u}_f \cdot \underline{M} \cdot \underline{u}_i \quad (\text{A2.53})$$

where the elements of \underline{M} are given by:

$$\begin{aligned} M_{fi}(t) &= M_{fi}(0) \\ &+ \frac{2}{N} \sum_{n \neq m} |\langle m | \sigma_f | n \rangle| |\langle n | \sigma_i | m \rangle| \{ \cos(\omega_{mn} t + \eta_{mn}) - \cos \eta_{mn} \} \end{aligned} \quad (\text{A2.54})$$

$$\eta_{mn} = \theta_{mn}^f - \theta_{mn}^i$$

$$\theta_{mn}^r = \arg \langle m | \sigma_r | n \rangle$$

The direction of initial polarization \underline{u}_i and the direction of observation \underline{u}_f are known in the external frame. One consequence of this expression for $\langle \sigma_{\underline{u}_f} \rangle(t)$ is that even if \underline{u}_f is perpendicular to

\underline{u}_i , $\langle \sigma_{u_f} \rangle(t) \neq 0$ provided that \underline{u}_i is not along a principal axis.

When H_T is solved in the $|X\rangle$, $|Y\rangle$, $|Z\rangle$, $|0\rangle$ basis, the four eigenfunctions which result are of the form

$$\psi_n = C_{1n}|X\rangle + C_{2n}|Y\rangle + C_{3n}|Z\rangle + C_{4n}|0\rangle, \text{ so} \quad (\text{A2.55})$$

$$\begin{aligned} \langle \psi_m | \psi_n \rangle &= C_{1m}^* C_{1n} + C_{2m}^* C_{2n} + C_{3m}^* C_{3n} + C_{4m}^* C_{4n} \\ &= 0 \quad \text{if } m \text{ does not equal } n \\ &= 1 \quad \text{if } m \text{ equals } n. \end{aligned} \quad (\text{A2.56})$$

$$\begin{aligned} \sigma_x | \psi_n \rangle &= C_{3n} | X \rangle + C_{4n} | Y \rangle + C_{1n} | Z \rangle + C_{2n} | 0 \rangle \\ \sigma_y | \psi_n \rangle &= -iC_{4n} | X \rangle - iC_{3n} | Y \rangle + iC_{2n} | Z \rangle + iC_{1n} | 0 \rangle \\ \sigma_z | \psi_n \rangle &= C_{2n} | X \rangle + C_{1n} | Y \rangle - C_{4n} | Z \rangle - C_{3n} | 0 \rangle, \text{ so} \end{aligned} \quad (\text{A2.57})$$

$$\begin{aligned} \langle \psi_m | \sigma_x | \psi_n \rangle &= C_{1m}^* C_{3n} + C_{2m}^* C_{4n} + C_{3m}^* C_{1n} + C_{4m}^* C_{2n} \\ \langle \psi_m | \sigma_y | \psi_n \rangle &= -iC_{1m}^* C_{4n} - iC_{2m}^* C_{3n} + iC_{3m}^* C_{2n} + iC_{4m}^* C_{1n} \\ \langle \psi_m | \sigma_z | \psi_n \rangle &= C_{1m}^* C_{2n} + C_{2m}^* C_{1n} - C_{3m}^* C_{4n} - C_{4m}^* C_{3n} \end{aligned} \quad (\text{A2.58})$$

In the case where $\underline{B}' = 0$ the only $\langle \psi_m | \sigma_j | \psi_n \rangle$ remaining are

$$\begin{aligned} \langle \psi_3 | \sigma_x | \psi_1 \rangle &= 1 = \langle \psi_1 | \sigma_x | \psi_3 \rangle \\ \langle \psi_2 | \sigma_x | \psi_4 \rangle &= 1 = \langle \psi_4 | \sigma_x | \psi_2 \rangle \\ \langle \psi_4 | \sigma_y | \psi_1 \rangle &= i = -\langle \psi_1 | \sigma_y | \psi_4 \rangle \\ \langle \psi_3 | \sigma_y | \psi_2 \rangle &= i = -\langle \psi_2 | \sigma_y | \psi_3 \rangle \\ \langle \psi_2 | \sigma_z | \psi_1 \rangle &= 1 = \langle \psi_1 | \sigma_z | \psi_2 \rangle \\ \langle \psi_4 | \sigma_z | \psi_3 \rangle &= -1 = \langle \psi_3 | \sigma_z | \psi_4 \rangle \end{aligned} \quad (\text{A2.59})$$

All η_{mn} are 0, and

$$\underline{\underline{M}}(t) =$$

$$\begin{bmatrix} M_{xx}(0) + \frac{1}{2}\cos\omega_{13}t & 0 & 0 \\ + \frac{1}{2}\cos\omega_{24}t & & \\ 0 & M_{yy}(0) + \frac{1}{2}\cos\omega_{14}t & 0 \\ & + \frac{1}{2}\cos\omega_{23}t & \\ 0 & 0 & M_{zz}(0) + \frac{1}{2}\cos\omega_{12}t \\ & & + \frac{1}{2}\cos\omega_{34}t \end{bmatrix}$$

(A2.60)

Simplifications:

in the absence of an applied field, the $\underline{\underline{M}}$ for each site is the same;

since ω_{24} , ω_{14} and ω_{34} are comparable to the vacuum hyperfine frequency and hence not readily observable, they can be dropped from further consideration;

since the most interesting part is going to be the part which oscillates, the $M_{ii}(0)$ can also be dropped.

The result is:

$$\underline{\underline{M}}(t) =$$

$$\begin{bmatrix} \frac{1}{2}\cos\omega_{13}t & 0 & 0 \\ 0 & \frac{1}{2}\cos\omega_{23}t & 0 \\ 0 & 0 & \frac{1}{2}\cos\omega_{12}t \end{bmatrix}$$

(A2.61)

In the special case where the initial polarization and direction of observation coincide, that is, $\underline{u}_f = \underline{u}_i$ and where \underline{u} , \underline{M} are in internal coordinates,

$$\langle \sigma_{\underline{u}} \rangle(t) = \underline{u} \cdot \underline{M} \cdot \underline{u} \text{ for one site.} \quad (\text{A2.62})$$

d. Spectrum for Three Sites

The observed spectrum for the case of three sites related by a three-fold symmetry axis can be calculated for this simple case. Using the \underline{D} 's as defined earlier, and with \underline{u}' the polarization direction in external coordinates, simply average the spectra from the three sites. That is,

$$\langle \sigma_{\underline{u}} \rangle(t) = \frac{1}{3} [\underline{D}_0 \cdot \underline{u}' \cdot \underline{M} \cdot \underline{D}_0 \cdot \underline{u}' + \underline{D}_+ \cdot \underline{u}' \cdot \underline{M} \cdot \underline{D}_+ \cdot \underline{u}' + \underline{D}_- \cdot \underline{u}' \cdot \underline{M} \cdot \underline{D}_- \cdot \underline{u}'] \quad (\text{A2.63})$$

where $\underline{D}_0 = \underline{D}(0)$, $\underline{D}_+ = \underline{D}(+120)$ and $\underline{D}_- = \underline{D}(-120)$

$$\begin{aligned} \langle \sigma_{\underline{u}} \rangle(t) = & \frac{1}{3} \sum_{n=0, \pm 120, -120} \{ [\cos(\phi+n)\cos\psi - \cos\theta\sin(\phi+n)\sin\psi]x' \\ & + [\sin(\phi+n)\cos\psi + \cos\theta\cos(\phi+n)\sin\psi]y' \\ & + \sin\theta\sin\psi z' \}^2 K_{13} \\ & + \{ [-\cos(\phi+n)\sin\psi - \cos\theta\sin(\phi+n)\cos\psi]x' \\ & + [-\sin(\phi+n)\sin\psi + \cos\theta\cos(\phi+n)\cos\psi]y' \\ & + \sin\theta\cos\psi z' \}^2 K_{23} \\ & + \{ \sin\theta\sin(\phi+n)x' - \sin\theta\cos(\phi+n)y' \\ & + \cos\theta z' \}^2 K_{12} \end{aligned} \quad (\text{A2.64})$$

$$\begin{aligned} \text{where } K_{13} &= \frac{1}{2} \cos\omega_{13} t \\ K_{23} &= \frac{1}{2} \cos\omega_{23} t \\ K_{12} &= \frac{1}{2} \cos\omega_{12} t \end{aligned} \quad (\text{A2.65})$$

Clearly, following some algebraic manipulation,

$$\begin{aligned}
\langle \sigma_u \rangle(t) = & \frac{1}{3} \left[\left\{ \frac{3}{2} \sin^2 \theta \sin^2 \psi (2z'^2 - x'^2 - y'^2) + \frac{3}{2} (x'^2 + y'^2) \right\} K_{13} \right. \\
& + \left\{ \frac{3}{2} \sin^2 \theta \cos^2 \psi (2z'^2 - x'^2 - y'^2) + \frac{3}{2} (x'^2 + y'^2) \right\} K_{23} \\
& \left. + \left\{ \frac{3}{2} \cos^2 \theta (2z'^2 - x'^2 - y'^2) + \frac{3}{2} (x'^2 + y'^2) \right\} K_{12} \right] \quad (\text{A2.66})
\end{aligned}$$

But $x'^2 + y'^2 + z'^2 = 1$

$$\begin{aligned}
\langle \sigma_u \rangle(t) = & \frac{1}{4} \left\{ [\sin^2 \theta \sin^2 \psi (3z'^2 - 1) + 1 - z'^2] \cos \omega_{13} t \right. \\
& + [\sin^2 \theta \cos^2 \psi (3z'^2 - 1) + 1 - z'^2] \cos \omega_{23} t \\
& \left. + [\cos^2 \theta (3z'^2 - 1) + 1 - z'^2] \cos \omega_{12} t \right\} \quad (\text{A2.67})
\end{aligned}$$

Note:

$$\begin{aligned}
\sin \theta \sin \psi &= \cos \gamma_{xx'} \\
\sin \theta \cos \psi &= \cos \gamma_{yy'} \\
\cos \theta &= \cos \gamma_{zz'} \quad (\text{A2.68})
\end{aligned}$$

the direction cosines, the angle between the corresponding external and internal axes. So

$$\begin{aligned}
\langle \sigma_u \rangle(t) = & \frac{1}{4} \left\{ [\cos^2 \gamma_{xx'} (3z'^2 - 1) + 1 - z'^2] \cos \omega_{13} t \right. \\
& + [\cos^2 \gamma_{yy'} (3z'^2 - 1) + 1 - z'^2] \cos \omega_{23} t \\
& \left. + [\cos^2 \gamma_{zz'} (3z'^2 - 1) + 1 - z'^2] \cos \omega_{12} t \right\} \quad (\text{A2.69})
\end{aligned}$$

Note the loss of all ϕ information and the loss of sign information for the direction cosines. This means that the site cannot be determined from zero magnetic field data alone, and all the information which can be obtained is obtained from a single orientation of the crystal.

In the presence of a magnetic field, all the angles will have an influence and so they can, in principle, be determined, but at a cost of having a spectrum of from 3 to 9 lines. If the applied magnetic field is along the symmetry axis, this simplifies the spectrum considerably, back to the 3 lines found in zero field. Unfortunately, for

the same symmetry reasons as for zero field, the ϕ dependence is again lost. It seems that in this instance, the information can only come from a complex spectrum.

I. APPENDIX 3: THE SUPERHYPERFINE INTERACTION HAMILTONIAN

For a spin 1/2 nucleus in zero magnetic field, with an anisotropic hyperfine interaction, where the axes of the superhyperfine tensor coincide with the axes of the anisotropic hyperfine tensor, the Hamiltonian yields the matrix:

$$\begin{bmatrix} -2A_{xx} & 0 & -iA_{zz}^N & 0 & 0 & A_{yy}^N \\ 0 & -2A_{xx} & 0 & iA_{zz}^N & -A_{yy}^N & 0 \\ iA_{zz}^N & 0 & -2A_{yy} & 0 & 0 & -iA_{xx}^N \\ 0 & -iA_{zz}^N & 0 & -2A_{yy} & -iA_{xx}^N & 0 \\ 0 & -A_{yy}^N & 0 & iA_{xx}^N & -2A_{zz} & 0 \\ A_{yy}^N & 0 & iA_{xx}^N & 0 & 0 & -2A_{zz} \end{bmatrix}$$

(A3.1)

where the basis is: $|X\alpha\rangle, |X\beta\rangle, |Y\alpha\rangle, |Y\beta\rangle, |Z\alpha\rangle, |Z\beta\rangle$ and X, Y, and Z defined as for the anisotropic hyperfine interaction in Appendix 2, and α and β are the spin states of the nucleus.

By rearrangement, the matrix can be made block-diagonal as follows:

$$\begin{bmatrix} -2A_{xx} & -iA_{zz}^N & A_{yy}^N & 0 & 0 & 0 \\ iA_{zz}^N & -2A_{yy} & -iA_{xx}^N & 0 & 0 & 0 \\ A_{yy}^N & iA_{xx}^N & -2A_{zz} & 0 & 0 & 0 \\ 0 & 0 & 0 & -2A_{xx} & -iA_{zz}^N & A_{yy}^N \\ 0 & 0 & 0 & iA_{zz}^N & -2A_{yy} & -iA_{xx}^N \\ 0 & 0 & 0 & A_{yy}^N & iA_{xx}^N & -2A_{zz} \end{bmatrix}$$

(A3.2)

The basis is now $|X\alpha\rangle, |Y\alpha\rangle, |Z\beta\rangle, -|X\beta\rangle, |Y\beta\rangle, |Z\alpha\rangle$. This has two identical blocks and so the spectrum will have three pairs of degenerate levels.

BIBLIOGRAPHY

Abragam 61

A. Abragam, *The Principles of Nuclear Magnetism*, Oxford University Press, London 1961.

Albert 84

E. Albert, A. Möslang, E. Recknagel, A. Weidinger, *Hyp. Int.* **17-19** (1984) 611.

Andersson 74

L.O. Andersson, 18th Ampere Congress, Nottingham, (1974) 129.

Arseneau 84

Donald J. Arseneau, David M. Garner, Masayoshi Senba, Donald G. Fleming, *J. Phys. Chem.* **88** (1984) 3688.

Barsov 83

S.G. Barsov, V.G. Baryshevskii, A.L. Getalov, V.A. Gordeev, S.P. Kruglov, L.A. Kuz'min, S.A. Kuten, S.M. Mikirtych'yants, G.V. Shcherbakov, Leningrad Nuclear Physics Institute preprint #879, Leningrad, (1983) [Russian].

Baryshevsky 78

V.G. Baryshevsky, S.A. Kuten, *Physics Letters* **67A** (1978) 355.

Bates 79

J.B. Bates, J.C. Wang, P.A. Perkins, *Phys. Rev. B* **19** (1979) 4130.

Beck 75

R. Beck, P.F. Meier, A. Schenck, *Z. Physik B* **22** (1975) 109.

Beder 78

Doug Beder, *Nuclear Physics* **A305** (1978) 411.

Beder 80

Douglas S. Beder, *Phys. Rev. B* **21** (1980) 3861.

Berger 64

M.J. Berger, S.M. Seltzer, *NASA SP* 3012 1964.

Berger 66

M.J. Berger, S.M. Seltzer, *NASA SP* 3036 1966.

Bevington 69

P.R. Bevington, *Data Reduction and Error Analysis for the Physical Sciences*, McGraw-Hill, New York, 1969.

Boekema 84

C. Boekema, *Hyp. Int.* **17-19** (1984) 305.

Bonner 76

W.A. Bonner, M.A. Van Dort, M.R. Yearian, H.D. Zeman, G.C. Li, *Israel J. Chem.* **15** (1976/77) 89.

Brewer 73

J.H. Brewer, K.M. Crowe, F.N. Gygax, R.F. Johnson, B.D. Patterson, D.G. Fleming, A. Schenck, *Phys. Rev. Letters* **31** (1973) 143.

Brewer 75

J.H. Brewer, K.M. Crowe, F.N. Gygax, A. Schenck, in *Muon Physics vol III* edited by Vernon W. Hughes and C.S. Wu, Academic Press 1975, 4.

Brewer 79

Jess H. Brewer, Douglas S. Beder, David P. Spencer, *Phys. Rev. Letters* **42** (1979) 808.

Brewer 79b

J.H. Brewer, D.P. Spencer, *Hyp. Int.* **6** (1979) 181.

Brewer 81

J.H. Brewer, D.P. Spencer, D.G. Fleming, J.A.R. Coope, *Hyp. Int.* **8** (1981) 405.

Brewer 81b

J.H. Brewer, P.W. Percival, eds. *Muon Spin Rotation Proceedings of the Second International Topical Meeting on Muon Spin Rotation*, *Hyp. Int.* **8** (1981) 307–853.

Brewer 82

J.H. Brewer, D.G. Fleming, P.W. Percival, from *Fourier, Hadamard and Hilbert Transforms in Chemistry*, ed. A.G. Marshall, Plenum Publishing Corporation, 1982, 345.

Brewer 85

J.H. Brewer, *Priv. Comm.*, 1985.

Brown 80

J.A. Brown, S.A. Dodds, T.L. Estle, R.H. Heffner, M. Leon, D.A. Vanderwater, *Solid State Communications*, **33** (1980) 613.

Carr 84

J. Carr, G. Gidal, B. Gobbi, A. Jodidio, C.J. Oram, K.A. Shinsky, H.M. Steiner, D. Stoker, M. Strovink, R.D. Tripp, *Hyp. Int.* **17–19** (1984) 887.

Celio 84

M. Celio, P.F. Meier, *Hyp. Int.* **17–19** (1984) 435.

Chen 84

Y. Chen, R. Gonzalez, K.L. Tsang, *Phys. Rev. Letters*, **53** (1984) 1077.

Clawson 81

C.W. Clawson, E.E. Haller, K.M. Crowe, S.S. Rosenblum, J.H. Brewer, *Hyp. Int.* **8** (1981) 417.

Clawson 82

Carl William Clawson, Ph.D. thesis, Lawrence Berkeley Laboratory, University of California, 1982.

Cowley 64

R.A. Cowley, *Phys. Rev.* **134** (1964) A981.

de Haseth 82

J.A. de Haseth, from Fourier, Hadamard and Hilbert Transforms in Chemistry, ed. A.G. Marshall, Plenum Publishing Corporation, 1982, 387.

Estle 84

T.L. Estle, S.L. Rudaz, E. Holzschuh, R.F. Kiefl, B.D. Patterson, W. Kündig, K.W. Blazey, Hyp. Int. **17-19** (1984) 623.

Estle 85

T.L. Estle, Priv. Comm. 1985.

Evans 55

R.D. Evans, The Atomic Nucleus (1964) 586.

Fleming 79

D.G. Fleming, D.M. Garner, L.C. Vaz, D.C. Walker, J.H. Brewer, K.M. Crowe, p. 279 in Positronium and Muonium Chemistry, ed. H.J. Ache, American Chemical Society, Washington, D.C. 1979.

Fleming 82

Donald G. Fleming, Randall J. Mikula, David M. Garner, Phys. Rev. **A26** (1982) 2527.

Fleming 83

Donald G. Fleming, Randall J. Mikula, Masayoshi Senba, David M. Garner, Donald J. Arseneau, Chem. Phys. **82** (1983) 75.

Fleming 84

D.G. Fleming, D.J. Arseneau, D.M. Garner, M. Senba, R.J. Mikula, Hyp. Int. **17-19** (1984) 655.

Friedman 57

J.I. Friedman, V.L. Telegdi, Phys. Rev. **105** (1957) 1681.

Frondel 62

C. Frondel, The System of Mineralogy, Volume III, Silica Minerals 7th edition John Wiley & Sons, Inc. 1962.

Garay 74

A.S. Garay, L. Keszthelyi, I. Demeter, P. Hrasko, Nature **250** (1974) 332.

Garner 78

D.M. Garner, D.G. Fleming, J.H. Brewer, Chem. Phys. Letters **55** (1978) 163.

Garner 79

D.M. Garner, Ph.D. Thesis, University of British Columbia 1979.

Garwin 57

R.L. Garwin, L.M. Lederman, M. Weinrich, Phys. Rev. **105** (1957) 1415.

Goldstein 50

H. Goldstein, Classical Mechanics, Addison-Wesley, 1950, 107.

Gonzalez 81

R. Gonzalez, Y. Chen, M. Mostoller, *Phys. Rev. B* **24** (1981) 6862.

Goodrum 72

J.W. Goodrum, *Journal of Crystal Growth* **13/14** (1972) 604.

Goshen 83

S. Goshen, M. Friedman, R. Thieberger, J.A. Weil, *J. Chem. Phys.* **79** (1983) 4363.

Graf 79

H. Graf, E. Holzschuh, E. Recknagel, A. Weidinger, T. Wichert, *Hyperfine Interactions* **6** (1979) 177.

Gygax 79

F.N. Gygax, W. Kündig, P.F. Meier, eds. *Muon Spin Rotation Proceedings of the First International Topical Meeting on Muon Spin Rotation*, *Hyp. Int.* **6** (1979) 1-450.

Gygax 84

F.N. Gygax, A. Hintermann, W. Rütuegg, A. Schenck, W. Studer, A.J. van der Wal, *Hyp. Int.* **17-19** (1984) 177.

Harshman 84

D.R. Harshman, R. Keitel, M. Senba, E.J. Ansaldo, J.H. Brewer, *Hyp. Int.* **17-19** (1984) 557.

Heffner 84

Robert H. Heffner, Donald G. Fleming, *Physics Today* **37** (1984) 38.

Henderson 72

B. Henderson, H.T. Tohver, *Phys. Status Solidi* **51** (1972) 761.

Holzschuh 81

E. Holzschuh, W. Kündig, B.D. Patterson, *Helvetica Physica Acta* **54** (1981) 552.

Holzschuh 82

E. Holzschuh, W. Kündig, P.F. Meier, B.D. Patterson, J.P.F. Sellschop, M.C. Stemmet, H. Appel, *Phys. Rev. A* **25** (1982) 1272.

Hughes 60

V.W. Hughes, D.W. McColm, K. Ziock, R. Prepost, *Phys. Rev. Lett.* **5** (1960) 63.

Isoya 83

J. Isoya, J.A. Weil, P.H. Davis, *Journal of Physics and Chemistry of Solids* **44** (1983) 335.

Ivanter 72

I.G. Ivanter, V.P. Smilga, *Sov. Phys. JETP* **34** (1972) 1167.

Jackson 62

J.D. Jackson, *Classical Electrodynamics*, John Wiley and Sons, 1962, 412.

James 71

F. James, M. Roos, MINUIT, CERN Computer 7600 Interim Programme Library (1971).

Jean 79

Yan-Ching Jean, Hans Ache, in D.C. Walker, *Origins of Optical Activity in Nature*, Elsevier Scientific Publishing Company, Amsterdam, Netherlands, (1979) 67.

Kadano 84

R. Kadano, J. Imazato, K. Nishiyama, K. Nagamine, T. Yamazaki, D. Richter, J.M. Welter *Hyp. Int.* **17-19** (1984) 109.

Karaseva 83

L.G. Karaseva, T.A. Karpukhina, B.V. Spitsyn, *Russian Journal of Physical Chemistry* **57(2)** (1983) 302.

Kiefl

R.F. Kiefl, Private Communication.

Kiefl 84

R.F. Kiefl, E. Holzschuh, H. Keller, W. Kündig, P.F. Meier, B.D. Patterson, J.W. Schneider, K.W. Blazey, S.L. Rudaz, A.B. Denison, *Phys. Rev. Lett.* **53** (1984) 90.

Kiefl 85

R.F. Kiefl, J.W. Schneider, H. Keller, W. Kündig, W. Odermatt, B.D. Patterson, K.W. Blazey, T.L. Estle, S.L. Rudaz, submitted to *Rapid Communications, Physical Review B* (1985).

Kinase 82

W. Kinase, N. Ohnishi, *Phys. Letters* **90A** (1982) 101.

Lee 56

T.D. Lee and C.N. Yang, *Phys. Rev.* **104** (1956) 254.

Leiss 57

J.F. Leiss, S. Penner, C.S. Robinson, *Physical Review* **107** (1957) 1544.

Le Page 80

Y. Le Page, L.D. Calvert, E.J. Gabe, *J. Phys. Chem. Solids* **41** (1980) 721.

Mogensen 74

O.E. Mogensen, *J. Chem. Phys.* **60** (1974) 998.

Myasishcheva 68

G.G. Myasishcheva, Yu.V. Obukhov, V.S. Roganov, V.G. Firsov, *Sov. Phys. - JETP* **26** (1968) 463.

Nagamiya 81

S. Nagamiya, K. Nagamine, O. Hashimoto, T. Yamazaki, *Phys. Rev. Lett.* **35** 308.

Norton 76

Norton, Beer, *J. Opt. Soc. Am.* **66** (1976) 259.

Noakes 85

D. Noakes, *Priv. Comm.* 1985.

Nuttall 81

R.H. Nuttall, J.A. Weil, *Can. J. Phys.* **59** (1981) 1696.

Oram 84

C.J. Oram, J.M. Bailey, P.W. Schmor, C.A. Fry, R.F. Kiefl, J.B. Warren, G.M. Marshall, A. Olin, *Phys. Rev. Lett.* **52** (1984) 910.

Pake 73

G.E. Pake, T.L. Estle, *The Physical Principles of Electron Paramagnetic Resonance*, W.A. Benjamin Inc., Reading, Massachusetts 1973.

Papp 75

N. Papp, K.P. Lee, *J. Mag. Res.* **19** (1975) 245.

Patterson 78

B.D. Patterson, A. Hintermann, W. Kündig, P.F. Meier, F. Waldner, H. Graf, E. Recknagel, A. Weidinger, T. Wichert, *Phys. Rev. Letters* **40** (1978) 1347.

Patterson 84

B.D. Patterson, *Hyp. Int.* **17-19** (1984) 517.

Patterson 84b

B.D. Patterson, E. Holzschuh, W. Kündig, P.F. Meier, W. Odermatt, J.P.F. Sellschop, M.C. Stemmet, *Hyperfine Interactions* **17-19** (1984) 605.

Percival 76

P.W. Percival, H. Fischer, M. Camani, W. Ruegg, A. Schenck, H. Schilling, H. Graf, *Chem. Phys. Lett.* **39** (1976) 333.

Percival 78

P.W. Percival, E. Roduner, H. Fischer, *Chem. Phys.* **32** (1978) 353.

Percival 79

Radiochimica Acta, **26** (1979) 1.

Percival 82

Paul W. Percival, Jean-Claude Brodovitch, Kenneth E. Newman, David P. Spencer, *Chem. Phys. Letters* **93** (1982) 366.

Percival 84

P.W. Percival, J.C. Brodovitch, K.E. Newman, *Hyp. Int.* **17-19** (1984) 721.

Percival 85

P.W. Percival, K.M. Adamson-Sharpe, J.C. Brodovitch, S.K. Leung, K.E. Newman, *Chemical Physics* **95** (1985) 321.

Perlson 74

B.D. Perlson, J.A. Weil, *J. Mag. Res.* **15** (1974) 594.

Roduner 84

E. Roduner, *Hyp. Int.* **17-19** (1984) 785.

Sachs 75

A.M. Sachs, A. Sirlin in *Muon Physics vol II* edited by Vernon W. Hughes and C.S. Wu, Academic Press, 1975.

Sahoo 85

N. Sahoo, K.C. Mishra, T.P. Das, Private Communication, 1985.

Sakudo 71

T. Sakudo, H. Unoki, Phys. Rev. Letters **26** (1971) 851.

Schenck 76

A. Schenck p. 159 in Nuclear and Particle Physics at Low Energies, Ed. J.B. Warren, Plenum Publishing Company, New York, 1976.

Schenck 81

A. Schenck, Helvetica Physica Acta **54** (1981) 471.

Schumacher 80

Rolf Schumacher, Ber. Bunsenges. Phys. Chem. **84** (1980) 125.

Senba 84

M. Senba, D.M. Garner, D.J. Arseneau, D.G. Fleming, Hyp. Int. **17-19** (1984) 703.

Smith 64

G.S. Smith, P.B. Isaacs, Acta Cryst. **17** (1964) 842.

Spencer 79

David P. Spencer, Donald G. Fleming, Jesse H. Brewer, Randy J. Mikula, in D.C. Walker, Origins of Optical Activity in Nature, Elsevier Scientific Publishing Company, Amsterdam, Netherlands, 1979.

Stadlbauer 84

J.M. Stadlbauer, B.W. Ng, Y.C. Jean, Y. Ito, D.C. Walker, Hyp. Int. **17-19** (1984) 715.

Stoneham 83

A.M. Stoneham, Priv. Comm. 1983

Swanson 58

R.A. Swanson, Phys. Rev. **112** (1958) 581.

Trower 65

W. Peter Trower, University of California Radiation Laboratory report #2426 (1965) 15.

Turner 85

R.E. Turner, Priv. Comm.

Vester 57

F. Vester, Seminar at Yale University, Feb. 7, 1957.

Walker 79

D.C. Walker, Origins of Optical Activity in Nature, Elsevier Scientific Publishing Company, Amsterdam, Netherlands, 1979.

Walker 81

D.C. Walker, Hyp. Int. **8**(1981) 329.

Willemsen 76

Herman W. Willemsen, Robin L. Armstrong, Peter P.M. Meincke, *Phys. Rev. B* **14** (1976) 3144.

Weil 71

J.A. Weil, *J. Chem. Phys.* **55** (1971) 4685.

Weil 75

J.A. Weil, *Rad. Eff.* **25** (1975) 261.

Weil 81

J.A. Weil, *Hyperfine Interactions* **8** (1981) 371.

Weil 81b

J.A. Weil, *Can. J. Phys.* (1981) **59** (1981) 841.

Weil 84

J.A. Weil, *Phys. Chem. Minerals* (1984) **10** (1984) 149.

Wu 57

C.S. Wu, E. Ambler, R.W. Hayward, D.D. Hoppes, R.P. Hudson, *Phys. Rev.* **105** (1957) 1413.

Yamazaki 84

T. Yamazaki, K. Nagamine, eds. *Muon Spin Rotation and Associated Problems*, *Hyp. Int.* **17-19** (1984) 1-1034.

Yasunaga 70

Hitosi Yasunaga, *Journal of the Physical Society of Japan* **28** (1970) 454.

Young 62

R.A. Young, *B. Post, Acta Cryst.* **15** (1962) 337.